LOW COMPLEXITY PSP-MLSE RECEIVER FOR H-CPM WITH RECEIVE DIVERSITY

Li Zhou

A thesis submitted in partial fulfilment
of the requirements for the degree of
Master of Engineering
in
Electrical and Electronic Engineering
at the
University of Canterbury,
Christchurch, New Zealand.
May 2009

This thesis is dedicated to my parents.

Abstract

This thesis is a study of harmonized continuous phase modulation (H-CPM) coupled with receive diversity as applied to mobile radio communication applications. H-CPM is the modulation technique specified by the American Public Safety Communication Official Project 25 (APCO P25) Phase 2 standards, which is focused on public safety applications. Practical implementation of an H-CPM maximum likelihood sequence estimator (MLSE) receiver requires complex reduction techniques to ensure a cost effective form. In addition, it must be able to handle a fast fading environment, which is often encountered in public safety applications. Here, the reduction of receiver complexity and the combating of fast fading situations are investigated via MATLAB simulation.

By using tilted phase and frequency pulse truncation techniques, the complexity of an H-CPM MLSE receiver is successfully reduced. In particular, the original 384-state receiver is first reduced to a 192-state receiver through the use of tilted phase. Then it is further reduced to 48-states and finally to 12-states by applying frequency pulse truncation. Simulation, assuming static channels, shows that the bit error rate (BER) performance of a 12-state receiver is essentially identical to that of a 384-state receiver, despite a 97% reduction in computational complexity.

To take into account the effects of fading, channel gain estimation via per-survivor processing (PSP) is incorporated into the reduced complexity MLSE receiver. Using a weighted-sum approach to the PSP gain estimates, it was found that at Doppler shifts of 5 Hz, 40 Hz and 80 Hz, the receiver performance was comparable to that obtainable by rival techniques [1]. To further reduce the effect of fading, receive diversity combining was investigated, where a three-antenna diversity scheme is applied to the reduced state PSP-based MLSE receiver. Three different combining techniques, namely selective combining (SC), equal gain combining (EGC) and maximum ratio combining (MRC) were compared. It was found via simulation that the best performance is achieved using MRC, with as much as 14dB improvement achieved by applying triple diversity MRC.

Acknowledgements

First and foremost I would like to thank my supervisors Dr. Philippa Martin, Professor Desmond Taylor and Dr. Clive Horn for their excellent guidance, invaluable support and constant encouragement. Their time and effort in providing me with insights and directions, both in the theoretical and simulation aspects of this project, is very much appreciated. I would also like to thank Tait Electronics Ltd, who provided me with this amazing thesis topic, resources for me to carry out my research, as well as the flexibility that allow me to finish this thesis while working. Of course, this thesis would not be possible without the funding provided by NZi3 Masters Scholarship.

Special thanks to Dr. Stephen Mann, Dr. Lee Garth and Professor James Cavers for their helpful inputs and enlightening advice. Their help in the fine details of the theory and simulation is essential to the success of this project. I also would like to acknowledge my past and present colleagues in the Communications Laboratory, who provided me with useful tips for this project and helped to make late night coding and thesis writing more bearable.

I offer my thanks to Wen Yuan Hu, Alan Wright, Chun Hong Yoon and Samara Alzaidi for their friendship, without which I would have collapsed under the burden of academic work. Most importantly, I am deeply indebted to my parents for their endless love, support and encouragement. I would like to thank my sister, who has always been there for me. Last but not the least, I am very grateful to my dearest husband, William, for believing me! I never would have made it without your continuous support emotionally and technically. Thank you for keeping my life so colorful, joyful, meaningful and full of surprises!

Table of Contents

List of Tables

List of Figures

Abbreviations and Acronyms

ACI	Adjacent Channel Interference.
ACS	Add-Compare-Select.
APCO	Association of Public Safety Communication Officials.
AWGN	Additive White Gaussian Noise.
BER	Bit-Error Rate.
Bps	bits per second.
CDMA	Code Division Multiple Access.
CIR	Channel Impulse Response.
CLT	Central Limit Theorem.
CPFSK	Continuous Phase Frequency Shift Keying.
CPM	Continuous Phase Modulation.
dB	decibel.
DECT	Digital Enhanced Cordless Telecommunications.
DPSK	Differential Phase Shift Keying.
DS-CDMA	Direct Sequence Code Division Multiple Access.
EGC	Equal Gain Combining.
FM	Frequency Modulation.
FSK	Frequency Shift Keying.
GMSK	Gaussian Minimum Shift Keying.
GSM	Global System for Mobile Communication.
H-CPM	Harmonized Continuous Phase Modulation.
Hz	Hertz.
iid	identically and independently distributed.
ISI	Intersymbol Interference.
LMR	Land Mobile Radio.
LMS	Least Mean Squares.
MAP	Maximum *a posteriori*.
MF	Matched Filter.
MIMO	Multiple-Input and Multiple-Output.
MPSK	M-ary Phase Shift Keying.
ML	Maximum Likelihood.
MLSE	Maximum Likelihood Sequence Estimator.
MRC	Maximal Ratio Combining.
MSK	Minimum Shift Keying.
P25	Project 25.
PAM	Pulse Amplitude Modulation.
pdf	probability density function.
psd	power spectral density.
PSK	Phase Shift Keying.
PSP	Per-Survivor Processing.
QPSK	Quadrature Phase Shift Keying.
RC	Raised Cosine.
REC	rectangular.
RSSD	Reduced State Sequence Detection.
RSSI	Received Signal Strength Indication.
SC	Selection Combining.
SNR	Signal-to-Noise Ratio.

SSP	State-Space Partitioning.
TCM	Trellis Coded Modulation.
VA	Viterbi Algorithm

Chapter 1

INTRODUCTION

1.1 General Overview

Wireless communication, in the most general sense, is the transfer of information over a distance without the use of electrical conductors. Although the term "wireless" is widely accepted as the synonym for the newest communication technologies, almost all forms of electromagnetic communications are actually wireless, with the exception of most optical and other cable based technologies. In fact, in the widest sense, one can argue that the use of a fire also smoke signals to communicate between troops in the medieval days is one of the earliest forms of wireless communication. Nowadays wireless communication systems still dominate the scene even if one confines oneself to electronic data transfers, which is what "wireless communication" usually refers to.

One of the most important forms of communication in human civilisation is verbal communication. The most common form of wireless voice transmission nowadays is mobile phone systems. However, while mobile phone systems tend to dominate the commercial market of wireless communication systems, there are many situations where wireless voice transmission is needed, and yet mobile phone systems are not adequate. One example is communication for public safety services. Commercial mobile phone systems use packet-switched and broadband technologies to support a broad range of multimedia applications [2]. In contrast, present day public safety land mobile radio (LMR) systems use narrow band technologies, which are sometimes circuit switched across the air interface, to support low-speed data services [3]. These two systems are different in market forces, requirements, spectrum policy and other factors [4]. In particular, the key difference is that public safety LMR systems have low user density (two orders of magnitude smaller than commercial

mobile phone systems) in a large geographic region. Moreover, reliability and availability are critical for public safety LMR systems since they are mission critical. In contrast, less reliability and availability for commercial mobile phone systems typically just mean less revenue and inconvenience. Therefore, public safety LMR systems typically need dedicated bandwidth to minimise the chance of collision, as well as to reduce the transmission delay due to high traffic. Finally, they need to be efficient in bandwidth and power for long distance communication over obstacles such as buildings or hills.

One development that is taking place for public safety communications is the development of the Association of Public Safety Communication Officials Project 25 (APCO P25) systems. APCO P25 is a standard agreed to by the US federal government, the US Association of Public Safety Communication Officials and the International Telecommunication Industry Association, for public safety digital land mobile radio. Also known as P25, these standards are designed to be backward compatible with analogue radios, to ensure a smooth transition of a two-way radio system from analogue to digital platforms. It is designed to provide interoperability for public safety professionals, as well as to enhance digital radio communication systems to achieve better spectrum efficiency, voice quality, user compatibility and system functionality [5].

P25 Phase 1 is already in use. Currently, P25 Phase 2 is under development. This thesis is mainly concerned with the development of the next generation P25 Phase 2 compatible base station, which will operate in 12.5 kHz channels and deliver 12k bits per second for the up-link using Harmonised-Continuous Phase Modulation (H-CPM) as the modulation [6]. Triple diversity, which is not specified in P25 Phase 2, is to be employed to combat multipath fading and hence improve performance and will be investigated in this project.

Figure 1.1 shows a schematic of a general communication link. It can be seen that a communication system is divided into three essential parts, namely, the transmitter, the receiver, and the medium through the data is transferred, known as the channel, where noise and distortion can take place. In designing any communication system, it is important to consider these three parts carefully.

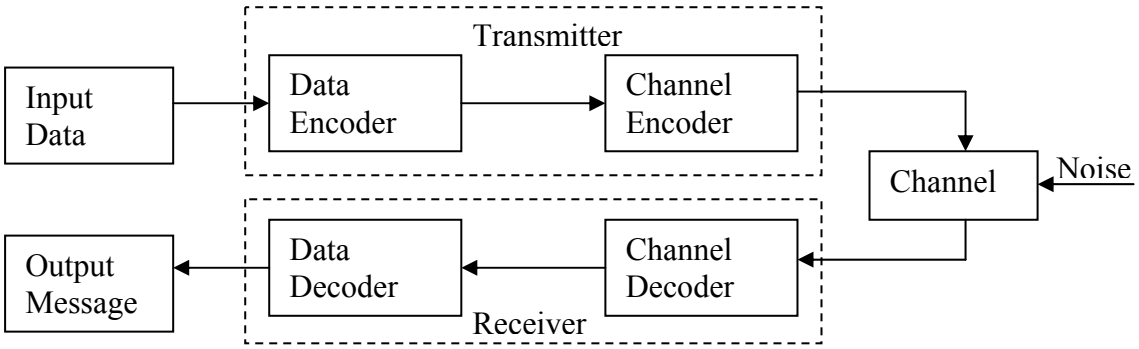

Figure 1.1 General digital communication link.

1.2 Data Transmission and H-CPM

The transmitter is the first stage of the communication system. Here the raw data is processed and transmitted. As shown in Figure 1.1, the transmitter consists of a data encoder and channel encoder or modulator, which converts the raw input data into an analogue bandpass signal, to be transmitted through a channel with specified bandwidth constraints. The act of converting digital data into an analogue bandpass signal through a specific coding scheme is known as modulation. Many different modulation techniques are available for data transmission. The APCO P25 standard specifies that for the up-link transmission, H-CPM must be used [6].

Continuous phase modulation (CPM) is a digital phase modulation with constant envelope [7, 8]. The idea of encoding information into carrier phase with complex patterns was proposed after 1974, based on the study of the most commonly used phase modulation CPFSK (continuous-phase frequency-shift keying) in the early 1970s [9]. In 1978 Anderson and Taylor explored the trellis structure of the CPFSK phase and found that varying the modulation index of CPFSK yielded reduced bandwidth and energy [10]. Then a number of researchers such as Aulin moved into the study of CPM [11]. In the 1980s, a thorough investigation of full response and partial response CPM schemes was carried out by Anderson, Aulin, Sundberg and Rydbeck [12-14].

CPM uses a phase-shaping filter to smooth the variation of the information-carrying phase so as to retain phase continuity. By keeping the phase continuous between symbols, the spectral efficiency of the transmission can be improved compared to common phase modulation schemes that have abrupt phase transitions,

such as quadrature phase-shift keying (QPSK) [15]. Furthermore, the use of the phase-shaping filter introduces memory into the modulation that can result in a "coding gain" compared to phase-shift keying (PSK) modulation [15, 16]. Hence CPM is generally considered as a form of "coded modulation" [9]. Moreover, it achieves gains in bandwidth while maintaining constant envelope for power efficiency without reducing the information data rate. In practical terms, CPM transmitters typically employ low cost, power efficient, non-linear Class C power amplifiers [7, 9]. A class C amplifier is 2 - 4dB more efficient than a linear class A or B amplifier. This prolongs the battery life of a terminal device by 50 -150% [9]. Typically CPM systems have high receiver complexity [17]. The base station receiver often has more processing resources and power available to support such a design. As can be seen CPM is efficient in both bandwidth and energy and is therefore particularly attractive for mobile communications where constant envelope modulation is desirable.

Minimum shift keying (MSK) and Gaussian minimum shift keying (GMSK) are the two most extensively used CPM schemes in the wireless communication scene. MSK, which is a special type of full response CPM, is commonly used for the digital personal communications (Digital Enhanced Cordless Telecommunications (DECT)) standards at 1.8GHz for indoor environments [18]. GMSK, a form of MSK, is the backbone of the global system for mobile communication (GSM) standard for mobile phones [12]. It is also used for other wireless systems such as Bluetooth and WLAN applications. MSK and GMSK are both forms of binary full response CPM modulation with modulation index equals 1/2, but GMSK uses an additional Gaussian filter with defined bandwidth to shape the data sequence prior to modulation. The Gaussian filter smoothes the phase transitions and achieves better spectral efficiency with lower side-lobes than MSK, but it introduces larger intersymbol interference (ISI) [19]. Another drawback of GMSK is that it needs a more complex receiver due to the ISI. However, an optimum receiver for MSK and GMSK is still easy to implement in practice, as the receiver only requires two matched filters (MF) followed by a maximum likelihood sequence estimator (MLSE) that searches the paths through a reasonable number of trellis states and decodes a data symbol after each symbol interval delay [15]. Other more powerful schemes of CPM such as nonbinary partial response CPM and CPM schemes with variable modulation index require a bank of matched filters followed by MLSE that searches the paths through a

large number of trellis states. The complexity introduced by the large filter bank and number of trellis states impedes their implementation in practice. Hence, MSK and GMSK are the two most commonly used CPM schemes in practice.

H-CPM is a partial response CPM that uses a different phase shaping filter from GMSK [20]. Similar to GMSK, H-CPM has a more compact spectrum with lower side-lobes than MSK. This is achieved by introducing additional memory into the modulation using partial response signalling without increasing the BER for the same signal to noise radio (SNR) [14]. It also uses a higher level modulation and has a longer correlation length in its phase shaping filter, which helps to avoid adjacent channel interference (ACI) and to yield better bandwidth efficiency than GMSK [21]. Hence, H-CPM is a good choice for P25 phase 2 uplink, since public safety radio systems employ narrow band technology where spectral efficiency is critical. The drawback is a high complexity receiver is required.

1.3 CPM demodulation

Once the signal is modulated and transmitted, it is passed into the channel, where it physically travels from the transmitter to the receiver. Inevitably, there are losses through the channel, in which some of the signal energy is lost. Furthermore, even with a lossless channel, the thermal noise in the receiver circuits will additively corrupt the transmitted signal. Effectively, at the receiver (in the best scenario), the received signal will be the transmitted signal plus an undetermined amount of noise. This random noise is well modelled as additive white Gaussian noise (AWGN).

Therefore, the receiver cannot simply reverse the process in the transmitter to retrieve the original data. Rather, it has to demodulate the received signal in such a way that the noise is taken into account. As the noise is random, the demodulated data will never be identical to the original data. The goal of the receiver is therefore to minimize the number of errors.

For CPM, three typical demodulation schemes can be found in the literature: discriminator demodulation, differential demodulation and coherent demodulation [22]. Coherent demodulation which requires perfect knowledge of the transmission carrier is used by the P25 Phase 2 standard. It is assumed in this thesis that perfect synchronization is available in the receiver so that the carrier phase and symbol

timing are accurately known. An optimum CPM receiver consists of a bank of matched filters followed by a MLSE that searches the paths through the trellis states for the minimum Euclidean distance path using the Viterbi Algorithm (VA) [16]. Figure 1.2 shows a block diagram for demodulating CPM using MLSE. The reason for using MLSE is to minimise the bit error rate (BER) performance in the presence of ISI. ISI results in the previously transmitted symbols interfering with the currently received symbol. It is largely caused by the partial response form of the continuous phase modulation used.

Coherent MLSE demodulation offers a potential 3dB improvement in SNR performance compared to the other two demodulation schemes. However, as a coherent demodulator performs an exhaustive search over the large number of possible trellis states, it inherently has high complexity in terms of processing power. Also the large size of the matched filter bank increases the implementation complexity. Generally speaking, more powerful (bandwidth and energy efficient) CPM schemes, like H-CPM, have higher implementation complexity, due to using a larger matched filter bank and more trellis states. As a terminal is very resource constrained, applying an optimum coherent receiver structure for H-CPM requires very careful implementation. On the contrary, as base station receivers in public safety LMR systems often have significant processing resources and power available. It is then practical to use coherent demodulation if a simplified receiver with good performance is proposed. Therefore, the first issue that needs to be addressed in designing an H-CPM receiver is how to reduce receiver complexity. Many complexity reduction techniques have been reported in the literature. For example, Fonseka presented a receiver structure that used a soft-decision phase detector preceding an MLSE decoder to reduce the receiver complexity [23]. Simmons proposed a simplified receiver structure with two simple low pass filters replacing the bank of matched filters [24]. Colavolpe et al. suggested a complexity reduction scheme based on a Laurent decomposition, which decomposes the CPM signals into a sum of linearly modulated components, simplifying the receiver front-end [25, 26]. In this thesis, trellis state reduction [27] [28] will be modelled and studied, to reduce the receiver design complexity.

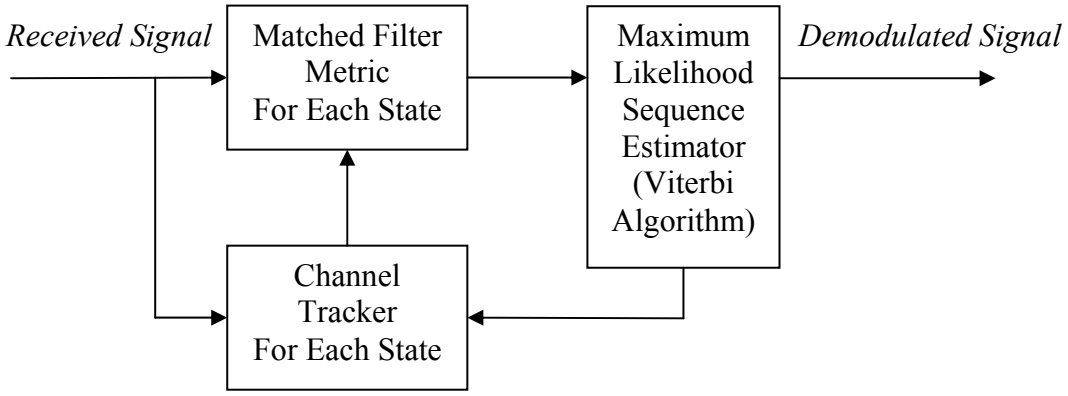

Figure 1.2 Schematic of a MLSE demodulator [6].

1.4 Multipath Fading and Channel Equalisation

Unlike cable or fibre based communication systems, a wireless system lacks a confined (wired) channel for data transmission. As a consequence, the transmitted signal usually reaches the receiver over multiple paths (multipath propagation), through reflections off different obstacles. These multipath propagated signals reach the receiver at different times and powers, and therefore may or may not be in phase with each other. If they are indeed out of phase, these multipath signals destructively interfere, leading to a weakened received signal with the amplitude reduction dependant on the phase difference between the multipath signals. This effect is known as fading, and is especially important in mobile radio networks as relative motion between the transmitter and the receiver often causes an inherent time-variation in the propagation path.

As coherent demodulation assumes an AWGN only channel (also known as a static channel), demodulation using the same receiver in a fading channel will pose problems. A standard way to overcome this problem is to use channel equalisation, whereby the faded signal received is passed through a channel equaliser which estimates the effect of the fading channel and compensates for its effect. The resulting signal can then be considered to be a "static" signal that can be readily demodulated using the coherent detector. While channel equalisation would introduce new errors due to imperfect channel equalisation, these errors are much less significant than those resulting from a non-equalised demodulator. The need for a channel equaliser in

a mobile radio system leads to the second major obstacle to the design of an H-CPM receiver, namely, the design of an algorithm which gives an accurate estimate of the fading channel.

Channel equalisation may be achieved using a conventional MLSE estimator. Figure 1.3 shows its block diagram. In this approach, a global channel estimator is used for all paths in the VA. The tentative decision made by the VA using this global estimate is then fed back to adaptively update the channel estimation. Note that one of

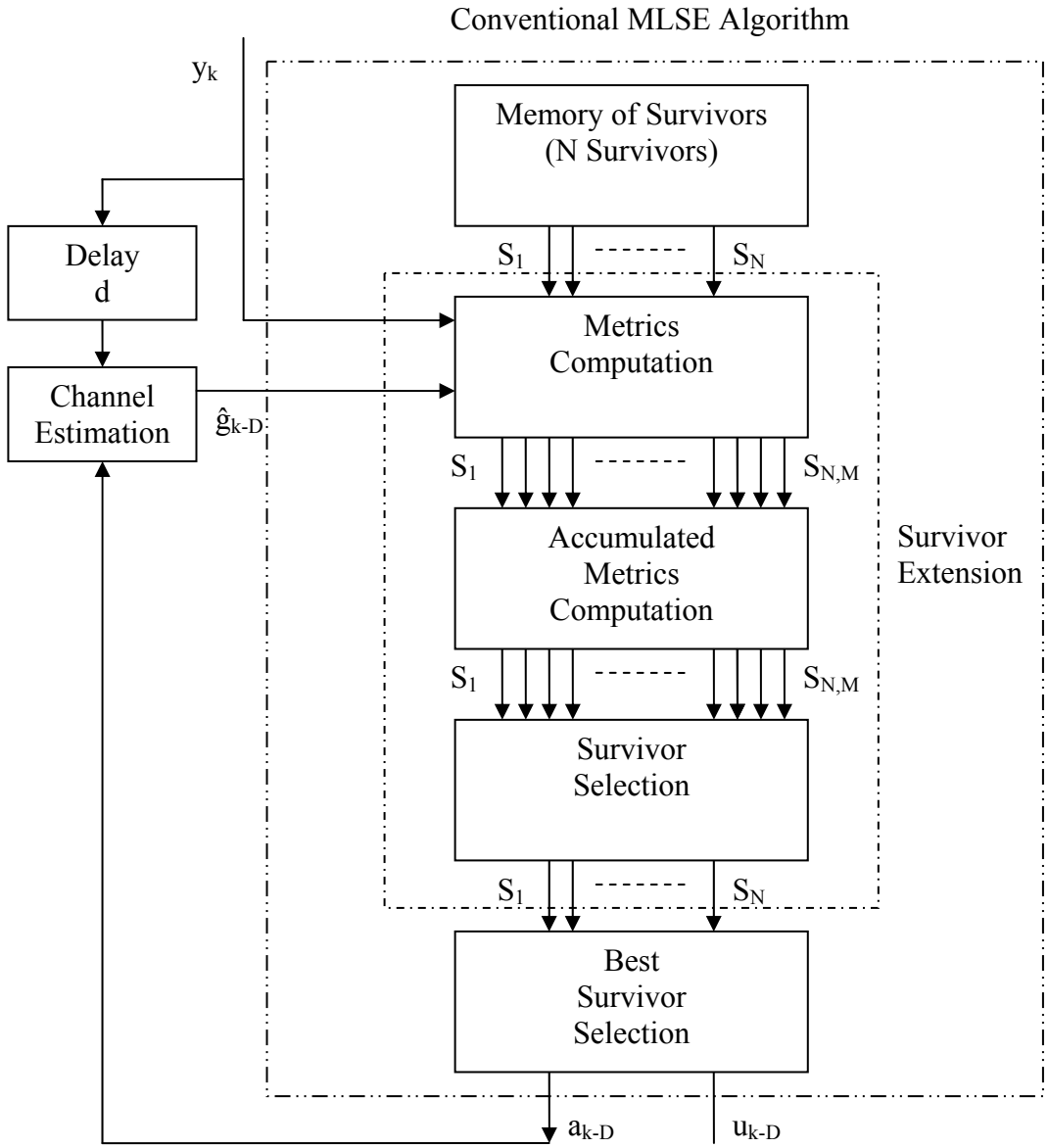

Figure 1.3 Conventional MLSE block diagram (adapted from [29]).

the intrinsic assumptions in the conventional MLSE method is that the channel parameters are known. Even though it is widely used, the conventional MLSE estimator approach is known to have problems. First, because of the need for decision feedback in the estimation of the channel, a delay is incorporated into the demodulation process. This unwanted delay prolongs the processing time and reduces the efficiency of the receiver. But more importantly, the presence of this delay means that the channel estimation will not be accurate in fast changing channels, such as some mobile radio channels. This is because the channel characteristics will have already changed by the time the channel estimation is obtained from the last VA tentative decision. Moreover, if a poor tentative decision is used in the channel estimation, the global nature of the channel estimate means this error will propagate through the whole trellis. Any tentative decisions affected by this poor estimate will be inaccurate, which in turn may lead to worse errors in the next channel estimate. One can see that this may lead to an avalanche effect of increasing inaccuracy.

To overcome these problems, per-survivor processing (PSP) was proposed by Raheli et al. for fast changing channels with unknown parameters [30], such as those encountered in mobile radio systems. Figure 1.4 shows a block diagram of a PSP based MLSE receiver. In PSP, channel estimation is done on a per-survivor basis, where for each surviving trellis path, a channel estimate is calculated from the current sample and the memory of survivors in that particular path. As the channel estimate is calculated prior to the survivor path selection, the delay is significantly reduced. Furthermore, as a separate channel estimate is kept for each survivor path, independent of any VA tentative decision, errors occurring in the channel estimation will be confined to a particular path. Therefore the error will not affect the output of the VA. As the best surviving path (the one with least error) will still be selected. The drawback is that PSP requires more processing power and memory.

PSP has been incorporated into many different modulation schemes to compensate for the fading effect encountered by coherent receivers. A list of examples is given below.

- Raheli et al. outlined the use of PSP on trellis coded modulation (TCM) systems [30, 31].

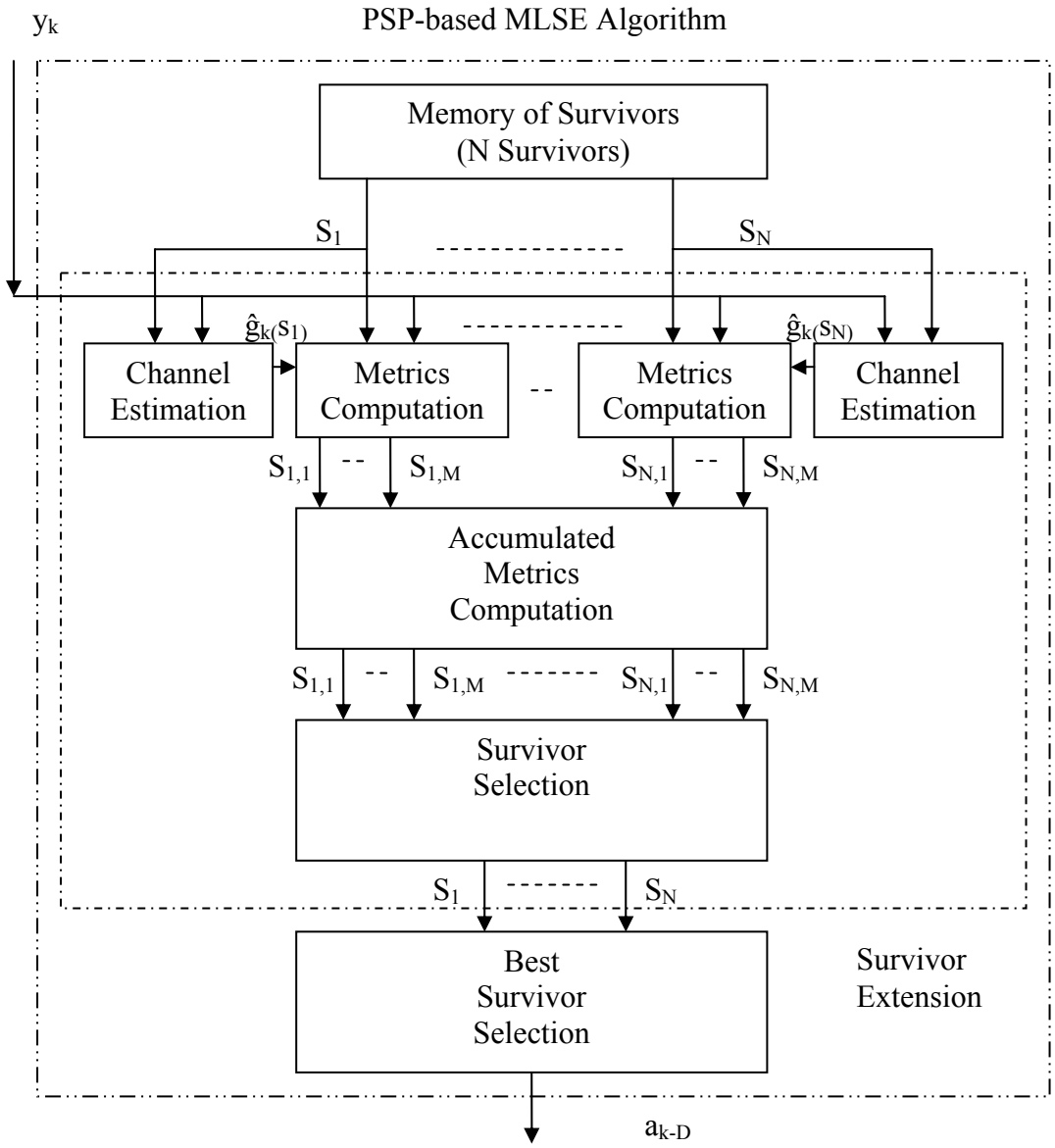

Figure 1.4 PSP-based MLSE block diagram (adapted from [29]).

- Miller has showed that the use of PSP for the demodulation of CPFSK signals gives significant detection efficiency advantage over conventional demodulation techniques [32].
- Patwary et al. reported the application of PSP-MLSE receiver for a time division multiple access (TDMA) and multiple-input and multiple-output (MIMO) system, and showed that it actually lead to a 75% reduction in computational complexity [33].
- The generalised PSP technique has also been applied to differential phase shift keying (DPSK) [31, 34], direct sequence code-division

multiple-access (DS-CDMA) systems [35], as well as for timing recovery [36].

It is clear that PSP is a powerful technique which can improve the efficiency and performance of a receiver system. Therefore, in designing the current base station receiver, PSP is applied to the coherent H-CPM demodulator to cope with the multipath fading caused by the mobile radio channel.

1.5 Diversity Combining

Diversity combining is a technique that is used to combat multipath fading in a wireless channel. When radio channels are separated sufficiently in any of the space, frequency, time or polarization domains, each channel experiences different fading conditions [37]. By combining the received signals, an improved signal is obtained. Receiver space diversity is the most commonly used form of diversity. The concept is relatively simple: instead of using a single receiver branch, multiple receiver branches, separated by at least one wavelength, are used to receive the signal from a single transmitter. Because the receivers are spatially separated, the signal received for each receiver typically will have experienced different fading conditions. In practice, for a typical mobile scenario, the receivers must be separated by at least 7.5 wavelengths to make correlation coefficients between antennas less than 0.7 meaning the fading experienced by these receivers will be mutually independent [38]. As a result, the received signals from the different receiver can be combined using various algorithms to extract the transmitted information. There are three typical diversity combining techniques used to combine the multiple received signals: selection combining (SC), equal gain combining (EGC) and maximal ratio combining (MRC) [37].

Diversity combining using two antennas, known as dual diversity, has long been studied and implemented [39, 40]. Triple diversity means three receive antennas are used. It can enlarge the useful diversity area compared to dual diversity (two antenna system), as triple diversity largely avoids blind spots and leads to close-to-equal coverage in all directions due to the fact that the three antennas forms a circular (2D) array. This is in contrast to dual diversity in which the two antenna can only

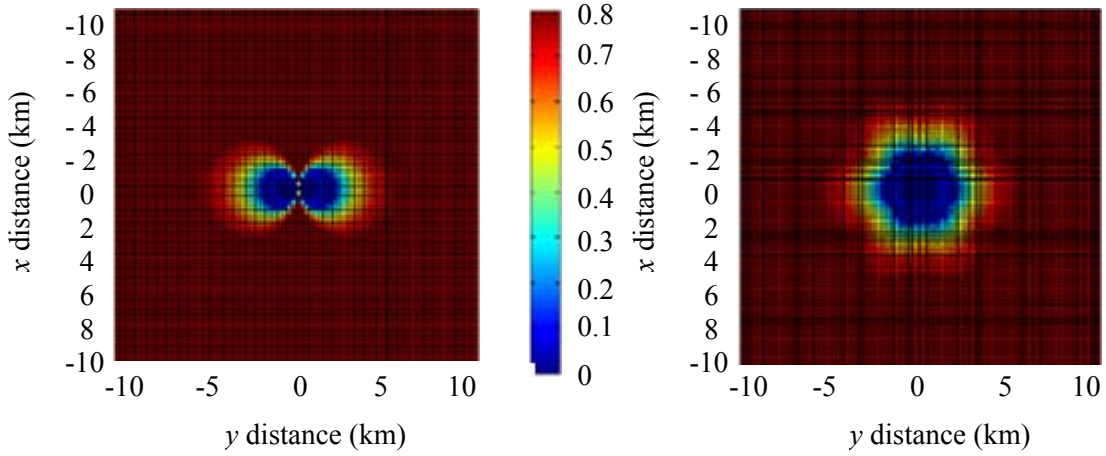

Figure 1.5a Dual diversity useful area [40].

Figure1.5b Triple diversity useful area [40].

form a linear (1D) array which lead to a significant coverage blind spot along the *x* (vertical) direction as seen in Figure 1.5a and b [40]. When more than three antennas are used, even though an even better coverage is obtained, the increment in coverage is not significantly better than when three receiver antennas are used. It is known that most diversity gain is achieved when the receiver is changed from no diversity (single antenna) to dual diversity. Diminishing additional diversity gains are obtained by increasing the number of antennas beyond two. In addition, as the number of antennas increases, it becomes more difficult to keep the correlation coefficients small for near-independent fading which is crucial for diversity performance [41]. The use of extra antennas also increases the hardware and implementation complexity considerably. Hence triple diversity will be used in this project to avoid coverage blind spots.

In the literature, the application of space diversity to CPM modulations with various demodulation detection schemes and channel models has been reported by a number of authors. Some of the important schemes are listed in Table 1.1. It can be seen that the use of diversity with variations of MSK and GMSK with non-coherent detection have been commonly reported in the literature. However, currently no reports can be found on the application of dual/triple diversity on a single-h H-CPM system in flat Rayleigh fading channels. In this Masters research, performance of all three combining techniques with H-CPM and three receiver antennas will be investigated to find the best practical combining technique for this application.

Reference	Type of CPM	Combining Technique	Demodulation Detection	Channel Model	Notes
[41]	GMSK	SC EGC	Coherent Detection	Frequency Selective	EGC outperforms SC by 1dB.
[42]	MSK	SC	Differential	two-delay Rayleigh-fading channel	
[43]	GMSK	MRC	Differential	AWGN Nakagami-m fading Slow frequency-nonselective	
[44]	Multi-h CPM	SC MRC		Rician Rayleigh /lognormal	MRC has better performance.
[45]	GMSK	SC	Limiter Discriminator	Nakagami	
[46]	Partial response CPM	MRC	Coherent Detection	AWGN Rayleigh	Assume the magnitude and phase of each path are exactly known at the combiner.
[47]	MSK	SC EGC MRC	Differential	AWGN Rayleigh	Postdetection
[48]	M-ary modulation, M-ary Orthogonal frequency shift keying (FSK)	MRC EGC	Coherent Detection for M-ary modulation, Non-coherent for M-ary Orthogonal FSK	Generalized gamma	Generalized gamma fading channel is a generalization of Rayleigh, Nakagami, and Ricean fading channels.
[49]	M-ary phase shift keying (MPSK)	Hybrid SC/MRC	Coherent Detection	Nakagami	
[50]	CPFSK	MRC	Differential	Rician	L= 1,2,3 M=2,4,8
[51]	QPSK	MRC	Coherent		MRC combining with PSP.

Table 1.1 Summary of the work done in the literature for CPM with diversity.

1.6 Thesis Outline

To summarise, the goal of this thesis is to study and design an efficient transceiver system using H-CPM as the modulation method in accordance with the P25 phase 2 standard and by applying triple diversity combining. Various demodulation techniques such as trellis reduction and PSP will be applied to improve the performance and the efficiency of the design. The design will be carried out using computer simulations, as opposed to the actual hardware design and implementation. In some sense, this study can be seen as a proof of concept or even a specification for an actual hardware implementation of the system.

In the next chapter, a detailed mathematical model of the H-CPM modulation will be presented, and an implementation of an H-CPM transmitter will be described, including some practical considerations. This is followed by a discussion of the different elements of a wireless channel with a description of how each of these can be modelled and simulated. Chapter 3 is dedicated to the design of an efficient receiver that addresses both the Gaussian noise and fading introduced by the channel, and the performance of different decoding algorithms will be presented. In Chapter 4, diversity combining applied to the optimal receiver will be studied. Chapter 4 and 5 include the original work in this thesis, namely, the design of a reduced complexity PSP based MLSE receiver for H-CPM on flat Rayleigh fading channels, and the comparative application of the three different space diversity combining techniques with dual/triple diversity on the H-CPM PSP-MLSE receiver. Finally, this thesis will conclude with a summary of results and future research directions in Chapter 6.

Chapter 2

TRANSMITTER AND CHANNEL

As shown in Chapter 1, a communication system consists of a transmitter, a channel and a receiver. While these are physically separate entities, they are very interrelated. In particular, to design an optimal receiver, the nature of the transmitted signal and the behaviour of the channel must both be considered. In this chapter, the formulation of the H-CPM transmitter and the multipath fading channel model will be described in detail, and the simulated transmitted signal and channel response will be presented and compared with expected results from a real system. This simulation model of the transmitter and channel will then be used to test and evaluate different receiver designs.

2.1 H-CPM Modulation

2.1.1 Formulation of CPM and H-CPM

In section 1.3, the usefulness of CPM modulation was outlined. It was mentioned that the constant envelope, spectral compactness and continuous phase nature of the modulation are the main reasons to its application in mobile communication systems. These properties can be naturally derived from the formulation of the CPM modulation. The CPM signal at time t is defined as [16, 52]

$$s(t) = \sqrt{\frac{2E}{T}} \cos[2\pi f_c t + \phi(t;\mathbf{I}) + \varphi_0], \; t \geq 0, \qquad (2.1)$$

where the transmitted information is carried in the so-called excess phase $\phi(t;\mathbf{I})$ [9, 16]. T is the symbol time, E is symbol energy, f_c is the carrier frequency, $\mathbf{I} = \{I_k\}$ is the sequence of M-ary data symbols that take the values $\pm 1, \; \pm 3, \cdots \pm (M-1)$ and φ_0 is the initial phase. The phase intercept φ_0 can be set to zero for coherent transmission

without loss of generality. The phase signal $\phi(t;\mathbf{I})$ is formed from the sequence of data symbols $\mathbf{I} = \{I_k\}$ as [9, 16]

$$\phi(t;\mathbf{I}) = 2\pi \int_{-\infty}^{t} \sum_{k=-\infty}^{n} h_k I_k g(\tau - kT) d\tau = 2\pi \sum_{k=-\infty}^{n} h_k I_k q(t - kT), \; nT \le t \le (n+1)T \quad (2.2a)$$

where

$$q(t) = \int_{-\infty}^{t} g(\tau) d\tau = \begin{cases} 0, t < 0; \\ \dfrac{1}{2}, t > LT, \end{cases} \quad (2.2b)$$

is the phase response that affects the phase transition over L symbols and $g(t)$ is the frequency pulse, which is a smooth pulse shape on the interval (0, LT), normalised such that $\int_{-\infty}^{\infty} g(t)dt = 1/2$. L is the duration of the pulse $g(t)$ in symbol periods and h_k is the modulation index for the kth symbol period. In the present work $h_k = h = \dfrac{m}{p}$ where m and p are relative prime positive integers. Note that the infinitely long and uncorrelated sequence of M-ary data symbols I_k can by definition only take the values $\pm 1, \; \pm 3, \cdots \pm (M-1)$, where M is a power of 2. It can be seen from (2.2a) and (2.2b) that since $g(t)$ has a smooth pulse shape without impulses or discontinuity, the resulting phase $\phi(t;\mathbf{I})$ of the CPM signal is continuous. Furthermore, from (2.1) it can be seen that the CPM signal inherently has a constant envelope of $\sqrt{\dfrac{2E}{T}}$.

The actual form of CPM is defined by the pulse length L, the modulation indices h_k, the number of levels, M, and the form of the frequency pulse function $g(t)$. If $L = 1$, the frequency pulse covers only one symbol interval, while if $L > 1$ then the frequency pulse covers more than one interval. It is clear that $L > 1$ introduces additional memory to the modulation scheme (the phase continuity of CPM means that it inherently has memory), and usually yields a more compact spectrum without necessarily sacrificing error performance [14]. Therefore, CPM can be divided into

two classes based on L, namely full response CPM (FR-CPM) with $L = 1$, and partial response CPM (PR-CPM) with $L > 1$.

The modulation index $h_{k,}$ is the maximum peak-peak frequency deviation ($2f_d$) [52]. It has a similar function to the index β in analogue Frequency Modulation (FM), and determines the phase change rate [52, 53]. If h_k is constant for every symbol, ie. $h_k = h$, then the system is referred to as a single-h CPM. However, if $h_k \epsilon \{h_1', h_2', \cdots, h'_H\}$ where $h_{k+H} = h_k$ (i.e. a cyclic set), the system is referred to as multi-h CPM [10]. This thesis is concerned only with single-h CPM modulation schemes. In general, in a single-h CPM system, increasing h can result in better error performance, but this results in a wider spectrum [53].

The number of data levels, M, is known as the alphabet size. It specifies the number of valid symbols in the modulation scheme. For an alphabet size M, a CPM symbol has valid values of $\pm 1,\ \pm 3, \cdots \pm (M-1)$. M is usually a power of 2. For a given data rate, increasing M generally has two effects, namely, it decreases the main lobe spectral width, and increases the susceptibility to noise [13]. Changing the value of M therefore introduces a trade off between error performance and spectral efficiency.

The frequency pulse *g(t)* is also known as the pulse shaping function. It is the "filter" which turns the data symbol value into a phase signal. Pulse shaping is used to shape the signal's spectrum to fit into the band limited channel. The only requirement on *g(t)* for a CPM scheme is that *g(t)* is a smooth pulse signal with no discontinuity or impulses, so that the resulting phase response *q(t)* is continuous. Further, *g(t)* is normalised such that the area under it is always 1/2. As the length of *g(t)* is specified by L, the length of the pulse is given by LT. Some commonly used pulse shapes include rectangular (REC), raised cosine (RC) and Gaussian functions.

By changing the four parameters defining CPM, a wide variety of CPM modulation schemes can be devised. Table 2.1 shows some properties of common CPM modulations with their corresponding values of L, h, M and *g(t)*. Note for some CPM schemes, a prefix 'L' is used to denote the length of the pulse. For example, a RC with pulse length 1 is denoted 1RC. The resulting frequency and phase pulse shapes are shown in Figure 2.1. Using the parameters L, h, M and *g(t)*, it is also possible to precisely define the modulation of principal interest in this thesis: H-CPM.

	L	***h***	***M***	***g(t)***
MSK (1REC)	1	0.5	2	$g(t)=\begin{cases}\dfrac{1}{2LT}\ ;\ 0\le t\le LT \\ 0 \quad ;\text{otherwise}\end{cases}$ (Rectangular)
Quaternary *3*RC [52]	*3*	4/16	4	$g(t)=\begin{cases}\dfrac{1}{2LT}\left[1-cos\dfrac{2\pi t}{LT}\right];0\le t\le LT \text{ (Raised Cosine)} \\ 0 \quad ;\text{otherwise}\end{cases}$
GMSK [52]	∞	0.5	2	$g(t)=\dfrac{1}{2T}\left[Q\left(2\pi B_b\dfrac{t-\frac{T}{2}}{\sqrt{ln\,2}}\right)-Q\left(2\pi B_b\dfrac{t+\frac{T}{2}}{\sqrt{ln\,2}}\right)\right];0\le B_bT\le 1$ $Q(t)=\int_t^\infty \dfrac{1}{\sqrt{2\pi}}e^{\frac{x^2}{2}}dt$ (Gaussian) where B_b is the bandwidth.

Table 2.1 Common classes of CPM.

H-CPM has the parameters: L = 4, h = 1/3, M = 4 with a frequency pulse defined as

$$g(t)=\begin{cases}\dfrac{1}{G}\left(\text{sinc}(\lambda(t-LT/2)/T)\right)\left(cos^2(\pi(t-LT/2)/T/L)\right) & \text{for } t\in[0,LT] \\ 0 & \text{elsewhere.}\end{cases} \tag{2.3}$$

where G is a normalization factor and λ is a modulation parameter. For H-CPM G = 2.60731391 for λ = 0.75 such that $q(t)$ = 1/2 for $t \ge 4T$. Each of the parameters is designed to optimise the effectiveness of the modulation scheme: L is chosen to ensure a long correlation length (L > 3) which helps to avoid adjacent channel interference (ACI) and to improve power efficiency without overly complicating the encoding algorithm [21]; h = 1/3 is employed here to conserve bandwidth at the cost of energy [9]; M = 4 turns out to be the best choice in a joint energy-bandwidth sense

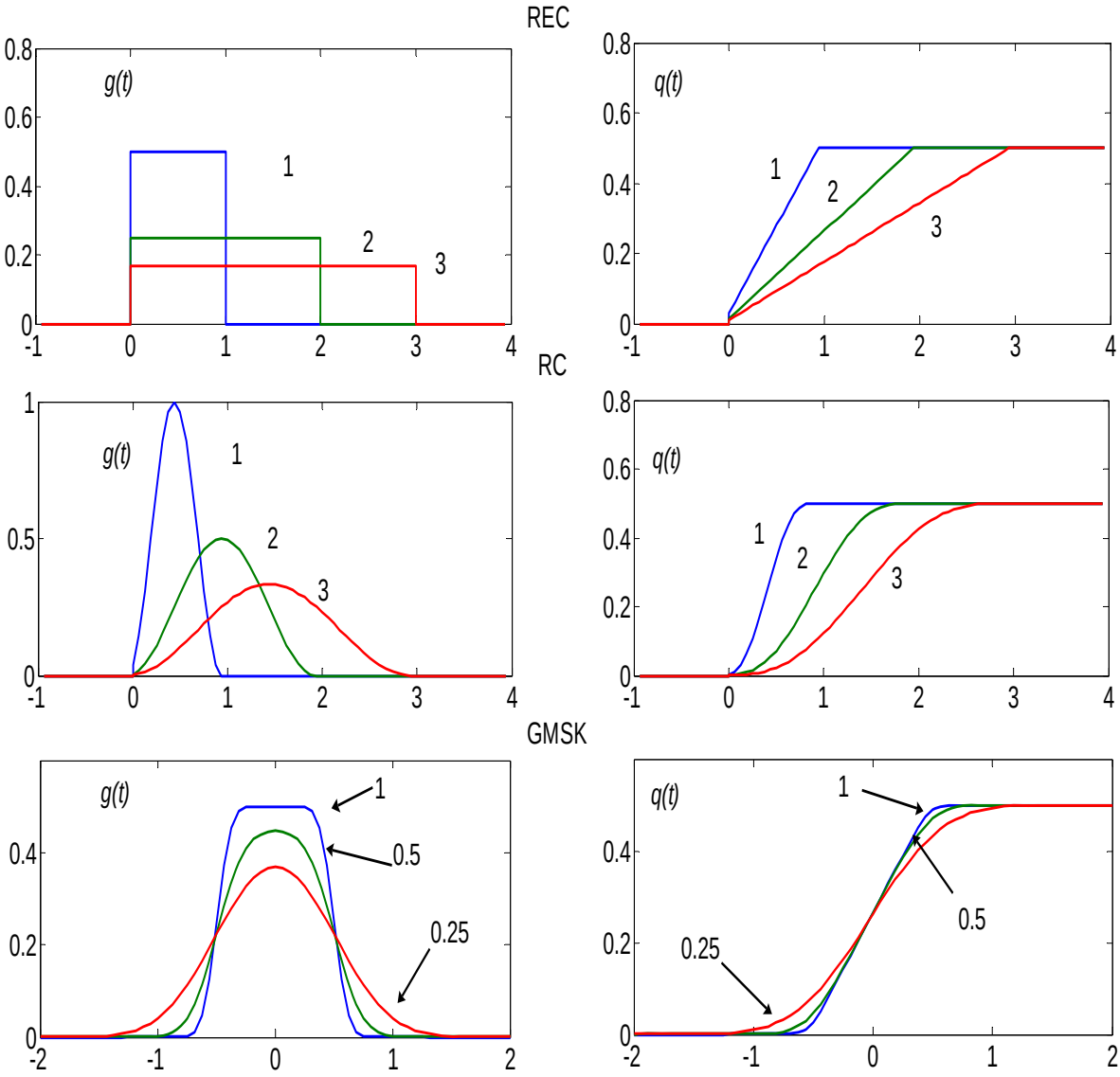

Figure 2.1 Basic frequency pulse (left) and phase pulse (right) of CPM, showing 1REC-3REC (*L*=1,2,3), 1RC-3RC(*L*=1,2,3), and GMSK with bandwidth parameter *Bb*=0.25, 0.5, 1. GMSK has infinite pulse length and *T*=1 in all cases [9]. Note that the x-axis in the figures is in symbol time *T*.

[9]. Note that in the H-CPM phase pulse shown in Figure 2.2, the period before $L = 1$ and after $L = 3$ has negligible effect on the phase change. Hence the effective phase pulse length may be considered to be 2. This helps to reduce the number of low energy phase states in demodulation while retaining the additional memory introduced to the signal due to using $L = 4$. Figure 2.3 shows the allowable phase shifts due to the input data symbols I_k for H-CPM.

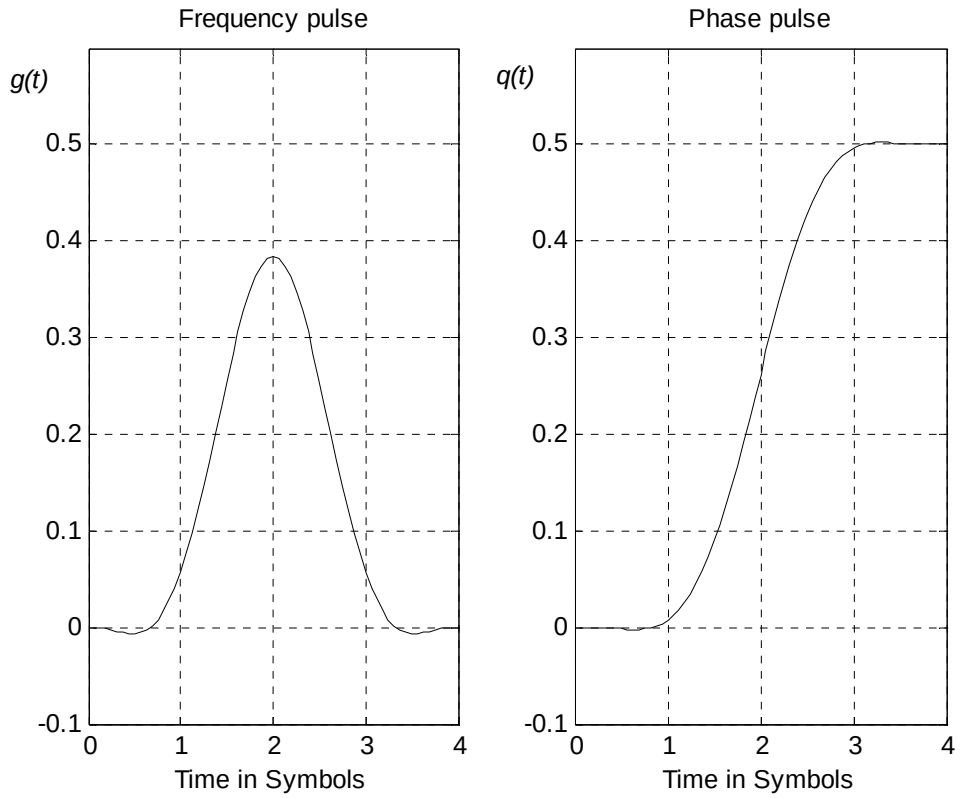

Figure 2.2 Frequency and phase pulse for H-CPM.

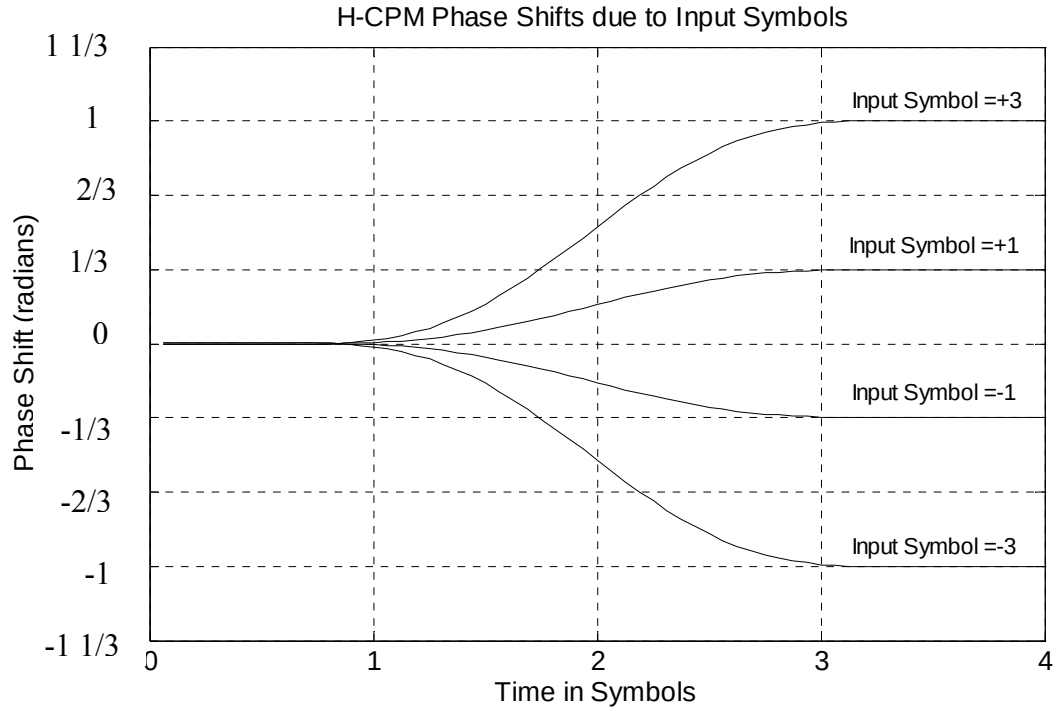

Figure 2.3 The phase shifts due to each input symbol for H-CPM.

2.1.2 Phase State and Correlative State

In this work we focus primarily on the P25 Phase 2 terminal [6]. The modelling of its transmitter is equivalent to modelling an H-CPM modulator. The most important part of the H-CPM modulator is the frequency pulse shaping filter *g(t)* which converts the information from the data signal into the phase signal $\phi(t;\mathbf{I})$ in the interval $nT \le t \le (n+1)T$. Recalling (2.2), the phase signal for a (single-*h*) CPM is given by

$$\phi(t;\mathbf{I}) = 2\pi h \sum_{k=-\infty}^{n} I_k q(t-kT)\,,\ nT \le t \le (n+1)T \tag{2.4}$$

From the last section, we know that $\int_{-\infty}^{\infty} g(t)dt = 1/2$ and $g(t) = 0$ for $t < 0$. This implies that $q(t) = 0$ for $t < 0$ and $q(t) = 1/2$ for $t > LT$, as $q(t) = \int_{-\infty}^{t} g(\tau)d\tau$. Therefore, (2.4) can be written as [16]

$$\phi(t;\mathbf{I}) = 2\pi h \sum_{k=-\infty}^{n} I_k q(t-kT) \tag{2.5}$$

$$= 2\pi h \sum_{k=n-L+1}^{n} I_k q(t-kT) + R_{2\pi}\left[\pi h \sum_{k=-\infty}^{n-L} I_k\right] \qquad nT \le t \le (n+1)T$$

$$= \theta(t;\mathbf{I}) + \theta_n \qquad nT \le t \le (n+1)T.$$

One can see that the first term is the convolution of the last *L* symbols including the current symbol with the pulse shaping function, while the second term is the running sum of all symbol values older than $t = (n-L)T$. The first term in (2.5) can be written as

$$\theta(t;\mathbf{I}) = 2\pi h \sum_{k=n-L+1}^{n-1} I_k q(t-kT) + 2\pi h I_n q(t-nT). \tag{2.6}$$

where the term $2\pi h \sum_{k=n-L+1}^{n-1} I_k q(t-kT)$ is known as the correlative phase component and is dependent on the previous data symbols $\{I_{n-1}, I_{n-2}, \cdots, I_{n-L+1}\}$, and the term $2\pi h I_n q(t-nT)$ defines the phase contributed by the data symbol I_n. The second term in (2.5) is known as the phase state θ_n,

$$\theta_n = R_{2\pi}\left[h\pi \sum_{k=-\infty}^{n-L} I_k\right], \; nT \le t \le (n+1)T, \tag{2.7}$$

and is determined by all symbols prior to $(n-L+1)T$. Examining (2.7), it can be seen that even though the summation appears to be infinite, the value of θ_n is in fact finite and is from a discrete set. This is due to the fact that θ_n is a phase, and therefore, by definition, can be reduced to a value between 0 and 2π. Furthermore, the data symbols I_k for H-CPM by definition can only take certain values determined by $M = 4$, namely, $I_k \in \{1, -1, 3, -3\}$. Given that $h = 1/3$, it can be shown that

$$\theta_n \in \left\{0, \frac{\pi}{3}, \frac{2\pi}{3}, \pi, \frac{4\pi}{3}, \frac{5\pi}{3}\right\} \tag{2.8}$$

This means that when encoding the n^{th} symbol, it does not matter what the actual values of the symbols before the $(n\text{-}L\text{+}1)^{\text{th}}$ symbol are, as long as their sum is known. This, however, is not true for the $(n\text{-}L\text{+}1)^{\text{th}}$ to n^{th} symbols, as the calculation of the correlated state, as specified in (2.7), requires the individual values of these L symbols. Therefore, during the interval $[nT, (n+1)T]$, the excess phase is defined by the data symbol I_n, the L-1 previous data symbols $\{I_{n-1}, I_{n-2}, \cdots, I_{n-L+1}\}$ collectively known as the correlative state, and the phase state θ_n. From this, one can define the H-CPM signal state as

$$S_n = \left(\theta_n, I_{n-1}, I_{n-2}, \cdots, I_{n-L+1}\right). \tag{2.9}$$

which specifies the H-CPM signal at a given symbol time n. Note that there are L-1 data symbols affecting the signal and each data symbol can take M values. Hence the number of CPM states is M^{L-1} times the number of phase states, θ_n [20]. For H-CPM,

$L = 4$, $M = 4$ and using (2.8) the number of phase states is 6. Therefore the number of phase states is $S = 384$. In fact, one can generalise for any single-h CPM modulation that the number of signal states is given by [16]

$$S = \begin{cases} pM^{L-1}, & m \quad even \\ \mathbf{2}pM^{L-1}, & m \quad odd \end{cases} \tag{2.10}$$

where $h = m/p$ [16].

This state representation of H-CPM is important and convenient in two ways. Firstly, it is an important part in the formation of the trellis for H-CPM modulation, which is essential for the application of VA demodulation techniques (see Chapter 3). Secondly, the state representation specifies the number of variables that need to be stored at each particular point in time. As the H-CPM signal state gives a simple specification of the modulated signal, this approach is used in the simulation of the H-CPM modulator in the transmitter. In particular, using the phase state and correlative state representation, one can rewrite the H-CPM signal (from (2.1)) as

$$s(t) = \sqrt{\frac{2E}{T}} \cos[2\pi f_c t + \theta(t;\mathbf{I}) + \theta_n] \tag{2.11}$$

which can be separated into inphase and quadrature components (by expanding the cosine function using trigonometry identities) to give

$$s(t) = \sqrt{\frac{2E}{T}} \left[\{ I(t) \cos(2\pi f_c t) - Q(t) \sin(2\pi f_c t) \} \right] \tag{2.12}$$

where $I(t) = \cos(\theta(t;\mathbf{I}) + \theta_n)$ and $Q(t) = \sin(\theta(t;\mathbf{I}) + \theta_n)$. A block diagram implementing this approach is shown in Figure 2.4.

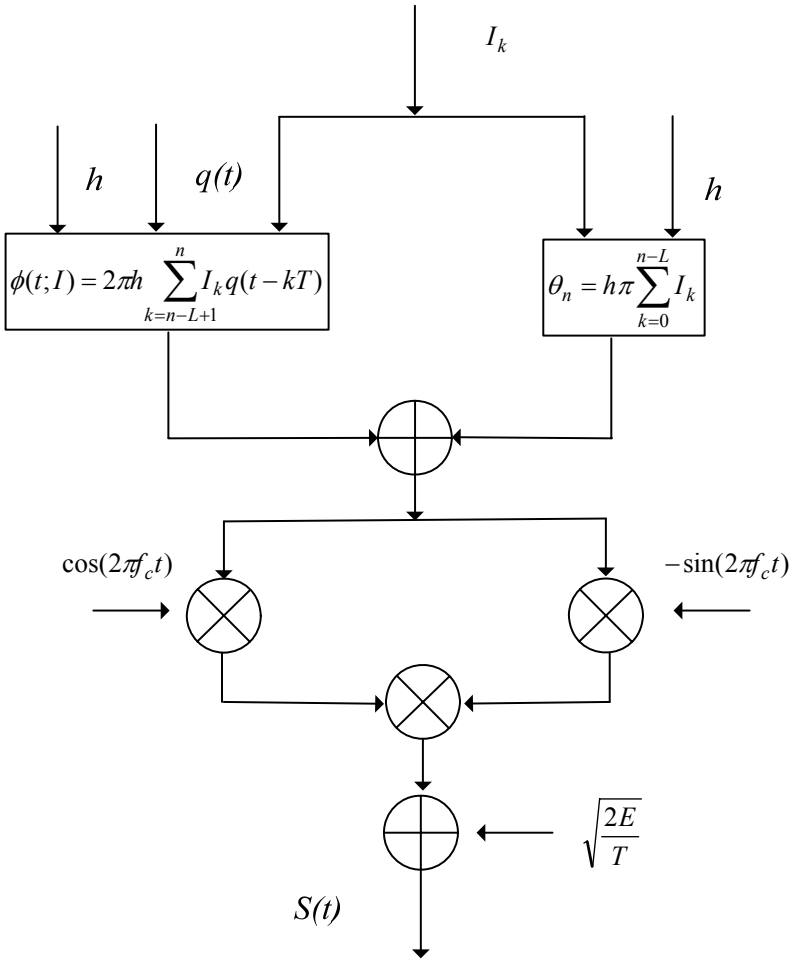

Figure 2.4 H-CPM transmitter block diagram.

2.2 Channel

With the transmitter implemented as in Figure 2.4, the next thing that needs to be considered is the modelling of the wireless channel. A wireless channel can be considered as a noisy filter which the transmitted signal needs to pass through before reaching the receiver. Therefore, to simulate a wireless communication system such as the one concerned here, one needs to formulate an appropriate filter which gives an accurate representation of the channel response. This channel modelling can be separated into modelling the AWGN and the multipath fading.

2.2.1 AWGN Channel

The AWGN channel assumes that the noise in the channel is a wideband noise with constant power spectral density across all frequencies and has a Gaussian amplitude distribution. In a wireless communication system, many noise sources are present, with the most significant being the receiver front end amplifier. As the noise is linearly additive, for all intent and purposes it can be regarded as a single AWGN source which additively corrupts the transmitted signal before it reaches the demodulator in the receiver. Hence an AWGN channel can be easily modelled by a summer which simply adds white Gaussian noise to the receiver input. For simulation purposes, random numbers that model white Gaussian noise are added to the transmitted signal samples. In particular, noise signals generated by a random number generator are added to the *I* and *Q* signal components to represent the H-CPM signal with noise. The magnitude of the I and Q noise signal components are scaled to model a desired signal to noise ratio (SNR).

2.2.2 Multipath Fading

All realistic channels, especially for mobile radio systems, suffer from multipath fading (which will simply be called fading from now on) as shown in Figure 2.5. Fading can result in multipath spread and intersymbol interference. It is caused by the interference of multipath propagated signals. Because of the multipath spread, fading is linear, but multiplicative. Therefore, a more complex model is needed to account for its effect. In this section, the Rayleigh channel model for mobile radio communication systems will be described, and the effect of various fading channel parameters such as coherence bandwidth and Doppler spread will be defined. A mathematical formulation will then be given, which forms the basis of the channel simulation.

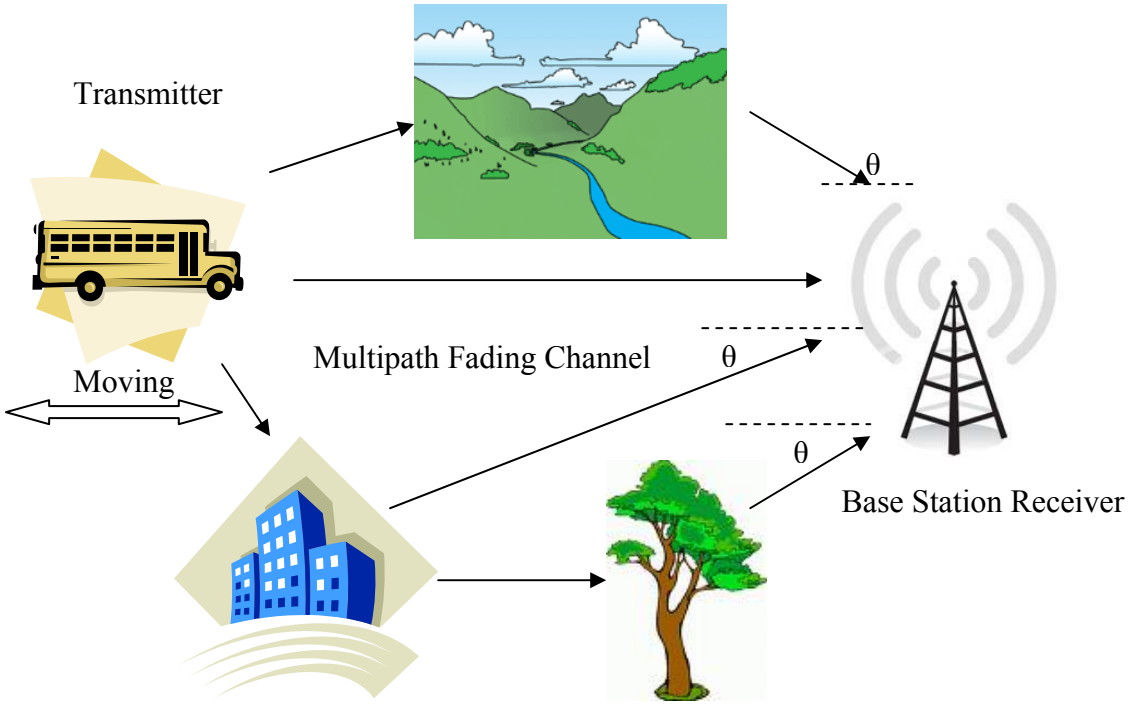

Figure 2.5 Principle of multipath fading channel.

2.2.2.1 Rayleigh Channel

There are a large number of fading channel models that have been used in the literature, depending on the nature of the communication channel. The most commonly used models are Rayleigh, Nakagami and Rician channels because they are easy to analyze and are fairly realistic [54]. Log normal fading model is typically used to describe shadowing and is almost always combined with other models. Typically, the Rayleigh and Rician models are the most suitable for land mobile radio channels. Figure 2.6 shows the probability density functions of the two models. The Rician model is used when the transmitter and receiver are in direct line-of-sight (with limited signal scattering). The received signal consists of a dominant non-faded or shadowed signal component and other faded signal components. In contrast, the Rayleigh model is used when the propagation between the transmitter and receiver is non-line-of-sight. In this project, mobile radio channels that have independent identically distributed (*i.i.d.*) Rayleigh fading are considered.

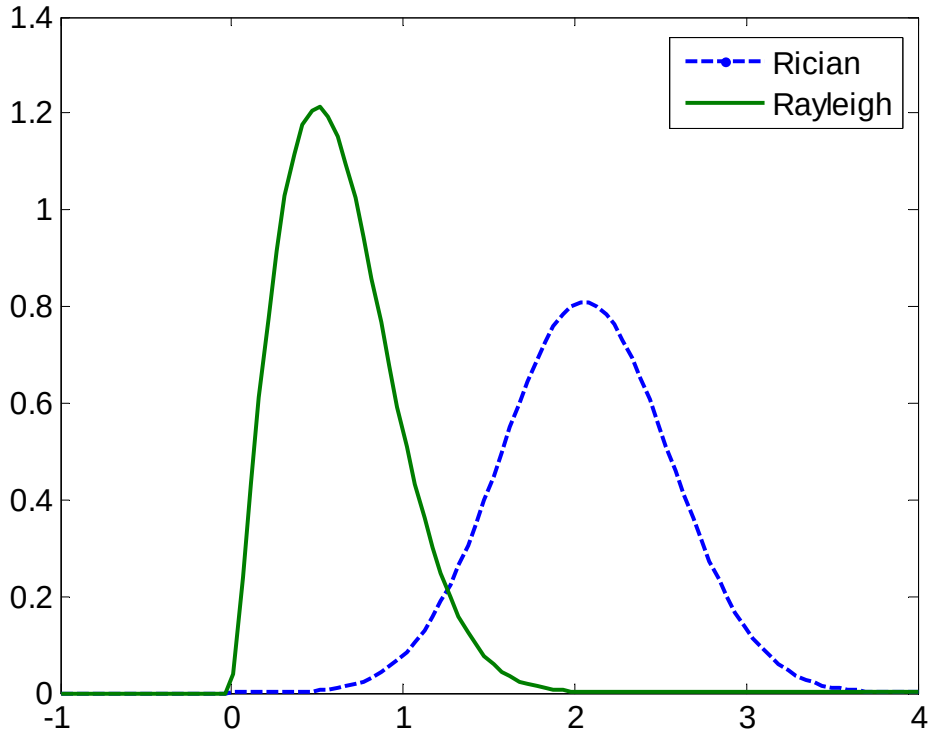

Figure 2.6 Probability density functions of Rayleigh and Rician fading models.

The signal envelope distribution for a Rayleigh fading channel has a Rayleigh distribution. Note that the magnitude of a complex Gaussian variable (with uncorrelated, *i.i.d* Gaussian random variables for the real and imaginary components) is Rayleigh distributed. The Rayleigh channel model ensures the phase shift due to fading is uniformly distributed between 0 and 2π, depending on the path difference. Further, we assume that the propagation paths are independent. Then, when there are a large number of scattering objects (buildings, hills), the result is a large number of propagation paths. With a large number of these *i.i.d.* channel paths we can apply the Central Limit Theorem (CLT), and conclude that the in-phase and quadrature component of the faded signal will each follow a Gaussian distribution with zero mean. As the phase is uniformly distributed in the interval (0, 2π), the envelope, *r*, of this fading follows a Rayleigh distribution, with probability density given by

$$p_R(r) = \frac{2r}{\Omega} e^{-r^2/\Omega} \qquad (2.13)$$

where $\Omega = E(R^2)$ is the variance of the random variable. The behaviour of the Rayleigh model is dependent on the fading behaviour, namely the rate of fading.

2.2.2.2 The Doppler Spectrum and Fading

While in theory any wireless channel will suffer from multipath fading due to the existence of obstacles and reflective paths, an important source of fading that is significant in a mobile radio channel is time variation in the relative positions of the transmitter and receiver. As a person is walking or driving along the road towards or away from the transmitter, a frequency shift is generated due to the Doppler effect. To recall, the Doppler effect is the change in the frequency of a propagating wave due to the relative velocity of the source and the observer. In this case, when the receiver moves, the relative velocity of the receiver and the source of the signal causes a Doppler shift in the received signal frequency. Since there are many scatterers in the channel, each of which can be treated as a signal source, the resulting multipath propagated signals not only have a different delay due to the path-length differences, but also have different Doppler shifts as the relative velocity between each obstacle and the receiver is different. It can be seen that each channel can be described in part by the maximum Doppler frequency $f_{d(\max)}$. When there are many scatterers, each with different Doppler, then a measure of the spread of Doppler shift in the different propagation paths is the Doppler power spectral density or spread function [55]. For Rayleigh fading a typical fade autocorrelation function is given as

$$R_g(\tau) = \sigma_g{}^2 J_0(2\pi f_{d(\max)}\tau), \qquad (2.14)$$

where J_0 is the zero order Bessel function of the first kind and $\sigma_g{}^2$ is the total power of the fading channel complex gains. An illustration of the Doppler power spectral density, and the corresponding autocorrelation are shown in Figure 2.7.

One can extend this to get an idea of the speed of the fading, meaning the rate at which the magnitude and phase changes. One can immediately see that this is directly related to the Doppler spread, as the larger the Doppler spread the faster the

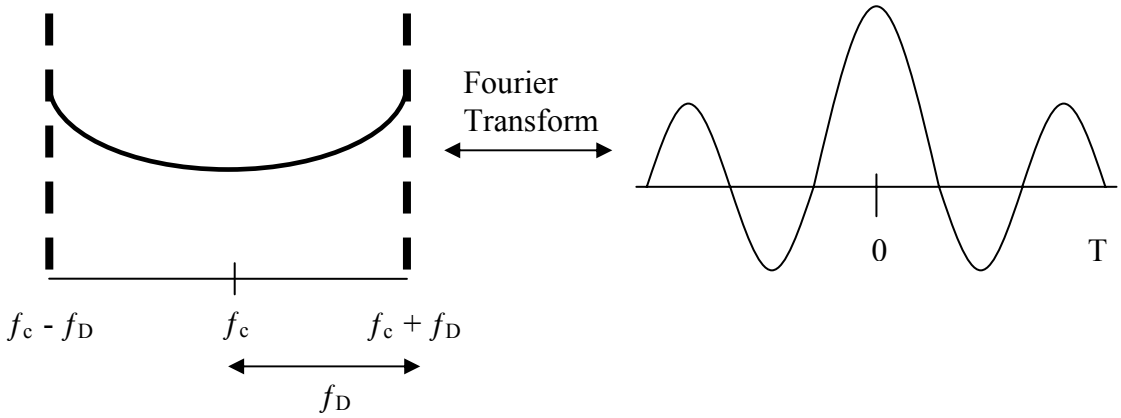

(a) Fading Doppler Spectrum (b) Fading Autocorrelation Function

Figure 2.7 Correlation and power density function for Rayleigh fading channel: (a) Doppler spectrum and (b) Normalized autocorrelation function.

rate of change of the phase difference between the signals. The standard way to quantify the fading rapidity is by using the coherence time, which is the maximum time delay that is allowed between two different signals for them to still be essentially coherent (in phase) with each other. The coherence time is defined as:

$$T_C = \frac{k}{f_{d(\max)}}, \tag{2.15}$$

where k is an arbitrary constant ranging from 0.25 to 0.5. It can be seen that if T_c is greater than the symbol period T, then within each symbol period the faded signals are still coherent. The resulting distortion will be relatively small. However, if $T_c < T$, distortion will occur within a symbol duration, resulting in severe distortion of the received signal that is difficult to correct. In general, if the product $f_{d(\max)}T$, called the normalized fade rate, approaches 0.01 or greater, a channel is referred to as fast fading. Conversely, if the normalized fade rate is close to zero, a channel is recognized as slow fading. For the special case when $f_{d(\max)}$ is zero, the channel response is stationary between the transmitter and receiver, and the channel is called a static channel. No fading occurs in a static channel and so the AWGN channel model can be used in this case.

Consider the P25 Phase 2 radio system [6] which transmits 6000 symbols per second (T = 1/6000 s). If we consider a 900 MHz band radio with a typical mobile velocity of 100kmh^{-1}, the maximum Doppler frequency is given by

$$f_{d(max)} = \frac{v \times f_{max}}{c} = \frac{\left(100 \times 10^3 / 3600\right) \times 900 \times 10^9}{3 \times 10^8} = 83 \text{ Hz.}$$

If $f_{d(\max)}$ is about 83Hz then the normalised fade rate $f_{d(\max)}T$, equals 0.014, which corresponds to a fast fading channel. Based on this, it can be seen that modelling the channel as a fast fading channel should be sufficient for the remainder of this thesis.

2.2.2.3 Frequency Selectivity

Recall that fading originates from interference due to multipath propagated signals. As two signals with very different frequencies cannot interfere with each other, one would expect that if two different signals with sufficient frequency difference are to pass through the same fading channel, the two signals will fade in an independent manner. The minimum frequency separation needed for two signals to fade independently is known as the coherence bandwidth, and is inversely proportional to the multipath spread of the fading channel.

The coherence bandwidth determines the frequency selectivity of the channel. Figure 2.8 presents a schematic of two possibilities that can occur with a fading channel. In the first case, the fading channel has a small coherence bandwidth $(\Delta f)_c$, where Δ denotes the differential operator. As a result, the transmitted signal with bandwidth W, marked by the rectangular window in Figure 2.8(a), is subjected to a large variation in the channel response at the different frequencies within the bandwidth. As a result, different frequency components in the transmitted signal will interfere in an uncorrelated fashion. This type of fading channel where the coherence bandwidth is smaller than the signal bandwidth is known as a frequency selective fading channel. On the other hand, if the coherence bandwidth is greater than the signal bandwidth as shown in Figure 2.8(b), the channel response experienced by the transmitted signal is more or less the same across the whole signal spectrum. The resulting fading is uniform and correlated for every part of the transmitted signal. Such a channel is known as a flat fading channel.

Transforming this into the time domain, we can see that a frequency selective signal will have a multipath spread that is greater than the symbol period. Such

frequency selective fading channels lead to ISI which often requires equalisers to mitigate its effect. Conversely, in flat fading channels, the ISI distortion is usually negligible due to the small multipath spread, making it much easier to decode. For the P25 Phase 2 system, it is expected that the channel can usually be treated as a flat fading channel. This assumption will be used for the rest of the thesis.

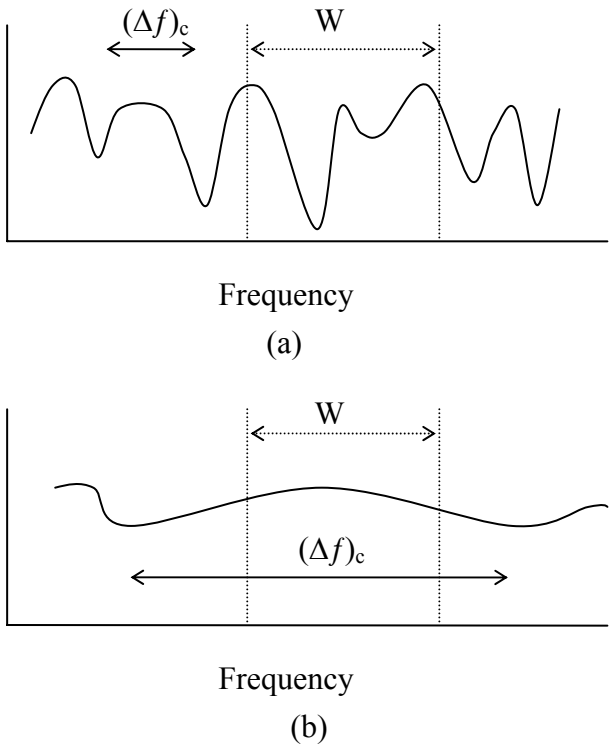

Figure 2.8 (a) Frequency-selective channel and (b) Frequency flat channel.

2.2.2.4 Simulation Model of Rayleigh Flat Fading Channel

The mobile radio channel for the P25 H-CPM communication system can be adequately represented by a Rayleigh flat fading channel with fast fading. From this, an appropriate channel model must be identified before the characteristics of this fading channel can be simulated. There are a number of implementation models that can be used for the Rayleigh channel. Jakes implementation of Clarks' model, called the Jakes model, is the most commonly used model in the literature [56].

Jakes model assumes that the transmitter is fixed with a vertically polarised antenna. It is further assumed that both the angle of arrival and the phase of the multipath signals are uniformly distributed from 0 to 2π, and that each of these has the

same amplitude. Then, the resulting superposition of the multipath propagated signal components is given by [56]

$$T(t) = K\left\{\frac{1}{\sqrt{2}}[\cos\alpha + j\sin\alpha](\cos\omega_m t + \theta_0) + \sum_{n=1}^{N_I}[\cos\beta_n + j\sin\beta_n](\cos\omega_m t + \theta_0)\right\} \qquad (2.16)$$

where K is the normalisation constant, α and β_n are phase values, θ_0 is the initial phase, and ω_m denotes the maximum Doppler shift (i.e. $\omega_m = 2\pi f_{d(max)}$). Note that α and β_n can be chosen arbitrarily, and determine the behaviour and characteristics of the resulting model. This model approximates Rayleigh fading, as with a large N_I, the CLT can be applied, specifying $T(t)$ as a complex Gaussian process, giving a Rayleigh distribution for $|T|$ as desired. Further, it can be shown that the autocorrelation of the envelope of $T(t)$ is a zero order Bessel function, which is characteristic of a Rayleigh fading channel [57], as illustrated in Figure 2.9.

From (2.16), it can be seen that Jakes Model essentially models the Rayleigh channel using a sum of sinusoids. Practically, Jake's Model can be realised by summing N_I oscillators, with each oscillator Doppler shifted from the carrier frequency by ω_n , given by:

$$\omega_n = \omega_m \cos\frac{2\pi n}{N};\ n = 1, 2, \ldots . N_I \qquad (2.17)$$

with N related to N_I via the relation $N_I = N/4 - 1/2$. Note that another oscillator with frequency ω_m, is also needed in the summation to take into account the maximum deviation due to Doppler spectrum. The phases β_n of these signals are set such that the final phase (including the effect of the Doppler shift) is uniformly distributed. This can be conveniently applied to the oscillators by using amplifiers with gains set to $2\sin\beta_n$ and $2\cos\beta_n$. The final step is to separate the in-phase $x_c(t)$ and quadrature $x_s(t)$ components of $T(t)$, corresponding to the real and imaginary parts, and representing the two directions in which the Doppler shift can affect the signal. Then, one can write

$$x_c(t) = 2\sum_{n=1}^{N_I}\cos\beta_n\cos\omega_n t + \sqrt{2}\cos\alpha\cos\omega_m t \qquad (2.18)$$

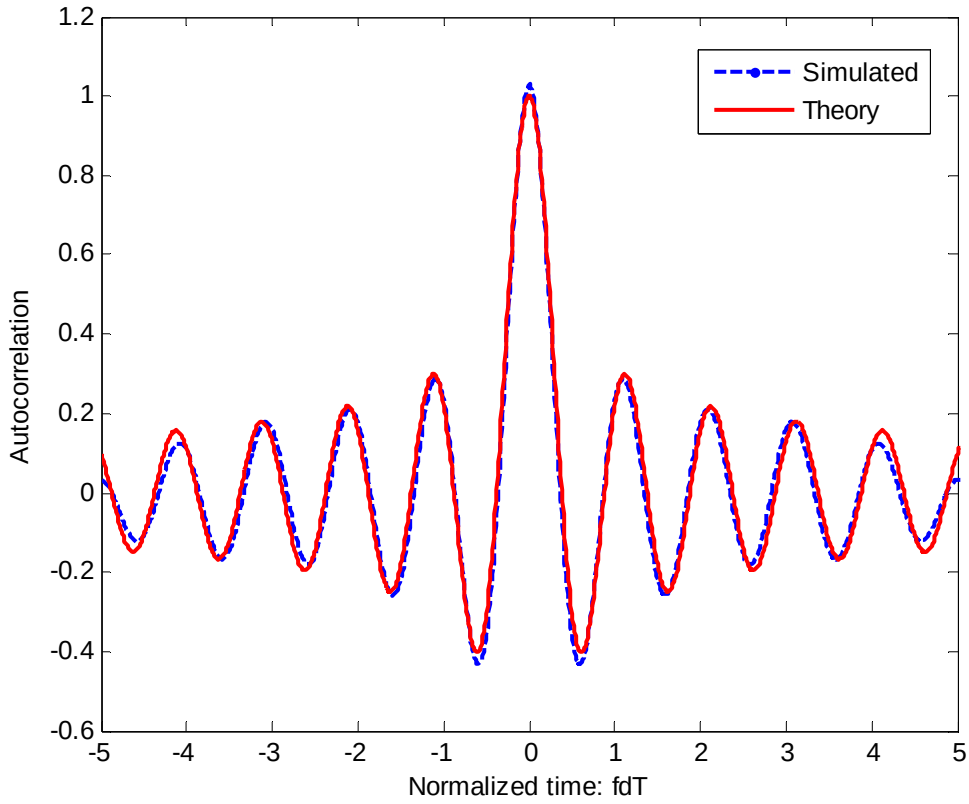

Figure 2.9 Autocorrelation of the simulated Rayleigh fading signal and zeroth order Bessel function for 60Hz Doppler and $N_I = 8$.

and

$$x_s(t) = 2\sum_{n=1}^{N_I} \sin\beta_n \cos\omega_n t + \sqrt{2}\sin\alpha\cos\omega_m t \qquad (2.19)$$

where the normalisation factors are arbitrarily set at $\sqrt{2}$. This is essentially the channel emulation as simulated by the Jakes Model. The final output signal, *y(t)*, is given by multiplicatively applying these fading components to the carrier signal, giving

$$y(t) = x_c(t)\cos\omega_c t + x_s(t)\sin\omega_c t \qquad (2.20)$$

Figure 2.10 shows the Jakes model simulator block diagram. Note that by choosing $\alpha = 0$ and $\beta_n = \pi n/(N_I + 1)$, the cross-correlation between $x_c(t)$ and $x_s(t)$ is zero, meaning the two components are uncorrelated. We now briefly define the channel simulation parameters used in this thesis. The autocorrelation function of the

simulated Rayleigh fading channel is shown in Figure 2.9 with N_I = 8 and $f_{d(\max)}$ = 60Hz. The theoretical auto-correlation function, namely the zeroth order Bessel function of the first kind, $J_0(2\pi f_{d(\max)}\tau)$ [57], is shown in Figure 2.9 for comparison. As we can see, the simulated result matches the theoretical curve well. Figure 2.11 shows the Doppler power spectrum of the simulated complex fading gain with N_I = 8 and $f_{d(\max)}$ = 60Hz. The shape of the spectrum matches that of the theoretical plot shown in Figure 2.7 (a). Figure 2.12 and Figure 2.13 show, respectively, the simulated fading signal amplitude and phase plot. As shown in Figure 2.12, the amplitude fluctuates with regular troughs and occasionally extraordinarily deep fades. Note between symbol 1520-1570 there is a large drop in magnitude as well as a 180º phase shift. This demonstrates that the "deep fades" in magnitude often correspond to rapid 180º phase changes.

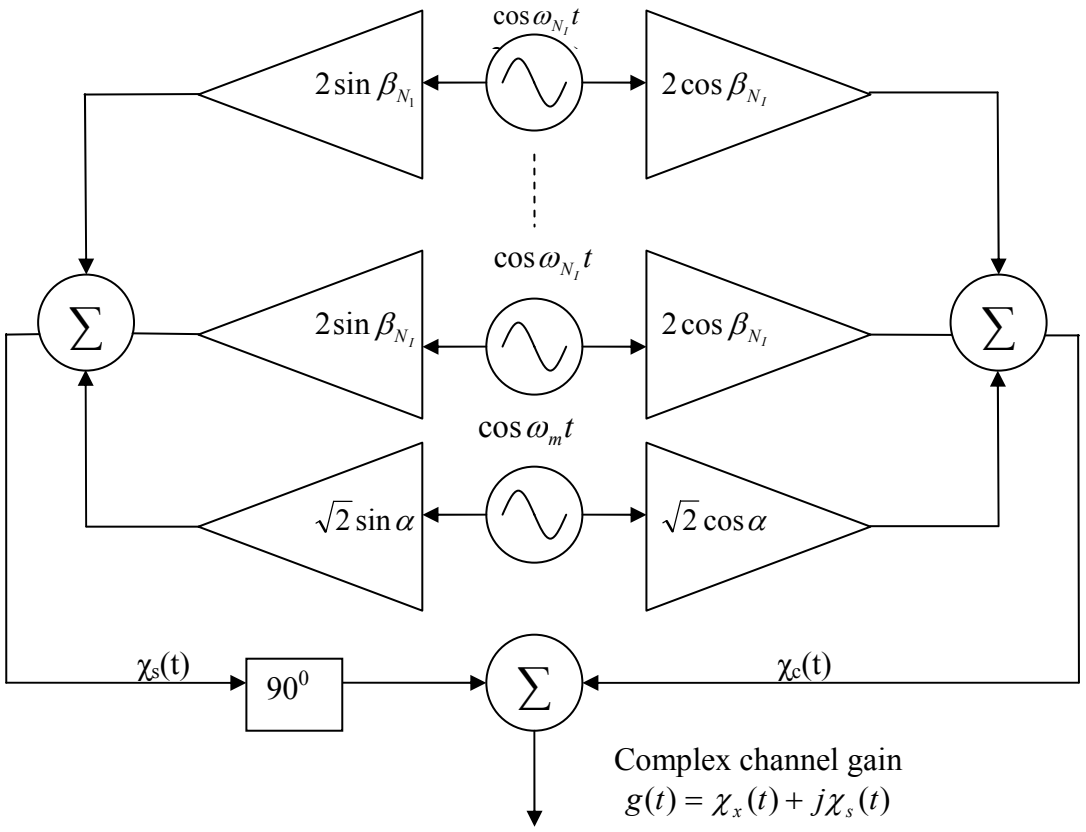

Figure 2.10 The Jakes model simulator block diagram [56].

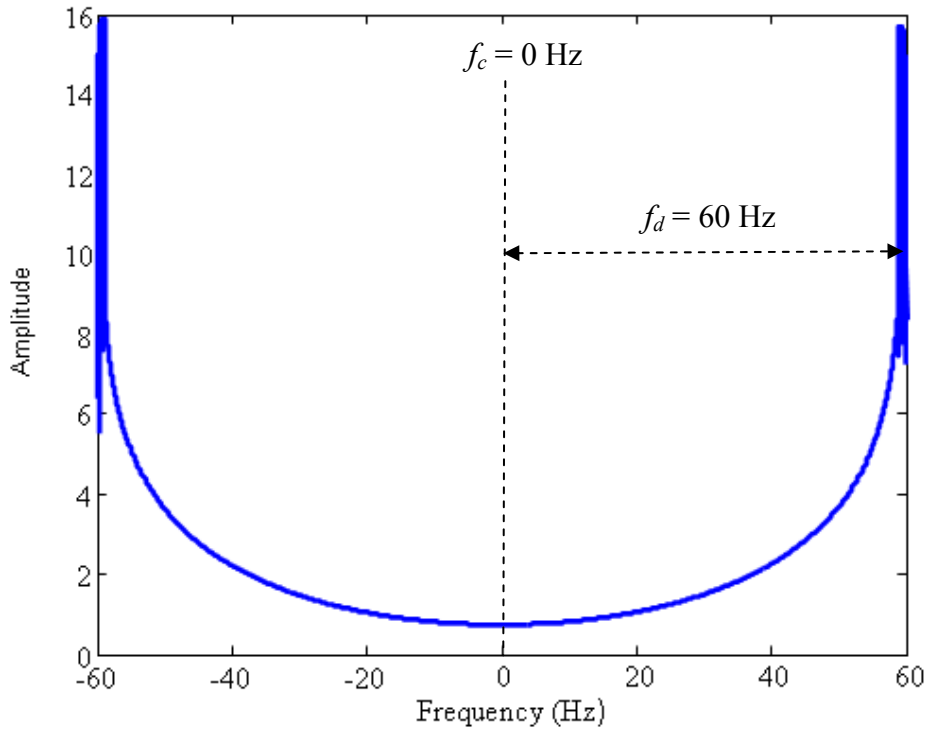

Figure 2.11 Simulated Rayleigh fading channel spectrum for Doppler frequency f_d = 60Hz and centre frequency f_c = 0 Hz with N_I = 8. Comparing with Figure 2.7, it can be seen that the simulation matches theoretical predictions.

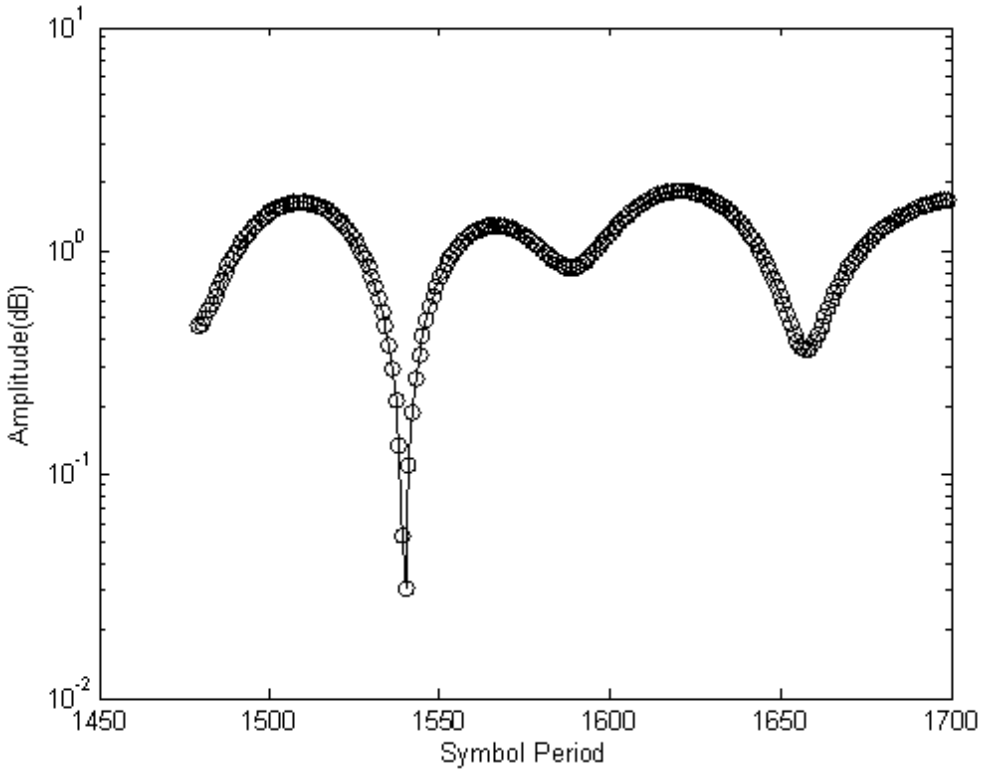

Figure 2.12 Logarithmic plot of the amplitude of the simulated Rayleigh fading Doppler 60Hz. Symbol intervals are indicated by circles.

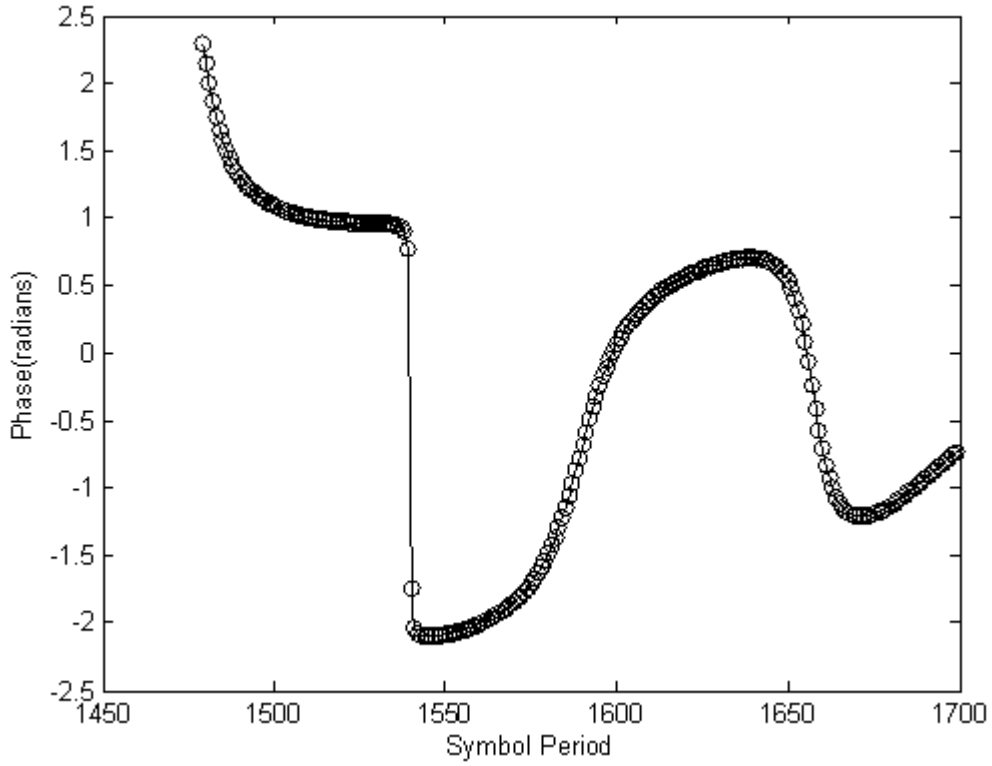

Figure 2.13 Phase plot for the simulated Rayleigh fading Doppler 60Hz. Symbol intervals are indicated by circles.

2.3 Summary

The preceding sections have outlined the H-CPM transmission model and the channel model used to simulate the P25 communication system. It was shown that the H-CPM transmitted signal can be represented by a transmitted state consisting of the correlative state and the phase state that contains all the information in an H-CPM signal. This state representation not only simplifies the transmitter simulation, but also forms the basis of the H-CPM demodulation algorithm. It was also shown that the transmission channel can be modelled by a Rayleigh distributed, frequency non-selective fast fading channel with AWGN. This will affect the amplitude and the phase of the received signal, posing problems for the demodulation.

In the next chapter, the effects of these different aspects of the transmitter and the channel model on the receiver design will be discussed in more detail, leading to the actual design of the optimal H-CPM receiver, and then to reduced complexity versions.

Chapter 3

MLSE RECEIVER

3.1 Introduction

Typically the transmitted wireless signal is corrupted by AWGN and distorted by Rayleigh channel fading. As a result, the received signal will often be very different to the transmitted signal. To accurately obtain the transmitted information, both the AWGN and fading must be compensated by the receiver. However, due to the random nature of the AWGN and fading, the processed signal will never be the same as the transmitted signal. Demodulation is the process of identifying the most likely transmitted symbols according to some criterion of optimality, based on the noisy, faded received signal [58]. In this chapter, reception in an AWGN environment is considered. Demodulation of H-CPM signals in a Rayleigh fading channel will be investigated in Chapter 4.

For CPM signals, three types of demodulation schemes are found in the literature: discriminator demodulation, differential demodulation and coherent demodulation [22]. Coherent demodulation has been chosen for the P25 Phase 2 standard [6] as it potentially offers a 3dB improvement in signal to noise ratio (SNR) performance. However, in general coherent demodulation requires a high-complexity receiver. Base station receivers usually have sufficient energy and powerful signal processing available. It is then practical to use coherent demodulation provided that a simplified receiver with good performance can be found. In this chapter, the design of a reduced complexity coherent receiver for H-CPM signals will be described.

The chapter begins with an introduction to maximum likelihood sequence estimation (MLSE), and a description of the H-CPM trellis and branch metric calculations. The Viterbi algorithm (VA) as a technique for implementing MLSE is then described showing details for H-CPM. Following this, a discussion of the

selection of the VA decision depth is given and the BER performance of the H-CPM receiver is presented. After that, two techniques – tilted phase [15] and frequency pulse truncation [59] are employed to reduce receiver complexity. These will be seen to result in negligible performance degradation. Finally, the simulated BER performance and the computational complexity of the MLSE H-CPM receiver are presented. These results show that the receiver design is practically suitable for a P25 Phase 2 base station, as well as more generic CPM systems.

3.2 Maximum Likelihood Sequence Estimation

Coherent demodulation requires phase and symbol synchronisation between the receiver and the received signal. Here, for simplicity, it will be assumed that the receiver has symbol synchronisation either through the use of pilot symbols or other synchronisation techniques.

One detection approach that is commonly used for coherent demodulation of CPM signals is MLSE. In general terms, the likelihood function $p(r(t) \mid s(t))$ is the conditional probability that a particular signal $r(t)$ is received given that the signal $s(t)$ is transmitted and is considered as a function of $s(t)$. Maximum likelihood (ML) detection is a rule that chooses the transmitted signal $s_i(t)$ which maximizes the likelihood function $p(r(t) \mid s_i(t))$. MLSE is the estimation of the transmitted symbol or bit sequence from the received signals based on the ML detection rule. In most cases, MLSE is implemented using the VA to find the sequence that maximises the likelihood function based on the present and past received symbols. The VA searches for the best path through a trellis corresponding to the transmitted signal by making use of a metric and the merging behaviour of the trellis corresponding to the signal or code structure [60]. Therefore, to design a MLSE detector utilising the VA for an H-CPM receiver, one must start with the trellis representation of the H-CPM signal.

3.2.1 H-CPM trellis

Recall from Chapter 2 that the H-CPM encoded symbol during each symbol interval can be represented using a linear combination of the phase state,

$$\theta_n = h\pi \sum_{k=-\infty}^{n-L} I_k, \tag{3.1}$$

and the correlative phase component,

$$\theta(t;\mathbf{I}) = 2\pi h \sum_{k=n-L+1}^{n-1} I_k q(t-kT), \qquad nT \le t \le (n+1)T, \tag{3.2}$$

defined by the correlative state (I_{n-1},…., I_{n-L+1}). The phase state θ_n can only take a finite number of values. For H-CPM, this set is $\left\{0, \frac{\pi}{3}, \frac{2\pi}{3}, \pi, \frac{4\pi}{3}, \frac{5\pi}{3}\right\}$. Similarly, as the correlative state is the sum of a finite number of symbols weighted by the phase pulse shaping function *q(t)*), and there are only a finite number of possible symbol values (1, -1, 3, -3 for H-CPM), the correlative phase components also has only a finite number of possible values. We consider H-CPM which has a response length of L = 4 symbol period, and therefore, every H-CPM encoded symbol received can be represented by a state $S = (\theta_n, I_{n-1}, I_{n-2}, I_{n-3})$. Since there are 64 combinations of I_{n-1}, I_{n-2}, and I_{n-3} and 6 values of θ_n, the resulting trellis has 384 states. For convenience, these states are usually numbered from 1 to 384.

Using the state representation, each current state is associated with the next state through the current symbol or transition. For example, without loss of generality, we label state 1 by S_1 = (0, 1, 1, 1), and let it be the current state. Then, if the transmitted symbol is -1, the next state is given by[1] S_{337} = (0 - π/3 = 5π/3, -1, 1, 1), as the current symbol I_n, I_{n-1} and I_{n-2} of the current state becomes I_{n-1}, I_{n-2} and I_{n-3} for the next state. Therefore, in the H-CPM trellis, state S_1 is associated with state S_{337} through an input symbol or transition of -1. Using the same method, one can formulate the entire H-CPM trellis, which can then be represented by a state transition matrix $\boldsymbol{S}$ of dimension 4 x 384, where $\boldsymbol{S}(n, m)$ specifies the next state corresponding to a current state, *m,* and a current input symbol or branch, *n*.

[1] using an arbitrary numbering system we call state (5pi/3, -1,1,1) state 337.

3.2.2 Branch Metrics

MLSE, as its name suggests, is a scheme which estimates the transmitted sequence by using the ML decision rule. The ML decision rule is based on the maximum a *posteriori* probability (MAP) criterion, which involves the maximization of the *a posteriori* probability [16]

$$P(\boldsymbol{s}_j|\,\boldsymbol{r}), \qquad j = 1, 2, 3 \ldots\ldots J \tag{3.3}$$

where $\boldsymbol{s}_j$ is one of the J possible transmitted sequences each K symbols long, where K could be infinite and $\boldsymbol{r}$ is the received sequence in the system of interest. By using the Bayes' rule for conditional probability $P(A|B) = P(B|A)P(A)/P(B)$, and the fact that $P(\boldsymbol{s}_j) = 1/J$ as all transmitted sequences are assumed equally probable, one can show that MAP detection is equivalent to the maximization of the conditional probability density function $p(\boldsymbol{r}|\boldsymbol{s}_j)$ [16], which is usually easier to evaluate. As previously mentioned $p(\boldsymbol{r}|\boldsymbol{s}_j)$ is called the likelihood function, and the decision rule which maximizes this probability with respect to $\boldsymbol{s}_j$ is the ML rule. The maximization of the likelihood function is equivalent to the maximization of the log-likelihood function $ln\ P(\boldsymbol{r}|\boldsymbol{s}_j)$ [16], and for any given sequence $\boldsymbol{s}_j$ can be shown to be proportional to the sum of the Euclidean distances over the sequence of symbols given by

$$D\left(\mathbf{r}, \mathbf{s}_j\right) = \sum_{k=1}^{K} \left(r_k(nT) - s_{jk}(nT)\right)^2 \tag{3.4}$$

where $r_k(nT)$ and $s_{jk}(nT)$ are the signal representation of r_k and s_{jk} at symbol time nT. $D\left(\mathbf{r}, \mathbf{s}_j\right)$ is known as a path metric and shows that the likelihood function can be maximized by minimizing the Euclidean distance between the k^{th} sample r_k in the received sequence and the k^{th} symbol s_{jk} in the hypothesized transmitted sequence $\boldsymbol{s}_j$ for all K received symbols. This Euclidean distance r_k and s_{jk} is known as the branch metrics, In other words, the path metrics is given by the sum of branch metrics of every symbol in the sequence.

As the received signal sample r_k and the possible transmitted symbols s_{jk} are complex signals, the Euclidean distance between them or the branch metrics is defined as

$$d_{jk}(nT) = \left| r_k(nT) - s_{jk}(nT) \right|^2 . \qquad (3.5)$$

The vector representation of these two signals is shown in Figure 3.1. Using vector arithmetic, one can define an error vector ***e*,**

$$\mathbf{r_k} = \mathbf{s_{jk}} + \mathbf{e} \qquad (3.6)$$

The error vector ***e*** in reality represents the error between the received symbol and a (possible) transmitted symbol. Note that from Figure 3.1, it can be seen that the Euclidean distance *d* is equivalent to the magnitude of the error vector ***e***. i.e.

$$d = \left| \mathbf{e} \right|^2 . \qquad (3.7)$$

Expanding (3.5) we obtain for each received signal sample

$$d_{jk}(nT) = \left| r_k(nT) \right|^2 - 2\,\mathrm{Re}(r_k(nT) s_{jk}^{*}(nT)) + \left| s_{jk}(nT) \right|^2 , \qquad (3.8)$$

where $s_{jk}^{*}(nT)$ denotes the complex conjugate of $s_{jk}(nT)$. Because of the constant envelope property of H-CPM, $\left| s_{jk}^{*}(nT) \right|^2$ is constant for all possible s_{jk}. Furthermore,

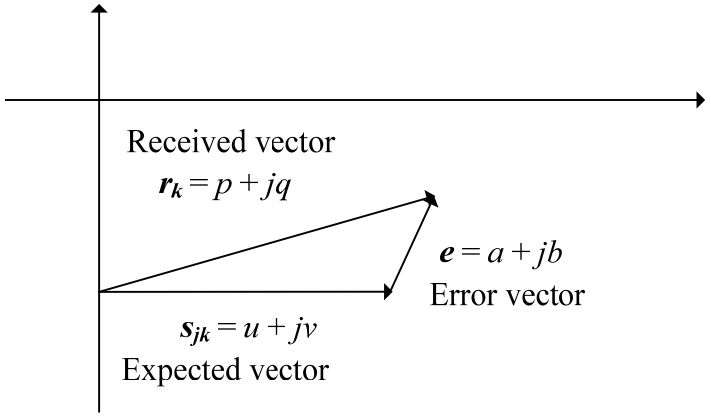

Figure 3.1 Illustration of the Euclidean distance between the expected vector and the received vector [61].

in the calculation of d for each s_{jk}, the received symbol r_k is the same. Therefore, the minimum Euclidean distance can be obtained by maximizing the middle term of (3.8), namely

$$\mathrm{Re}(r_k(nT)s_{jk}^{*}(nT)) \tag{3.9}$$

for each symbol. In practice, we may write the complex base band signal samples in the form

$$r_k(nT) = p + jq \tag{3.10}$$

and

$$s_{jk}(nT) = u + jv. \tag{3.11}$$

We may then write the branch metrics in terms of real base band components as,

$$B = Re((p + jq) * (u - jv)) \tag{3.13}$$

$$B = Re(pu + quj - pvj + qv) \tag{3.14}$$

so that

$$B = pu + qv \tag{3.15}$$

This process is illustrated in Figure 3.2. It can be seen in the figure the ratio between Branch metrics 1 and Branch metrics 2 remains the same even if the signal magnitude is reduced under AWGN. This demonstrates that the envelope variation of *r(t)* does not affect the branch metrics decision. From these individual branch metrics, one can then calculate the path metric, thereby maximizing it.

In order to obtain a ML sequence estimate for the sequence of received symbols, one must search through the trellis over the current and previously received symbols to find the trellis path with the maximum overall path metric in (3.4) (rather than maximum individual branch metrics for each symbol). This is calculated using the branch metrics that were calculated in (3.9) for each of the received symbols in the sequence. The most efficient way to do this is by using the VA, which is a search algorithm that will be described in the next section. Note the branch metrics can be evaluated in practice using a matched filter (MF) bank [7]. The size of the MF bank is given by $2M^L$ [7]. Figure 3.3 shows the optimum MLSE receiver structure for CPM.

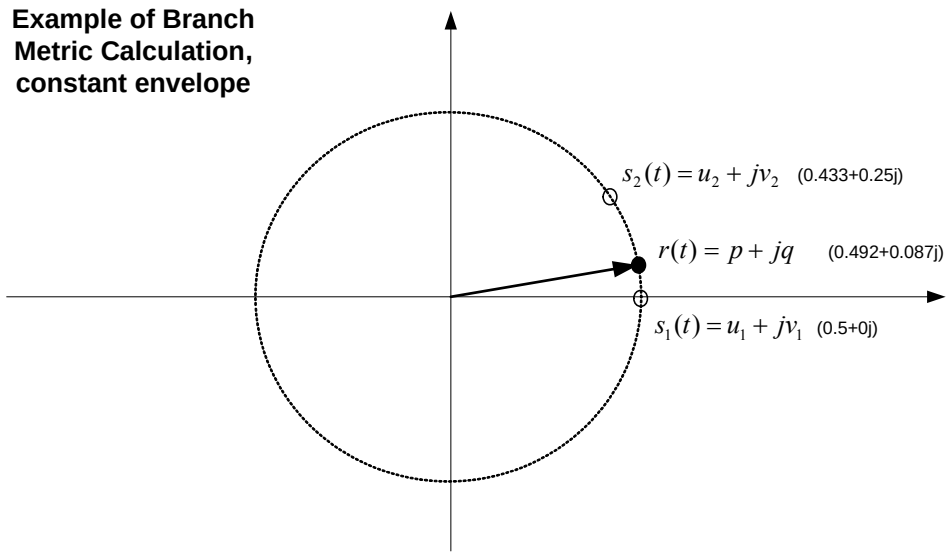

Branch Metric 1	Branch Metric 2	Branch Metric Ratio	Conclusion
$(p*u_1)+(q*v_1)$	$(p*u_2)+(q*v_2)$	$(p*u_1)+(q*v_1)/(p*u_2)+(q*v_2)$	The received signal is more likely to have been in State 1 than State 2
(0.492*0.5) + (0.087*0) = 0.246	(0.492*0.433) + (0.087*0.25) = 0.2348	0.246 / 0.2348 = 1.04	

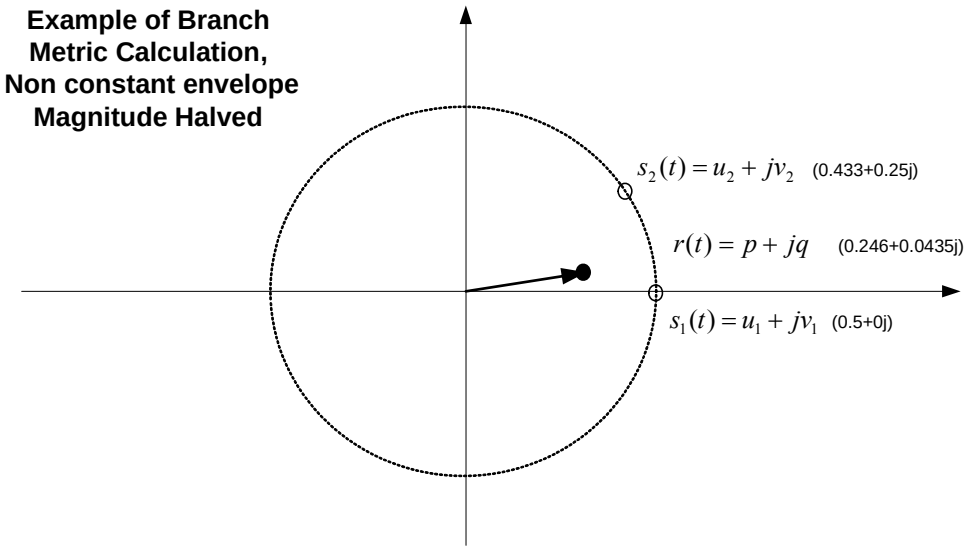

Branch Metric 1	Branch Metric 2	Branch Metric Ratio	Conclusion
$(p*u_1)+(q*v_1)$	$(p*u_2)+(q*v_2)$	$(p*u_1)+(q*v_1)/(p*u_2)+(q*v_2)$	The received signal is more likely to have been in State 1 than State 2 i.e the envelope variation has not affected the decision
(0.246*0.5) + (0.0435*0) = 0.123	(0.246*0.433) + (0.0435*0.25) = 0.1174	0.123 / 0.1174 = 1.04	

Figure 3.2 Metric calculation example [2].

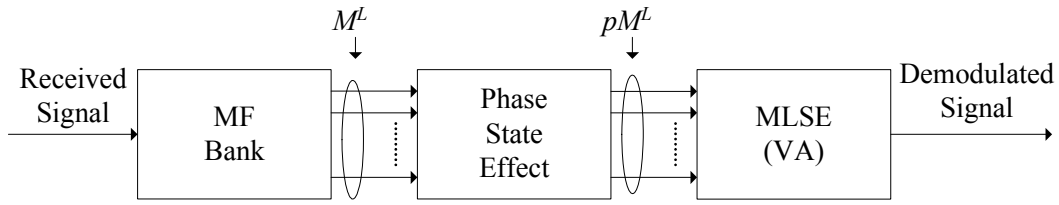

Figure 3.3 The optimum MLSE receiver structure for CPM [8].

3.2.3 The Viterbi Algorithm

The VA is an efficient searching algorithm that finds the best or shortest path through a trellis. It was proposed by Viterbi in 1967 [62] as a means of decoding convolutional codes. The algorithm is an application of forward dynamic programming which searches for the shortest unidirectional route in a graph exhaustively and synchronously [9]. It ensures a ML estimate of the transmitted data sequence is obtained [7].

In practice an approximate version of the VA is used, since it is not usually feasible to trace back through the whole trellis due to the required long delay. In a practical VA, surviving paths are saved only over a certain length of path history, N_{win}. The algorithm returns an estimate for the oldest symbol in the best partial sequence of length N_{win}, based on the current estimation of the most likely path [7]. This length N_{win} is called the decoder decision depth or observation window [9]. N_{win} is also known as the decoding delay as each symbol is decoded after N_{win} symbol times. Ideally N_{win} should be long enough that no significant performance loss will be introduced [9], and such that the resulting delay is tolerable. The best criterion for choosing N_{win} depends on channel conditions such as the SNR and the transmit signal memory length [7]. In practice, N_{win} is typically chosen to be five times the frequency pulse length of L symbols for CPM [16].

3.2.3.1 H-CPM

Recall that the H-CPM states are represented as $S = (\theta_n, I_{n-1}, I_{n-2}, I_{n-3})$. Figure 3.4 shows a small portion of the complete state trellis for H-CPM. Each state is

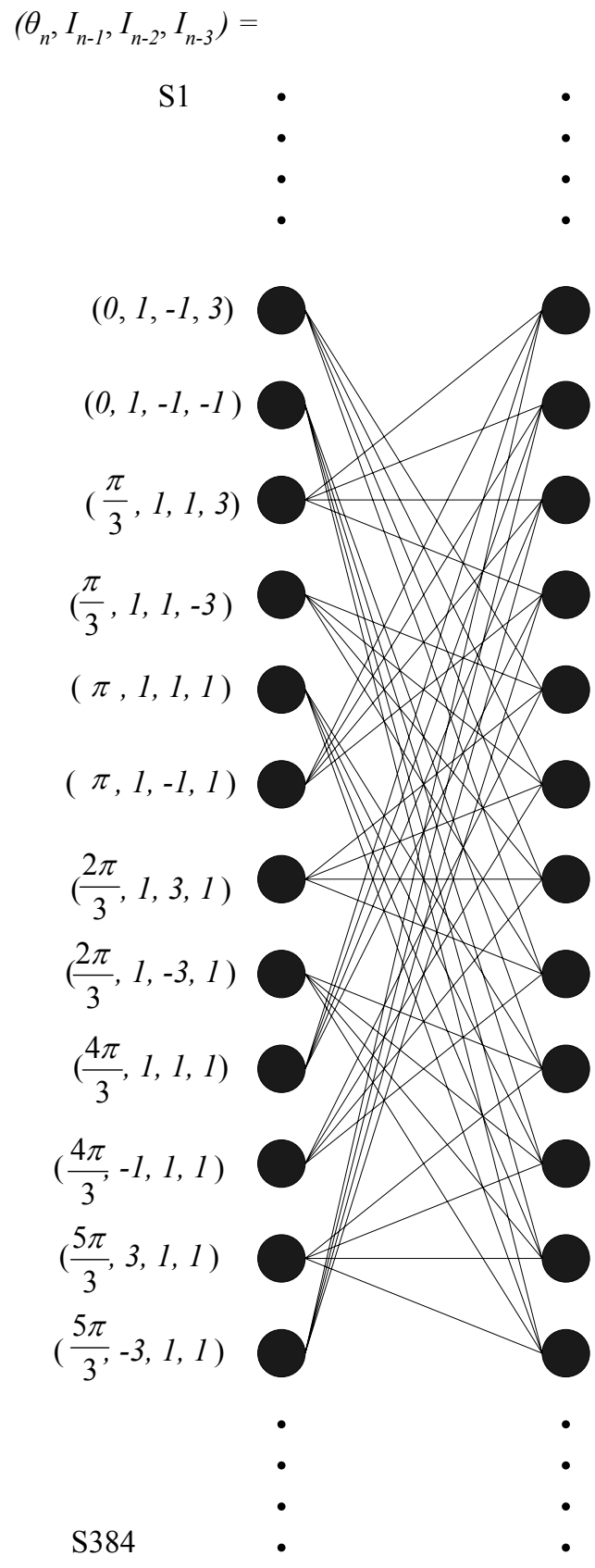

Figure 3.4 Partial representation of the H-CPM trellis.

directly linked to four other states, corresponding to the four possible state transitions or data symbols (± 1 and ± 3). The solid dots represent the different H-CPM states. Figure 3.5 shows an example of how the VA decodes the transmitted symbol sequence for H-CPM. Assume a sequence of 1's is transmitted. We will use $S1$ as an example for illustrating the process. At $t = T$, given a signal $s(t)$ is received, we want to find out what the conditional probability that the $S1$ signal is transmitted. We calculate the branch metrics between $s(t)$ and four possible ancestor states $S66$, $S195$, $S196$ and $S321$. Then the path metrics are calculated by adding these branch metrics to the accumulated path metrics of $S5$, $S11$, $S15$ and $S2$ calculated at the previous symbol time for the previous state. Once the four path metrics are calculated, only the path with the maximum path metric value is kept and stored. This process is known as the add-compare-select (ACS) [63]. The selected and stored path is called the surviving path.

For H-CPM, this process is repeated for all 384 states and 384 survivor paths are kept. As mentioned in section 3.2.3, the surviving paths are saved only over a path history of N_{win} symbol times. Then the VA selects the path with the maximum path metric as the winner surviving path and returns an estimate for the oldest symbol in that path. The process is repeated until all transmitted symbols are decoded.

3.2.4 Simulation Results

The H-CPM encoded symbols are generated randomly and transmitted, as described in Chapter 2, through an AWGN channel. They are then decoded using the above VA implementation. The results are compared to the actual transmitted symbols to estimate the bit error rate (BER) performance as a function of SNR. The SNR is calculated as E_b/N_o, where E_b is the energy per bit and N_o is the noise power spectral density. This definition will be used in the rest of the thesis.

Section 3.1.3 described how it is important to choose the correct memory depth of N_{win} symbols in the VA to minimize performance loss and decoding delay. Normally, N_{win} is chosen to be four or five times the frequency pulse length of L symbols [16]. A wide range of values of N_{win} has been used in the present simulations in order to determine an appropriate value and the results are shown in Figure 3.6.

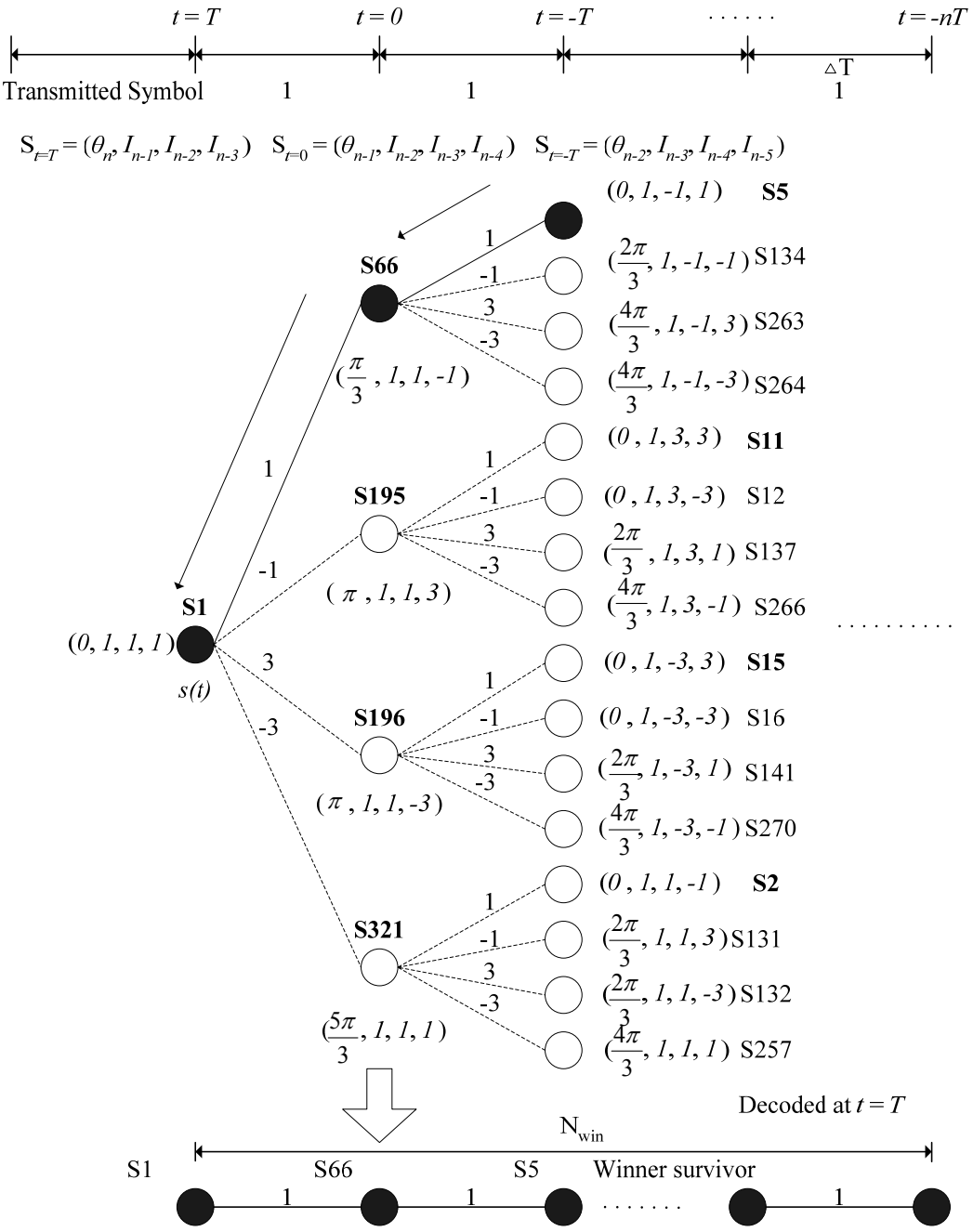

Figure 3.5 Viterbi decoding example for H-CPM. The symbol sequence is represented by the state sequence *S*1→*S*66→*S*5 … up to time *t* = *T*. At *t* = *T*, the winner survivor gives the decoded symbols.

As seen in Figure 3.6, when N_{win} is chosen to be close to the frequency pulse length of L = 4, errors are introduced at high SNR as seen for N_{win} = 3 and 5. This is to be expected. As already stated, N_{win} is usually around 4-5 L [16]. The better BER performance obtained when N_{win} = 20 is consistent with this. Moreover, if we further

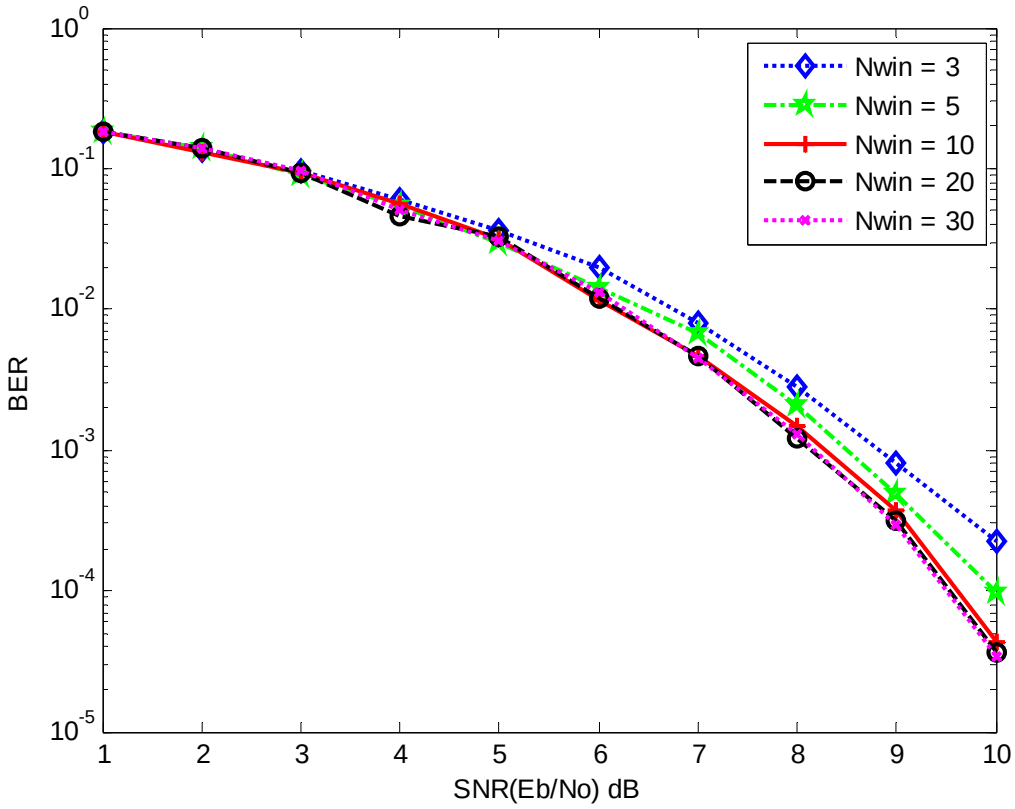

Figure 3.6 BER performance for 384 states, $S = (\theta_n, I_{n-1}, I_{n-2}, I_{n-3})$, $L = 4$ and $Nwin = 3, 5, 10, 20$ and 30.

increase the N_{win} size, little further performance gain is observed, even at $N_{win} = 30$. Furthermore, if $N_{win} = 2.5L = 10$ is used, the performance degradation is very small compared with $N_{win} = 20$, while a significant reduction of memory usage is achieved. Hence, in this thesis, $N_{win} = 2.5L = 10$ is chosen as the decision depth for VA decoding of the H-CPM signal.

Figure 3.7 shows the H-CPM receiver BER performance comparison between the simulated 384 state version and Tyco's 12-state realization for an AWGN channel [1]. Note that the simulated 384-state simulation assumes perfect channel information. Tyco's 12-state realization incorporates some format channel estimation to track the channel information. No detailed implementation information is available for Tyco's 12-state realization. As shown in Figure 3.7, the simulated 384-state case has a similar shape to Tyco's 12-state version. At low SNR, the two receivers have almost identical BER performance, while at high SNR, the simulated 384-state case outperforms Tyco's 12-state realization. This is expected since the full trellis of H-CPM has 384 states.

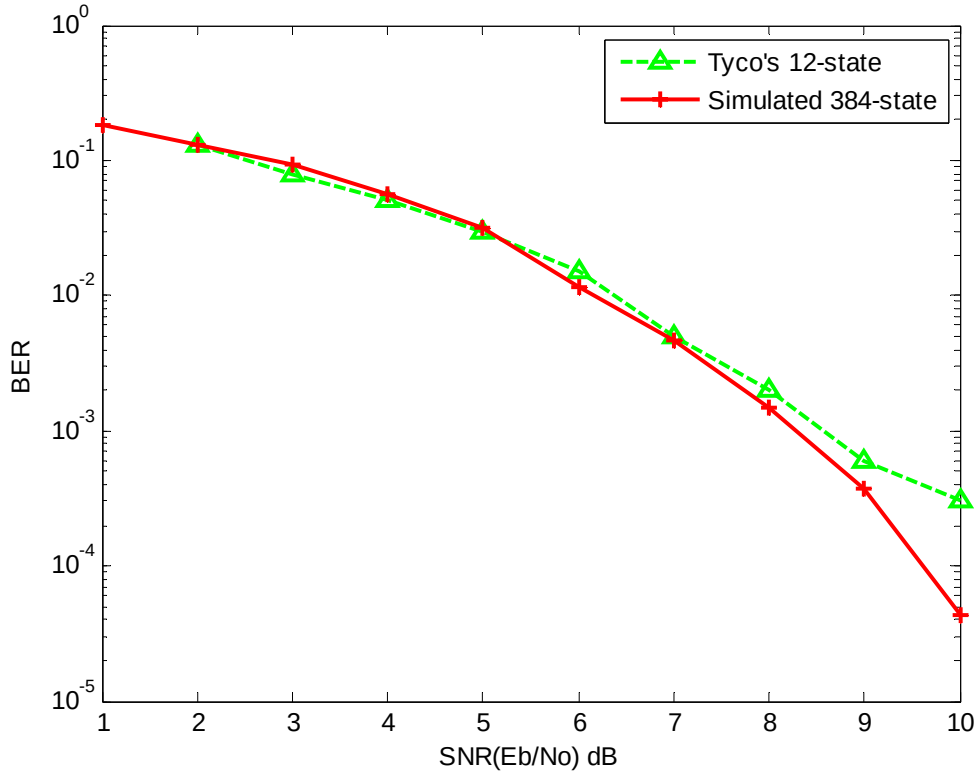

Figure 3.7 BER performance of the simulated 384-state simulation, $S = (\theta_n, I_{n-1}, I_{n-2}, I_{n-3})$, $N_{win} = 10$ and Tyco's 12-state realization with channel estimation for an AWGN channel [1].

3.3 Receiver Complexity Reduction

A problem with the above MLSE detector is complexity. The VA requires a search through all trellis states that are present at each symbol time. The number of distinct state transitions or symbols is actually fairly small compared to the number of states. However, the complexity of the algorithm increases exponentially with the number of trellis states or equivalently with the number of symbols L over which the phase response $q(t)$ extends. For example, consider the 384-state decoding of H-CPM. There are 4 possible transmitted symbols, so that at each symbol time T the algorithm must calculate 4*384 branch and path metrics and select 384 survivors. Coupled with the memory needed to store previous states, surviving paths and previous symbols, it is easy to see that the resulting receiver requires significant resources and computing power.

As mentioned in Chapter 1, there are several different approaches to reducing receiver complexity. One way is through reduced-search schemes that only search the part of the trellis where the transmitted sequence is likely to be [9]. The two main

categories of reduced-search schemes are the breadth-first decoders whose search is forward and unidirectional, and depth first decoders or backtracking decoders that can backtrack and are typified by sequential decoders [9]. The *M*-algorithm is one of the best known breadth-first decoders. It keeps only the *M* paths with the best cumulative path metrics. Another well known breadth-first decoding algorithm is the *T*-algorithm [64]. While the *M*-algorithm keeps a constant number of paths, the *T*-algorithm keeps a variable number of paths which depends on a threshold level and the best metric path. Comparing the average number of paths that the *T*-algorithm keeps with that of the *M*-algorithm, it is seen that at lower SNR, the *T*-algorithm needs a larger number of survivors. However, at moderate or higher SNR, the *T*-algorithm needs to store fewer survivors. One other breadth-first decoder that has received attention in the literature is state-space partitioning (SSP) [65]. SSP was introduced by Larsson for partial response CPM. It divides the trellis states into *C* classes [65]. Then for each state class, only one path, namely the one that is closest to the received signal, is selected and retained. By reducing the parameter *C*, a reduced complexity receiver is obtained, and thus C controls the overall computational effort. SSP can be implemented with a decision feedback scheme developed in [66] called reduced state sequence detection (RSSD) [65]. The drawback is that it exhibits error propagation due to the decision feedback. Finally we note that the size of the MF bank does not change with any of these reduced-search algorithms [67].

Two other well-known complexity-reducing techniques are the use of pulse amplitude modulation (PAM) signal representations [7, 68] and the use of orthogonal basis function models[69]. The PAM approach is also known as the Laurent expansion approach and was first developed by Mengali et al [68]. Using this technique, a CPM signal is decomposed into a linear combination of PAM components [67, 70]. Then at the receiver, a small number of PAM components form pseudo-symbols and the resulting pulses are used to approximate the actual signals so as to obtain reduced complexity [67]. As the number of pulses is reduced, the size of the MF bank and the number of trellis states are simultaneously reduced by the PAM model [67]. Orthogonal basis function techniques on the other hand project CPM signals onto a set of orthonormal basis functions that entirely span the signal space to replace the MF bank [69]. By using only a small subset of these projections to decode the signal, complexity is reduced. This technique only reduces the size of the MF bank, but not the number of trellis states [28, 69].

More easily implemented techniques which reduce the underlying trellis complexity and hence the receiver complexity are the so-called reduced-state schemes. Here the actual trellis structure is simplified by exploiting in part the redundancy in the trellis. There are several such schemes available. The frequency pulse truncation technique was first proposed by Svensson, Sundberg and Aulin [59]. There the frequency pulse used in defining the phase response *q(t)* is truncated [3]. As the amplitudes of the frequency pulse tails are small, the resulting phase response can be truncated, thereby simultaneously reducing both the number of trellis states and the number of matched filters, with little performance degradation. As this truncation actually reduces the correlative-state vector, it is a form of correlative state reduction [28]. Another complexity-reducing technique, which is normally used along with other complexity-reducing techniques, is called the tilted phase approach [7, 28]. It is based on the decomposition model of [15]. It transforms the periodically time-varying trellis usually encountered in CPM into a time-invariant form that usually has only half the number of phase states of the original trellis. It affects only the number of phase states and not the number of correlative states.

Almost all these complexity-reducing techniques involve tradeoffs between performance and implementation complexity. Table 3.1 summarises the properties of the various techniques in terms of the type of complexity reduction [28].

Technique	**Phase State Reduction**	**Correlative State Reduction**	**MF Reduction**
Tilted Phase	✓		
M-algorithm		✓	
T-algorithm		✓	
Frequency Pulse Truncation		✓	✓
SSP	✓	✓	
PAM		✓	✓
Basis Functions			✓

Table 3.1 Comparison of the properties of the complexity-reducing techniques [28].

As seen in Table 3.1, there is no single technique that leads simultaneously to phase state reduction, correlative state reduction and MF reduction, but a combination of the techniques can achieve this. In the present work, the tilted phase approach combined with frequency pulse truncation will be applied to obtain a low complexity H-CPM receiver. This combination reduces both the number of trellis states and the size of the MF bank. Furthermore, the resulting scheme will be seen to be robust against error propagation and simple to implement. In particular for the H-CPM signal format, state reduction is achieved via a three step approach. The tilted phase approach [15] is first used to reduce the number of states to 192. This is followed by frequency pulse truncation which further reduces the number of states to 48 by reducing the number of correlative states. Finally, a further four-fold reduction is achieved by applying a second selective frequency pulse truncation process to obtain the final 12 state receiver.

3.3.1 Tilted Phase

Recall that the phase state of H-CPM can have one of the following 6 values

$$\theta_n \in \left\{0, \frac{\pi}{3}, \frac{2\pi}{3}, \pi, \frac{4\pi}{3}, \frac{5\pi}{3}\right\}. \tag{3.16}$$

One can arrange the phase states in a phase diagram as shown in Figure 3.8.

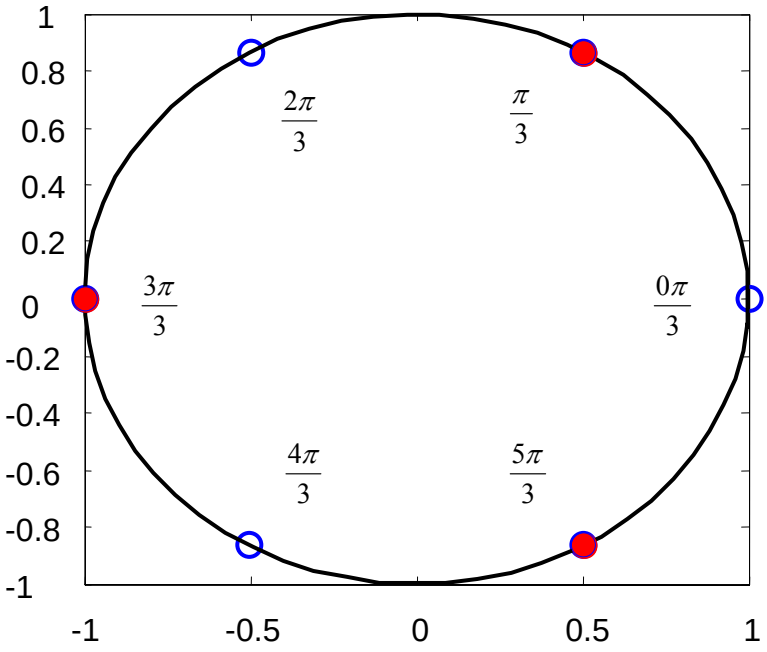

Figure 3.8 Phase states of H-CPM.

The phase states can be represented by two subsets corresponding to even and odd symbol times respectively. The hollow and solid symbols in the figure represent the two subsets.

The modulation index h of CPM is denoted m/p, where m and p are relatively prime integers. For the H-CPM scheme, $m = 1$ and $p = 3$. In the tilted phase state representation described by Rimoldi [15], the amount of computation needed is reduced by using the two subsets of states from the trellis at even and odd symbol times [71]. The actual number of trellis states is still 384, but at each symbol time, only 192 states are actually used in the VA, and hence the receiver complexity may be reduced by 50%. To understand how this works, one must refer to the H-CPM phase state. Recall the phase state $\theta_n = R_{2\pi}\left[h\pi \sum_{k=-\infty}^{n-L} I_k \right]$, $nT \le t \le (n+1)T$. We define new data symbol values $U_k = (I_k + M\text{-}1) / 2$, where $M = 4$ (for H-CPM) is the alphabet size as defined in Chapter 2. These replace the original data symbol I_k, which allow us to decompose θ_n into a data independent phase tilt υ_n and a data dependent phase state ϑ_n, given in [15, 28] as

$$\theta_n = R_{2\pi}\left[\pi h \sum_{k=0}^{n-L} I_k \right] = \upsilon_n + \underbrace{2\pi h \sum_{k=0}^{n-L} U_k}_{\vartheta_n} \tag{3.17}$$

where, by convention, $I_{-\infty} = \cdots = I_L = I_{-3} = I_{-2} = I_{-1} = 0$. Note that υ_n is obtained through the recursion

$$\upsilon_n = \upsilon_{n-1} - \pi h(M-1), \tag{3.18}$$

which causes the phase offset and the resulting phase state in each symbol period to alternate between the so-called even phase state set and odd phase state set. For example, at $t = 0$, which is an even symbol time, $\upsilon_{n-1} = 0$, which for H-CPM gives $\upsilon_n = -\pi$. At $t = T$, which is an odd symbol time, υ_n can be recursively obtained as -2π, which (modulo 2π) gives 0 phase offset. Therefore for H-CPM, at odd symbol times, υ_n provides no phase offset, while at even symbol times, it gives a $-\pi$ phase offset.

Now we consider the data dependent part for the phase state θ_n. Taking a modulo 2π representation of θ_n gives [15]

$$R_{2\pi}\left[2\pi h\sum_{k=0}^{n-L}U_k\right]=R_{2\pi}\left[2\pi\left(\frac{m}{p}\right)\sum_{k=0}^{n-L}U_k\right]=R_{2\pi}\left[2\pi\left(\frac{m}{p}\right)R_p\left[\sum_{k=0}^{n-L}U_k\right]\right] \quad (3.19)$$

where $R_p[\cdot]$ is the modulo p operator. Clearly θ_n takes only p data-dependent phase values. This is only half as many as the actual number of phase states. For H-CPM, $U_k \in \{0,1,\cdots,3\}$ and θ_n takes the possible values

$$\theta_n \in \left\{0,\frac{2\pi}{3},\frac{4\pi}{3}\right\}. \quad (3.20)$$

Taking into account the phase offset at even and odd symbol times as determined by the data independent phase tilt υ_k, the set of 3 possible values of the phase state θ_n at odd symbol times is given by

$$\theta_n \in \left\{0,\frac{2\pi}{3},\frac{4\pi}{3}\right\}. \quad (3.21)$$

At even symbol times, the set of 3 possible values of the phase state θ_n is given by

$$\theta_n \in \left\{\frac{\pi}{3},\pi,\frac{5\pi}{3}\right\}. \quad (3.22)$$

Figure 3.9 shows the H-CPM phase trellis showing how the two sets of phase states are used at alternate even and odd symbol times.

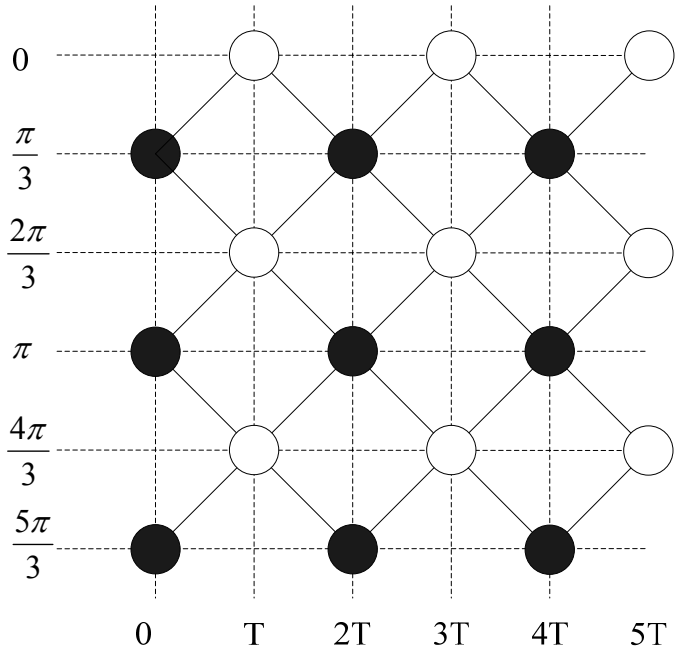

Figure 3.9 Phase trellis for H-CPM.

It turns out that for all CPM schemes, at any given symbol time, the value of θ_n can take only p possible values, even though the total number of possible θ_n values may be either p if m is even, or $2p$ if m is odd [71]. In the case where m is odd, the set of $2p$ possible θ_n values is split in half, with each set used only at either even symbol times or odd symbol times, respectively [71]. In particular, at odd symbol times, the phase state takes the possible values

$$\theta_n \in \left\{0, \frac{2\pi}{p}, \frac{4\pi}{p}, \cdots, \frac{(p-1)2\pi}{p}\right\} \tag{3.23}$$

while at even symbol times, it has the values

$$\theta_n \in \left\{\frac{\pi}{p}, \frac{3\pi}{p}, \frac{5\pi}{p}, \cdots, \frac{(2p-1)\pi}{p}\right\}. \tag{3.24}$$

The proof of this is shown in [71]. This alternating property of the phase state set results in a cyclically time variant structure of the trellis with a period of 2 symbol times for CPM schemes with odd m [71]. This time variant trellis can be represented

as an equivalent time invariant trellis called the tilted trellis which can be used with the VA [15]. The tilted trellis is arrived at by applying the phase offset of (3.18) to "correct" the phase state values. With this approach, the effective number of states used to decode H-CPM is halved in each symbol interval without any performance loss. Note that this in fact changes the time-variant trellis into a time-invariant one.

Figure 3.10 shows the comparative error performance of the 384-state and 192-state receivers using the tilted trellis for an AWGN channel. It can be seen that the error performances of the two designs are virtually identical, even though the complexity of the 192-state receiver is half that of the 384-state receiver. This is as expected and confirms the usefulness of the tilted trellis design.

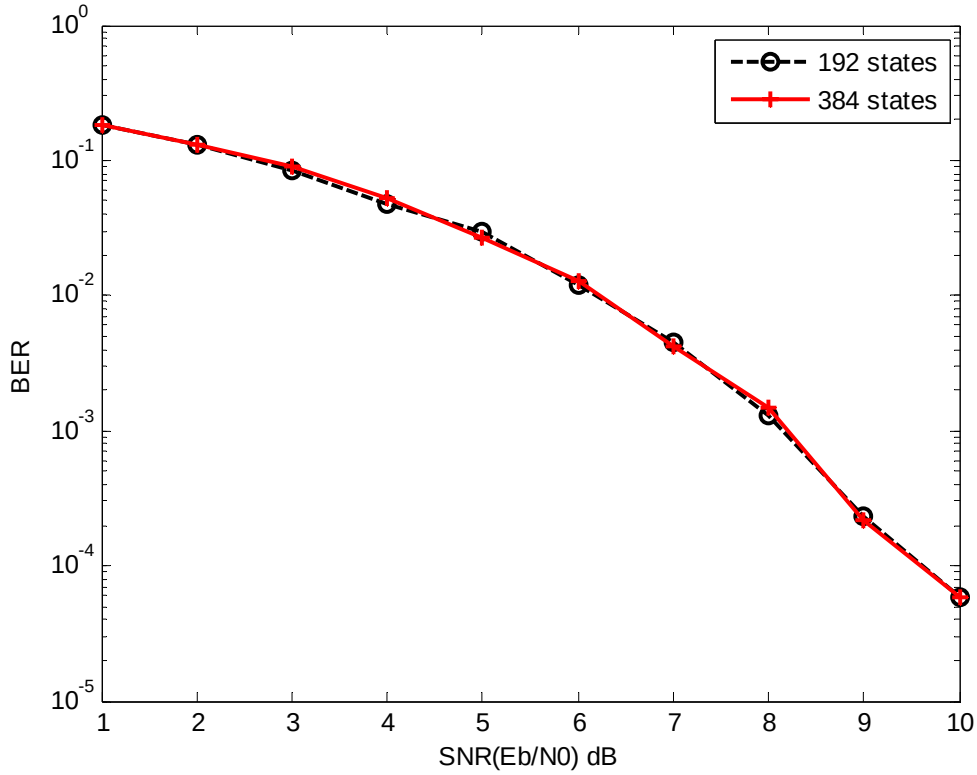

Figure 3.10 H-CPM receiver BER performance for 384 states, $S = (\theta_n, I_{n-1}, I_{n-2}, I_{n-3})$, $Nwin = 10$ and for 192 states with tilted phase, $S = (\theta_n, I_{n-1}, I_{n-2}, I_{n-3})$, and $Nwin = 10$.

3.3.2 Frequency Pulse Truncation

Figure 3.11 shows how frequency pulse truncation is applied to the H-CPM signal. Figure 3.11a, shows the effect of the phase response $q(t)$ on the transmitted signal for the H-CPM ($L = 4$) encoding, starting from $t = 0$ (current transmission) and

tracing back to the previous symbols. From $t = 0$ to $t = -4T$, the value of $q(t)$ increases from 0 to 0.5. This time span corresponds to the correlative state of the transmitted signal, as described by (3.2), and the correlative state is defined by the three symbols I_{n-1}, I_{n-2} and I_{n-3} immediately preceding the current symbol. This is represented in Figure 3.11a as the white regions in the graph. On the other end, for $t \leq -4T$, the value of $q(t)$ is constant at 0.5, and the sum of all the symbols transmitted in and before this time frame gives the phase state θ_n of the transmitted signal. This is shown in Figure 3.11a as the shaded region.

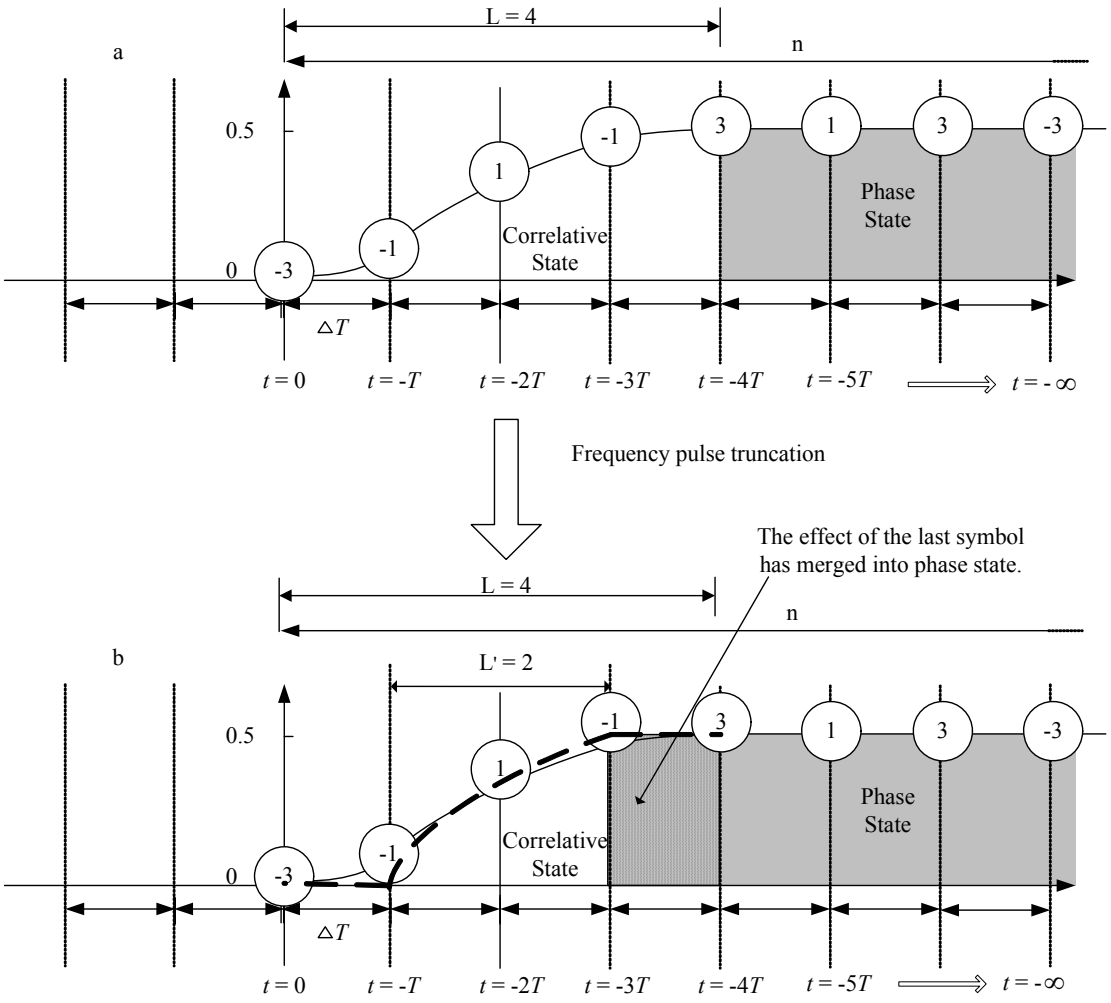

Figure 3.11 The change in the correlative state and phase state upon application of frequency pulse truncation (figure adapted from [61]). Note that this is equivalent to performing a phase truncation as the phase pulse is simply the integral of the frequency pulse.

The implementation of frequency pulse truncation relies on the shape of $q(t)$. In particular, it can be seen from Figure 3.11a that at $t = -3T$, the value of $q(t)$ is very close to 0.5. Therefore, one can assume that the value of $q(t)$ at $t = -3T$ is approximately 0.5, in which case the effect of the last symbol I_{n-3} can be merged into θ_n. This reduces the pulse time varying response length L by 1, which according to (2.10), reduces the number of trellis states from 192 to 48. Note that this makes no difference to the allowable values of the phase state θ_n.

A further reduction in the number of states can be achieved by considering the value of $q(t)$ at $t = -T$. It can be seen that at $t = -T$, the value of $q(t)$ is very small. This leads us to approximate it as $q(T) \approx 0$, which essentially ignores the effect of the symbol at $t = -T$ on the correlative state. The resulting phase response duration is further reduced by 1, giving $L' = 2$, which means that the number of trellis states at each symbol time is reduced to 12. The new states corresponding to a reduced trellis are represented by $S = (\theta_n, I_{n-2})$, based on which the VA then decodes the signal. This approach is also called correlative state reduction, as the last element of the correlative state vector has been merged into the phase state vector [67] and the first element of the correlative state vector has been ignored. The final appearance of the phase response and the corresponding correlative and phase state are shown in Figure 3.11b as the dashed trajectory.

Figure 3.12 shows the reduced 12 state H-CPM trellis with the two numbers representing the phase state θ_n and previous symbol I_{n-2} which uniquely identify each state. It also demonstrates the H-CPM alternating phase states feature as described in Section 3.2.1. Figure 3.13 shows the error performance of the reduced complexity receiver designed using frequency pulse truncation in an AWGN channel. It can be seen from Figure 3.13 that there is a slight degradation in the error performance as the number of trellis states is reduced from 192 to 48. This is expected as, unlike the tilted phase, an approximation is made in the frequency pulse truncation process, and thus, a small extra error is introduced into the decoding process. Similarly, the state reduction from 48 states to 12 states also leads to some further error performance degradation, although to a lesser extent. Furthermore, limitations caused by a finite simulation length may also contribute to some of the performance variations seen. In particular, at high SNR the BER becomes less accurate due to the small number of errors that can be generated in a reasonable timeframe. Note that the performance loss becomes noticeable only at high SNR. At low SNR, the AWGN dominates, and the inaccurate

phase effect introduced by the frequency truncation is negligible. With the same amount of AWGN, there is hardly any performance difference between different receivers. At high SNR, the AWGN is very small, and the inaccurate phase effect introduced by frequency pulse truncation dominates performance. As the result of the different degrees of approximation to the phase, performance degradation starts to appear. According to the figures, this degradation is still very small. This leads to the conclusion that the significant effects of the correlative state are retained.

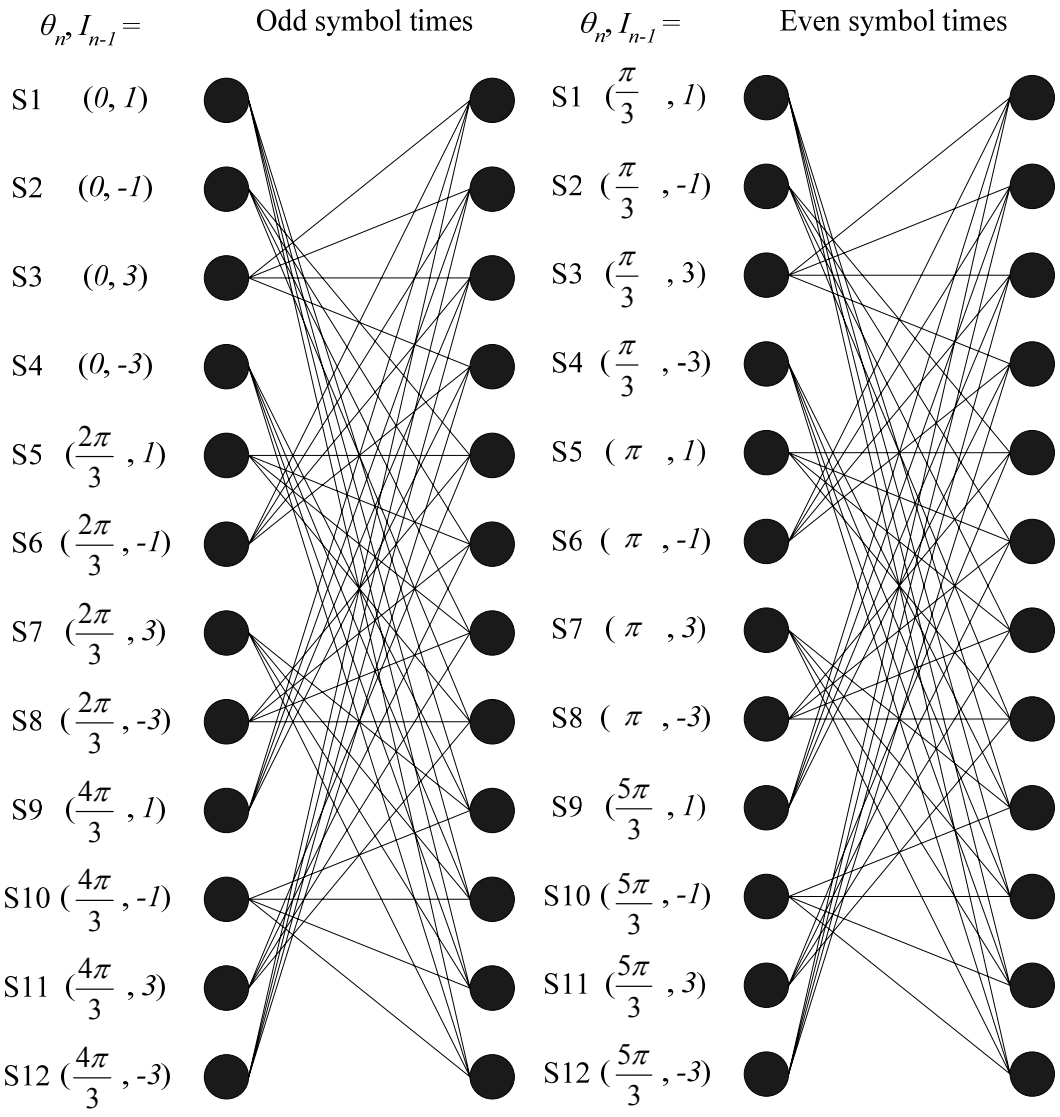

Figure 3.12 Trellis example of the reduced state H-CPM receiver.

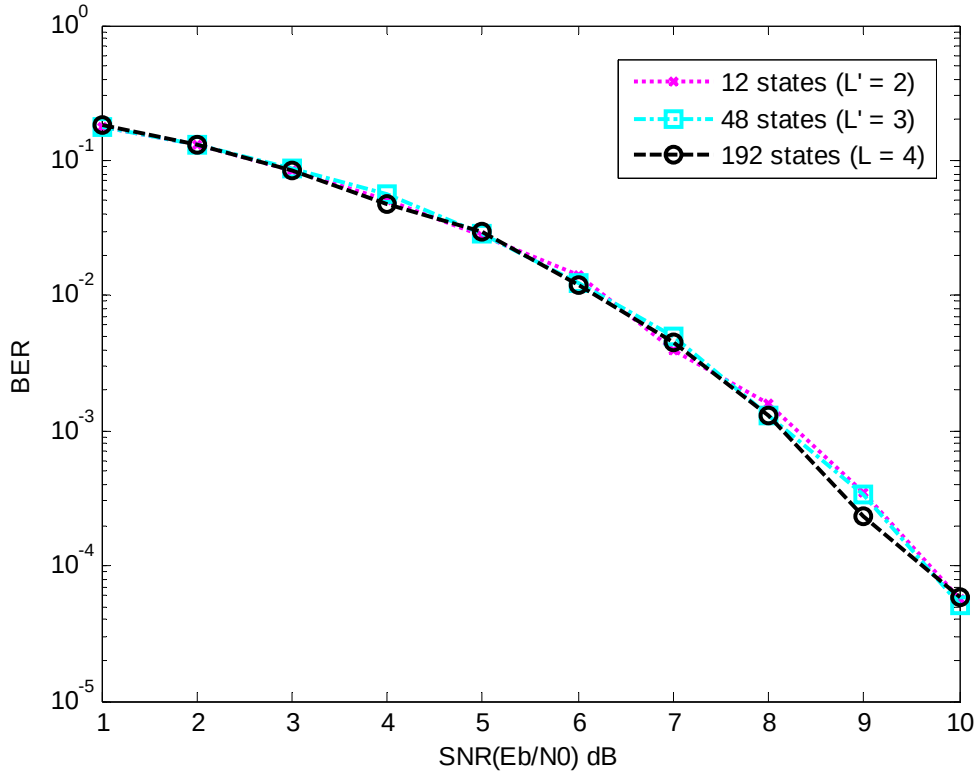

Figure 3.13 BER performance of the sub-optimum (*L* = 4, *L'* = 3 and *L'* =2) H-CPM receivers. *Nwin* = 10.

3.3.3 Discussion

From Figure 3.10 and Figure 3.13 it can be seen that by using the tilted phase and frequency truncation techniques, we can reduce the complexity of the receiver with almost no degradation in the resulting error performance. This is further emphasized in Table 3.2, which shows the performance versus complexity trade-off for the trellis state reduction processes. It can be seen that as the number of trellis states is reduced, the computational load, which involves the computation of all possible branch metrics for each branch in the trellis, is reduced dramatically, with the initial state reduction from 384 to 192 halving the computational load, and the reduction to 12 states led to a reduction of computation time by over 95%. This is accompanied by a BER degradation of 0.07 dB at 2% and 5% BER. This is a very small change, and for all practical purposes may be neglected. Table 3.3 shows the corresponding error performance of the receiver for an AWGN channel. The remainder of the thesis will focus on the 12-state receiver.

Number of states	Number of branches/state	Total number of branches	Computational reduction	Loss (dB) at $BER = 10^{-4}$
384	4	1536	-	-
192	4	768	50%	-
48	4	192	87.5%	0.3dB
12	4	48	96.875%	0.3dB

Table 3.2 The performance/complexity trade-off for receiver trellis state reduction.

	384	192	48	12
5% BER	4.10 dB	3.90 dB	4.00 dB	4.17 dB
2% BER	5.40 dB	5.45 dB	5.45 dB	5.47 dB
0.01% BER	9.38 dB	9.44 dB	9.64 dB	9.68 dB

Table 3.3 BER performance of H-CPM receiver for an AWGN channel. The performance amongst the four are essentially the same within statistical variation.

3.4 Summary

In this chapter, an optimum MLSE H-CPM receiver structure has been specified. Tilted phase and frequency pulse truncation techniques have then been applied to reduce receiver complexity, resulting in a sub-optimum low complexity structure. Simulation results have shown that a properly designed 12-state low-complexity MLSE H-CPM receiver suffers about 0.07 dB performance degradation at 2% and 5% BER under AWGN conditions with a 96.875% increase in computation efficiency. In the next chapter, a Rayleigh fading channel will be considered, and receiver performance with per-survivor processing (PSP) based channel estimation will be investigated.

Chapter 4

CHANNEL ESTIMATION

In Chapter 3, the optimal MLSE H-CPM receiver was described. Using tilted phase and frequency truncation, it was shown that a receiver with low complexity can be designed, giving a computation efficiency increase of over 95% with almost no degradation in performance in AWGN channel. It is obvious that a 12 state MLSE receiver can form the basis of the receiver design for the P25 base station system. However, so far only AWGN has been considered. As we know, apart from AWGN, multipath fading also has important effects on the received signal that need to be considered in the demodulation. This will be the focus of this chapter.

4.1 Branch Metrics and Channel Gain

The low complexity receiver designed in Chapter 3 needs the channel gain estimated prior to actual demodulation in fading channels. Under the effects of fading, the received signal is given by

$$r(nT) = g(nT)s(nT) + e(nT), \tag{4.1}$$

where $g(nT)$ is the fading process, also known as the channel gain and $e(nT)$ is the AWGN component. Recall from (3.7) that the Euclidean distance is given by the magnitude of the error. Incorporating the channel gain into (3.7), the distance becomes

$$d(nT) = \left|e(nT)\right|^2 = \left|r(nT) - g(nT)s(nT)\right|^2, \tag{4.2}$$

which can be expanded as

$$d(nT) = \left|r(nT)\right|^2 - 2\,Re(r(nT)g^*(nT)s^*(nT)) + \left|g(nT)s(nT)\right|^2. \qquad (4.3)$$

Again using the same argument as Chapter 3, we get the branch metric

$$B(nT) = Re(r(nT)g^*(nT)s^*(nT)). \qquad (4.4)$$

Again, practically, we can separate the real and imaginary components of *r(t)*, *g(t)* and *s(t)*, and represent these complex functions as

$$r(nT) = p + jq, \qquad (4.5)$$

$$s(nT) = u + jv, \qquad (4.6)$$

$$g(nT) = m + jn, \qquad (4.7)$$

from which we get

$$B(nT) = Re((p + jq) * (u - jv) * (m - jn)), \qquad (4.8)$$

$$B(nT) = Re((mpu + mquj - mpvj + mqv - jnpu + nqu - npv - jnqv)). \qquad (4.9)$$

Hence

$$B(nT) = mpu + mqv + nqu - npv \qquad (4.10)$$

is new branch metric that needs to be evaluated for fading channels. Note that when $g(nT) = 1 + 0j$ (corresponding to a static channel), then the branch metric becomes $B(nT) = pu + qv$ which is the result obtained in Chapter 3 as (3.15). Therefore, it can be seen that the branch metric includes channel gain can be used in MLSE for both AWGN and fading channels. From this, an estimation of the channel gain $g(nT) = m + nj$ representing the fading effect of the channel must be obtained.

4.2 Conventional Channel Estimation

Conventionally, MLSE receivers estimate the channel gain by using an inter-module technique in which the information is shared between the data-aided estimators and the VA module. Figure 4.1 shows the block diagram of a conventional MLSE receiver with built-in channel estimation. In this approach, one global channel estimator for all paths in the VA is used [72]. It feeds back tentative

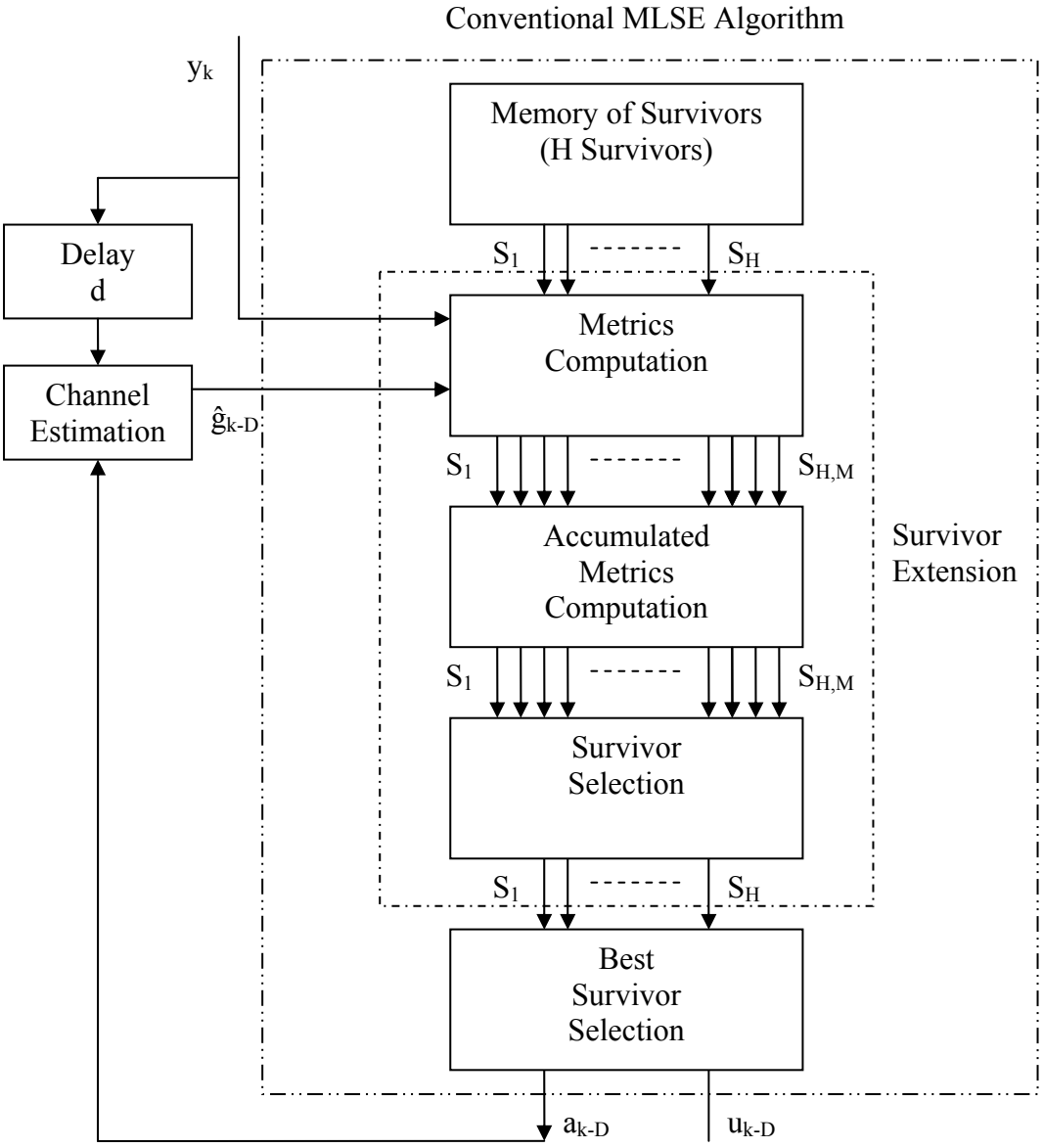

Figure 4.1 Conventional MLSE receiver (adapted from [29]).

decisions made by the VA and updates the channel estimate adaptively. The problem with conventional MLSE is that it introduces a delay in channel estimation as the channel estimate is only calculated after the VA. In a rapid changing channel, the delays in this approach may lead to inaccurate estimations. Moreover, if poor tentative decisions are used in channel estimation, the resultant degraded estimator will cause further performance degradation in future detection. Then worse tentative decisions will be produced and so on. It becomes a vicious cycle of error propagation. A solution to this problem is to use an alternative algorithm, namely per-survivor processing (PSP) estimation.

4.3 PSP

PSP is a channel estimation technique which is based on the surviving paths in the VA. Figure 4.2 shows the algorithm of a PSP-based MLSE processor. As can be seen in the block diagram, in a PSP approach different channel responses are estimated along the surviving paths that are associated with each state in the trellis of the VA simultaneously. Each surviving path maintains and updates its own channel estimate based on the corresponding hypothesized transmitted data sequence [72, 73], and that gain is only used for that surviving path to calculate branch metrics. The existence of individual gains for surviving paths means that each gain estimated is confined within the surviving path, along with its error. Thus unlike conventional MLSE, if one of the gain for a particular surviving path is corrupted with noise or distortion, then the rest of the surviving paths may not be affected, and as decision making is based on the best surviving path, this error would not propagate through the decoding sequence. Further, as the gain is estimated based on the previous surviving paths, in general, the more reliable the surviving path is, the more reliable the channel estimation associated with it is. This therefore increases the reliability in a self-propagating manner (i.e. the better the surviving path, the better the gain, which in turn leads to a more accurate surviving path). Finally, as the gain for each surviving path is calculated based on previous survivors right at the start of the algorithm without feedback from the tentative decision, the delay between receiving and decoding a symbol is significantly reduced. Hence PSP is suitable for fast time-varying channels with a great reduction in the effects of error propagation.

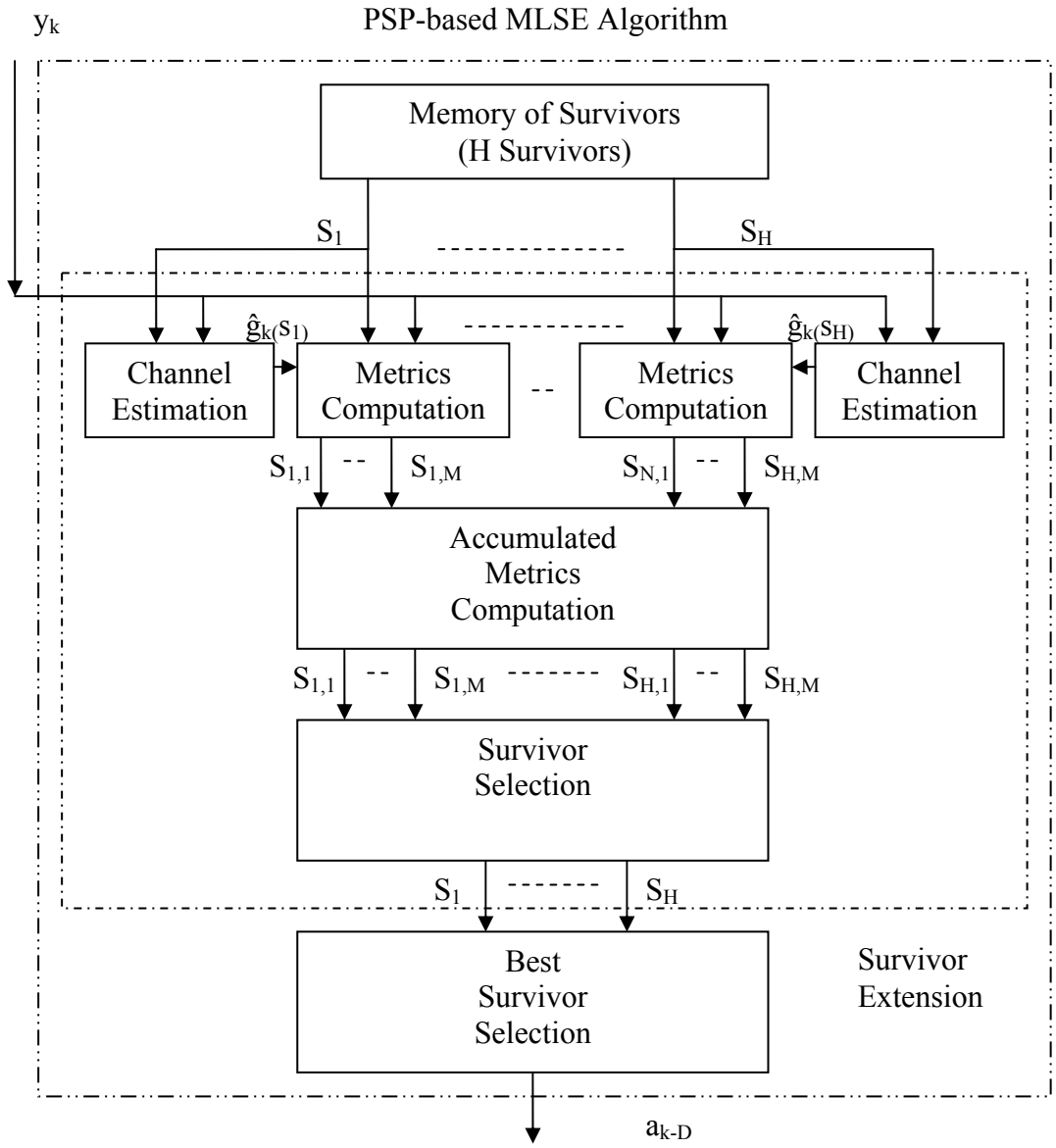

Figure 4.2 PSP-based MLSE block diagram (adapted from [29]).

Typically, the PSP-based MLSE receivers outperform the conventional MLSE receivers, especially under fast fading conditions. Therefore PSP is chosen for the design of MLSE H-CPM receivers. The drawback of the PSP-based MLSE receivers is their large computational complexity as channel estimation is required for each survivor rather than requiring only one global channel estimate.

4.4 Implementation of PSP

The main concern when designing a PSP-based MLSE receiver is the design of the channel estimation algorithm. From the block diagram shown in Figure 4.2 it can be seen that the channel estimation is derived from the previous entries of the surviving path. This is because the previous symbols in the surviving path contain information about the channel. In particular, if we assume that the surviving path is correct, then the decoded symbol and the received symbol from the previous symbol time in that surviving path must be related through the channel gain at that particular point in time. In fact, it can be shown that the correlation function between the received signal $r(t) = p + jq$ and the tentative decoded signal $s(t) = u + jv$, given by

$$corr(r,s) = (pu + qv) + j(qu - pv) \tag{4.11}$$

is a noisy estimate of the channel gain [74]. Hence one can obtain an accurate estimate of the channel gain by reducing the noise component in the correlation function. This can be done by averaging, possibly in a weighted manner, N successive estimations to obtain a more nearly noise free gain estimate [74].

In this thesis, two averaging algorithms are considered. The first is standard averaging where each of the N previous estimations is weighted equally, ie.

$$g(nT) = \frac{1}{N}\left[corr(r,s) + g((n-1)T) + g((n-2)T) + ...g((n-N+1)T)\right] \tag{4.12}$$

This simple averaging is easy to implement, but usually provides less accurate estimates of the gain in a fast changing channel due to the equal importance of current and past channel conditions. In the second approach, a weighted sum is used by assuming a Jakes' Doppler spectrum [74]

$$g(nT) = w_0 corr(r,s) + w_1 g((n-1)T) + w_2 g((n-2)T) + ...w_N g((n-N+1)T) \tag{4.13}$$

where $\boldsymbol{w}^T = [w_0\ w_1\ w_2\ \ldots\ w_n]$ is defined by the Yule-Walker equation [16]

$$\boldsymbol{w} = \boldsymbol{R}_y^{-1} \bullet \boldsymbol{p}. \tag{4.14}$$

Hence $\boldsymbol{R_y}$ is the covariance matrix

$$\mathbf{R}_{\mathbf{y}_{i,j}} = 2\gamma_s J_0\left(2\pi f_{d(\max)} T\left(i-j\right)\right) + \delta\left(\left(i-j\right),0\right). \qquad (4.15)$$

γ_s is the SNR of the channel and J_0 is the zero order Bessel function, where the cross correlation vector $\boldsymbol{p}$ (of length L) is given by

$$\mathbf{p}_i = \sqrt{2\gamma_s J_0\left(2\pi f_{d(\max)} T\left(i+1\right)\right)}. \qquad (4.16)$$

This approach takes into account the speed of fading, and weights the successive estimates accordingly. It is expected that this weighted sum approach will give a more accurate estimate for fast fading channels. To compare the two, each technique is implemented into the MLSE reduced state receiver designed in Chapter 3. They generate channel gain estimates for each surviving path, which are incorporated into the branch metrics as described by (4.8). Performance of the PSP-based MLSE receiver is then simulated for a Rayleigh fading channel with Doppler frequencies of 0Hz, 5Hz, 40Hz, 80Hz and 333Hz. These are typical Doppler frequencies used to test the performance of modern mobile radio wireless systems. The corresponding BER performances are then compared.

4.5 Simulation Results

Figure 4.3 shows the performance of the PSP algorithm considered here using an averaging length of $N = 5$ which is a typical value used. Performance is compared to a receiver with perfect channel information on an AWGN channel. An AWGN channel is used here to highlight the effect of the PSP algorithm itself on the error performance. The performance of the MLSE receiver with channel estimation by

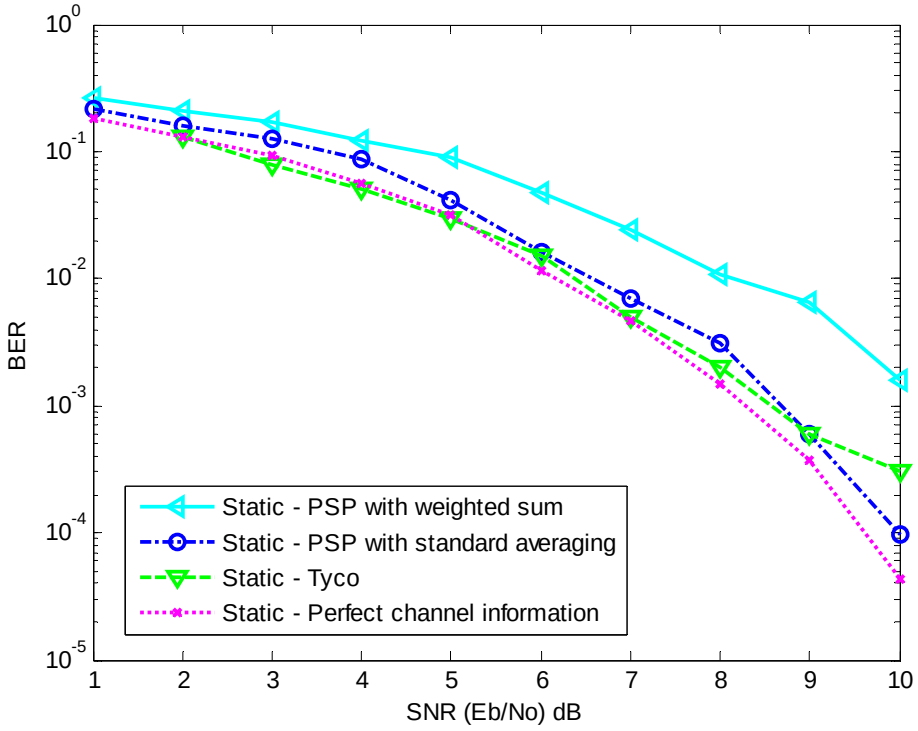

Figure 4.3 The performance of the PSP based MLSE receiver in AWGN compared with the performance of the MLSE receiver with perfect channel information and Tyco's receiver.

Tyco Ltd is also shown on the figure for comparison. Note that pilot symbols are used with channel estimation by Tyco Ltd and no other information on the channel estimator designed is available. It can be seen from the figure that the application of the PSP algorithm does degrade the error performance. This is expected as the extra estimation step involved in calculating the gain will inevitably lead to some error that is especially noticeable when the gain estimation is not actually needed. This is because the additive noise is random and can only be minimized by increasing SNR [8]. The graph shows that the performance degradation for the standard averaging technique is much less than that observed for the weighted sum technique in the displayed SNR range. In particular, while the performance of the averaging PSP algorithm under static conditions is essentially the same as a receiver without PSP, the performance of the weighted sum algorithm is more than 2 dB inferior for BER $< 10^{-2}$. It can also be seen from the figure that the performance of the Tyco system is slightly better than that observed for the averaging PSP. This could be due to the additional channel information provided when the pilot symbols are used.

Figure 4.4 shows the performance of the final PSP algorithm design (using weighted sum averaging) in Rayleigh fading channels at Doppler frequencies of 5 Hz, 40 Hz, 80 Hz, the three typical Doppler frequencies used to test the performance of a modern mobile radio wireless system. Also a Doppler frequency of 333 Hz corresponding to the Doppler spread expected for transmissions from a helicopter, which is commonly used in public safety operations. A more detailed comparison between the different PSP approaches at different conditions are shown in Figure 4.5 and Figure 4.6 for the standard averaging technique and the weighted sum PSP respectively. As a comparison, the performance of the MLSE receiver without PSP under the different Doppler spreads is also shown in each figure. It can be seen from the figures that both techniques offer a performance improvement over standard MLSE with no PSP in fading channels. This confirms the necessity of channel estimation and the usefulness of PSP in fast fading channels. Looking first at Figure 4.5, it can be see that while the improvement observed is quite dramatic (over 10dB improvement) against MLSE without PSP, the actual BER observed over the

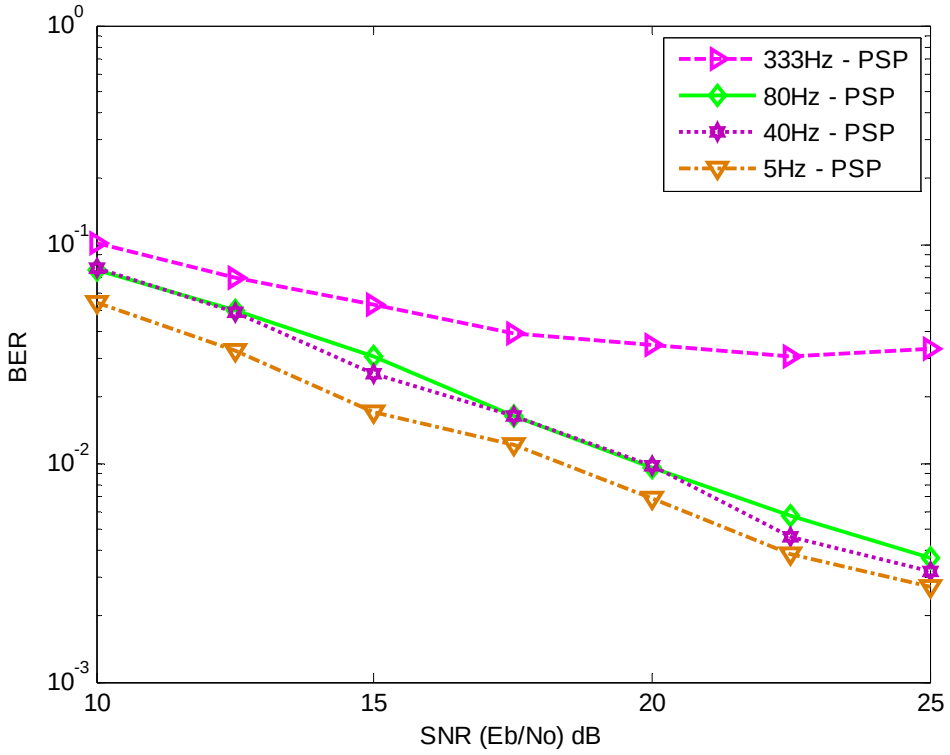

Figure 4.4 BER performance of PSP based MLSE receiver at a Doppler frequency 5Hz, 40Hz, 80 Hz and 330Hz in a Rayleigh fading channel. Symbol time $T = 1/6000$. Weighted sum averaging is used here.

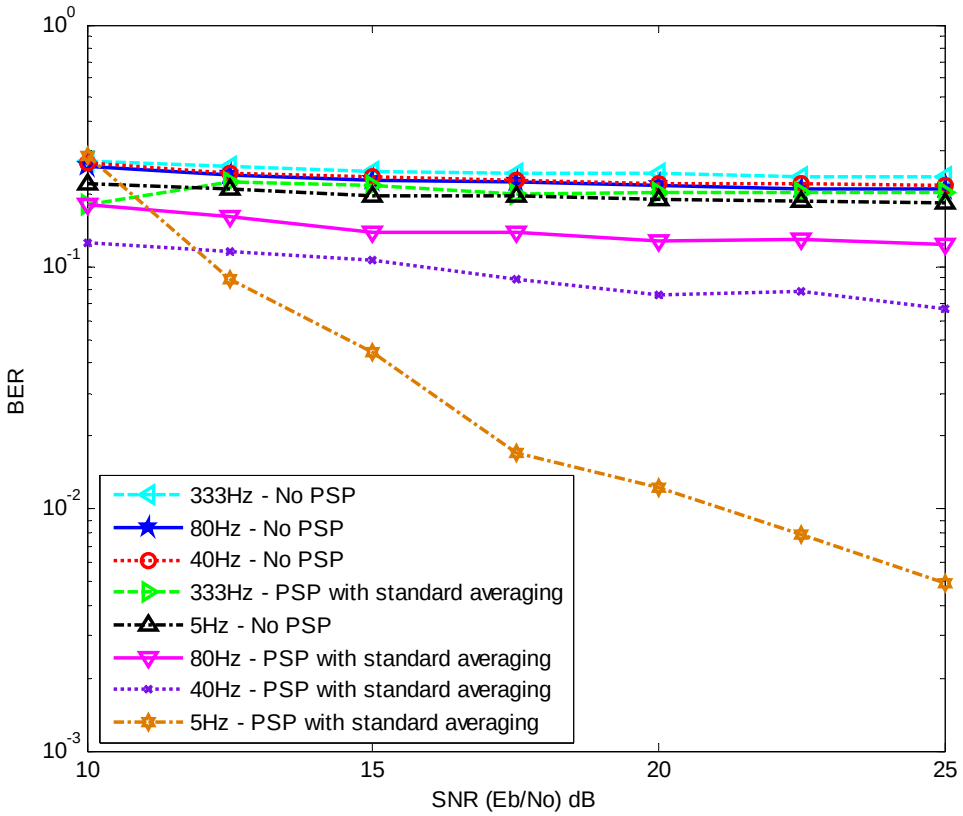

Figure 4.5 BER performance of PSP-based MLSE receiver using standard averaging compared to BER performance of the PSP-based MLSE receiver without PSP in Rayleigh fading channel. Symbol time $T = 1/6000$.

specified SNR range is quite high. In particular, apart from the 5 Hz curve, performance at all other Doppler frequencies are very poor, with BER above 10^{-1} even at high SNR for Doppler frequencies of 80 Hz and 333 Hz. The performance at Doppler frequency of 40 Hz is slightly better, although the BER is still around the 10^{-1} mark even at SNR = 25 dB. At Doppler frequency of 5 Hz, however, the averaging technique seems to be doing quite well, with over an order of magnitude reduction of BER at high SNR.

Figure 4.6 shows the performance of the weighted sum PSP. Compared to the standard averaging, it can be seen that BER performance has improved substantially. While at 5 Hz, the performance between the two is similar, at higher frequencies the weighted sum technique has brought the BER down substantially below 10^{-1} for the SNR range of interest. In fact, the increase in Doppler spread does not seem to have a dramatic impact on the receiver performance. At a BER of 10^{-2}, the performance at 5

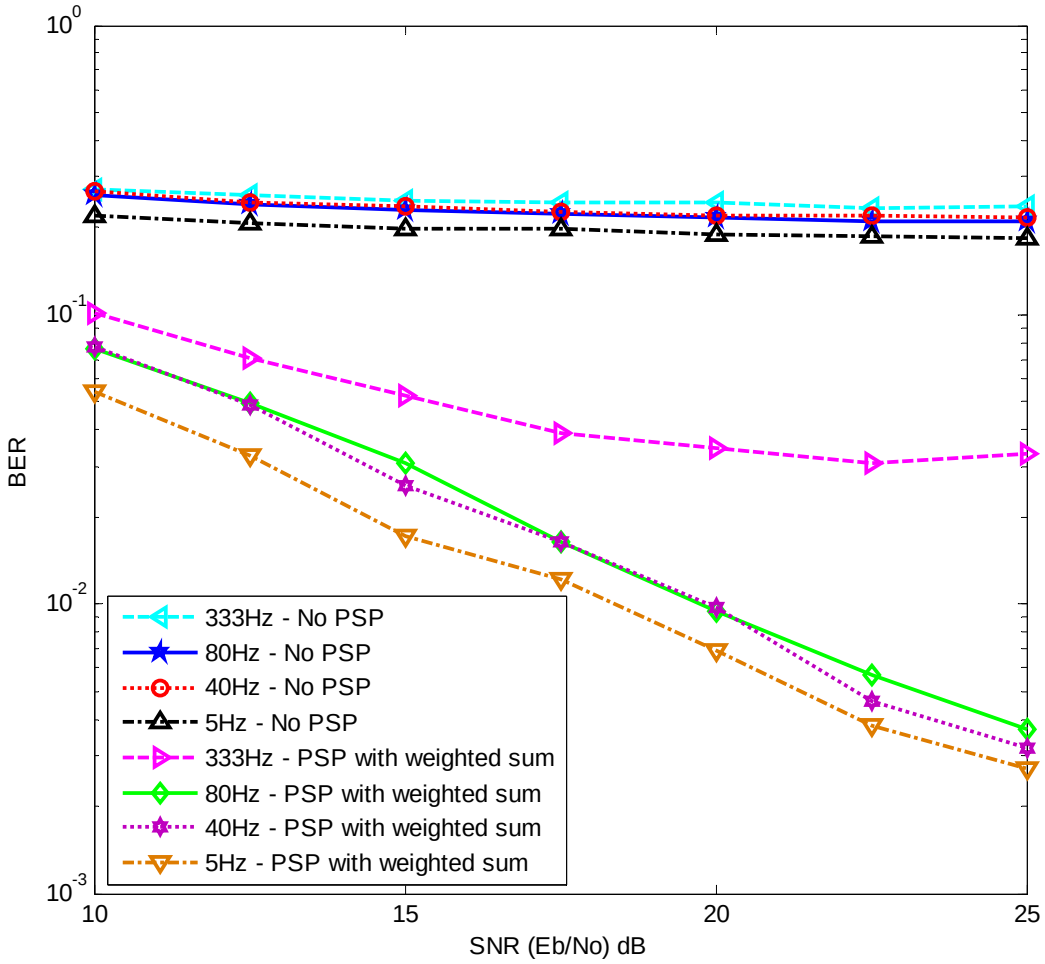

Figure 4.6 BER performance comparison of PSP based MLSE receiver with weighted sum and MLSE receiver without PSP in a Rayleigh fading channel. Symbol time $T = 1/6000$.

Hz is only about 2 dB better than that at 40 Hz, and the performance at 80 Hz is essentially the same as that at 40 Hz. Even at the extremely high Doppler spread of 333 Hz, the degradation compare to 5 Hz is only of the order of 5 dB at a low SNR of 5×10^{-2}. At higher SNR, the BER saturates at ~0.04. From these results, it can be seen that although the averaging technique performs better under static conditions, the weighted sum approach is a better technique under fast fading conditions.

Figure 4.7 compares the PSP results obtained here to those obtained by Tyco Ltd in a Rayleigh fading channel at Doppler frequencies of 5 Hz, 40 Hz and 80 Hz, using the weighted sum approach. It can be seen that the performance of the receiver design described here is the same if not slightly better than that obtained by Tyco. This is especially clear under higher Doppler frequency of 80 Hz, which shows 1.5 dB

improvement at 10^{-2} BER. This clearly shows that the PSP receiver design here is reasonable for the P25 system.

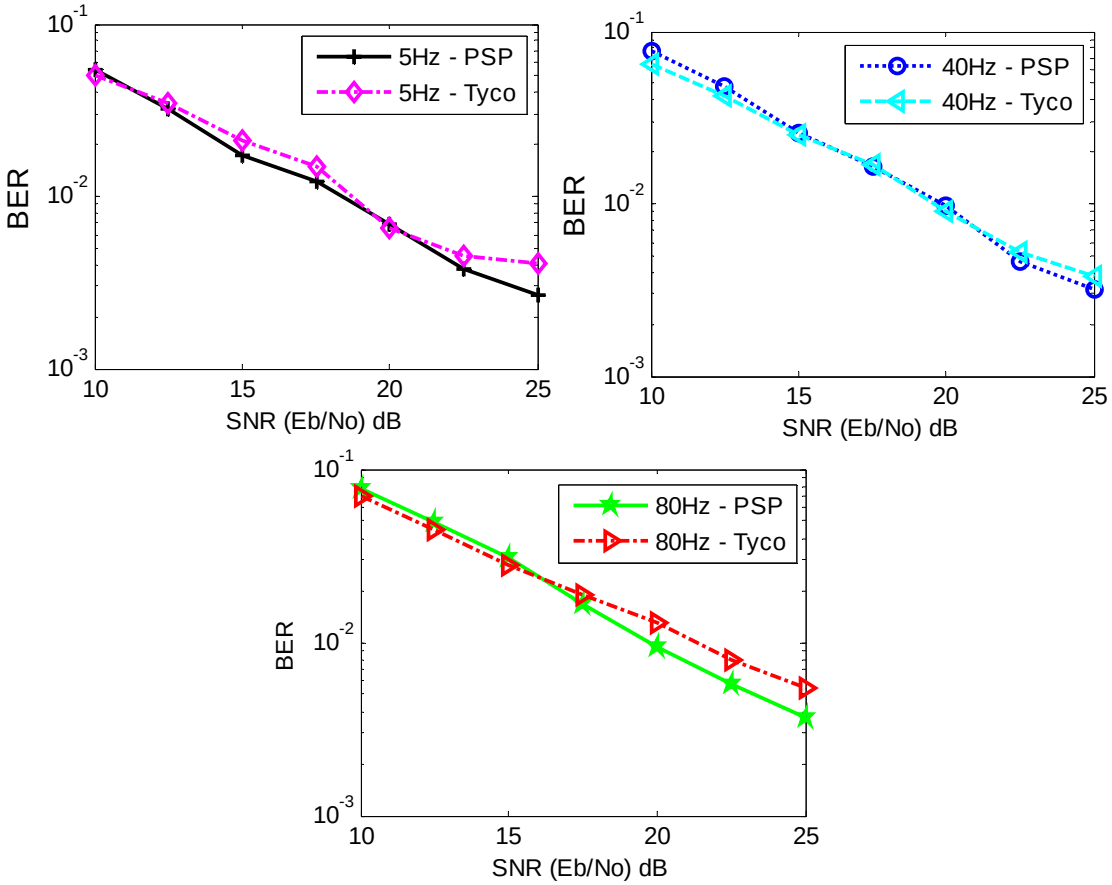

Figure 4.7 BER performance comparison of PSP based MLSE receiver with weighted sum and Tyco's receiver in a Rayleigh fading channel. Symbol time T = 1/6000.

4.6 Discussion

From the simulations, it was observed that the two algorithms for calculating the coefficients for gain estimation behave quite differently. In particular, it was observed that the standard averaging technique performs very well under static condition, but performs badly under fading conditions. On the other hand, the weighted sum technique performs badly under static conditions, but very nicely under fading conditions. This can be explained through the nature of the two algorithms. In the standard averaging algorithm, the weight of each previous gain estimate is the same. Under static conditions, the channel condition is always the same. Therefore,

the standard averaging averages out the noise in the "gain estimates" under static conditions. Under fading conditions, the faster the fading is, the faster the channel condition changes, and therefore, putting equal weight on past estimates result in an inaccurate estimation of the channel gain. On the other hand, with the weighted sum approach, the weight is calculated using the Doppler spread taking into account the extent of correlation between past estimates, and therefore, the gain estimate is more accurate. However, using this on the static condition result in worse performance as the inherit randomness will mean that the correlation between past estimates will never be 1, which is what it should be under static conditions. Another further complication that might have an effect is the fact that the Bessel function used in calculating the coefficients is designed specifically for a Rayleigh fading channel. Therefore, the resulting coefficients calculated for 0 Hz fading which should correspond to a static channel might not actually be the optimal set for static conditions. A new basis function for calculating the coefficients might be needed to provide a more suitable set of coefficients. This, however, is outside the scope of this thesis.

It is clear that there is a trade off between improving the receiver's response for the fading channel, and the sensitivity of the receiver in static conditions. According to the current design, this tradeoff is accommodated by a selective rule which uses the standard averaging technique for static conditions, and the weighted sum technique for fading channels, thereby fully incorporating PSP into the H-CPM receiver. Nevertheless, it is realized that this selection rule is by no means easy to implement, as it will be difficult for a receiver to identify in real time whether a channel is static or not. In fact, it will be difficult in real time to determine the Doppler spread of the channel, which is needed to calculate the weighting coefficients $\boldsymbol{w}$. There are a number of approaches to estimate the Doppler spread which can be incorporated into this model [75]. This is however outside the scope of this thesis.

More practically, one can also use an adaptive algorithm which feedbacks the instantaneous error calculated from the estimated signal and the received signal to adjust the estimated gain obtained from PSP. A possible approach will be to use the least mean square (LMS) algorithm to adaptively change the weight coefficients based on minimizing the error in a mean square sense. In particular, the LMS estimation follows the general equation

$$w(n+1) = w(n) + 2\mu e(n)w(n) \qquad (4.17)$$

where *w(n)* is the variable of interest, *e(n)* is the observed error and μ is a rate constant that is system dependent. Conventionally, *e(n)* would be the error observed from the decoded symbol as compared to the transmitted symbol. However, in the PSP sense, this cannot be used as it will defeat the per-survivor low delay approach. Using the difference between the gains estimated from the correlation function and the previous gain estimates is a possibility. However, this option has not been investigated in this study as it is outside the scope of this thesis. Nonetheless, it is expected that the application of LMS with the PSP algorithm designed here would result in a versatile H-CPM receiver that could satisfy the requirements for a P25 base station system.

4.7 Summary

In this chapter, we have seen that a fading channel requires a channel gain estimator to compensate for the effect of fading before MLSE can be applied. We have described the use of PSP for this channel estimation, which gives the advantage of less error propagation and more accurate results compared to conventional channel estimation techniques. PSP was implemented based on the branch metrics approach, which required an estimation of the complex form of the channel gain, obtained from the correlation function of the received signal and the possible transmitted state. Both standard averaging and weighted sum approach were used to reduce the noise component in the gain estimation. It was found that while the standard averaging technique keeps the error performance of a PSP receiver in static condition essentially the same as one without PSP, the weighted sum approach is more appropriate for fast fading conditions. The performance of the PSP receiver at Doppler frequencies of 5 Hz, 40 Hz and 80 Hz reduced the BER by more than an order of magnitude compared to MLSE receivers without PSP. The difference in the behavior of the static channel and the difficulty in obtaining an accurate Doppler spread suggests that an adaptive approach to renew the weighted sum coefficients is needed.

Chapter 5

DIVERSITY

As we have seen previously, a fast fading channel poses problems in the receiving and decoding of the H-CPM signal due to the variability of the channel, which prevents accurate estimation of its parameters. It was seen in Chapter 4 that this can be overcome by using a low delay PSP algorithm to estimate the behavior of the channel. Another way that the effect of fading can be mitigated is by using diversity at the receiver. Diversity can be implemented in the time, frequency or spatial domains. Here we focus on the use of space diversity employing multiple antennas at the receiver. This chapter is focused on the design of a diversity combining scheme that can be used in parallel with the MLSE PSP algorithm to improve the error performance of the H-CPM receiver.

5.1. Types of Diversity

The concept of receive diversity is relatively simple. It consists of techniques to improve the reliability of a received signal by combining two or more copies of the signal containing the same information, but received through different and independent channels. Combining the received signals appropriately can increase SNR and improve performance by reducing the fluctuations caused by fading.

There are a number of diversity schemes that can be used to achieve this. For example, in frequency diversity, the same information is transmitted at more than one carrier frequency. The carrier frequencies are separated by more than the coherence bandwidth of the channel, and the receiver combines the signals at these frequencies [37, 76]. Time diversity is obtained by repeatedly transmitting the same information in different time slots and combining the received signals at the receiver [37]. This type of diversity is highly effective in a fast fading environment since independent fading is experienced within a small time interval. However, in slow fading channels,

as the fading is more correlated, less independent fading is obtained unless a large decoding delay is allowed [77] and the effect of diversity is decreased. Time diversity is achieved by using a coding structure known as interleaving where the interleaving code or pattern is known by the receiver. Polarization diversity utilizes the polarization state of electromagnetic waves, where the same antenna can be used to obtain vertically and horizontally polarized signal components, which show sufficient decorrelation to allow diversity gain [37]. However the diversity order is restricted to two as only vertical and horizontal polarizations can be used. In this thesis, a more common form of diversity, space diversity, will be considered.

Receiver space diversity is an effective tool to minimize the effects of multi-path fading and co-channel interference without sacrificing spectral efficiency. However, this is at the expense of extra hardware [46]. Receiver space diversity is achieved by using $N > 1$ receive antennas. Each antenna receives a copy of the desired signal subject to independent fading due to the multi-wavelength distance between antennas, the distance from the mobile, and the height of the receive antennas [78]. The independence between channels can be quantified by a correlation coefficient which has a value ranging from 0 to 1, where 1 corresponds to totally correlated channels, and 0 to independent channels [79]. In practice, a correlation coefficient 0.7 represents a practical limit below which most of the available diversity gain is achieved [80]. It is known that antennas separated by at least 7.5 wavelengths are needed to make the correlation coefficient between antennas less than 0.7 [79]. For example, for VHF (150 MHz) base stations, the separation between antennas has to be at least 15m, while for UHF (450 MHz) and 800 MHz base stations, the separation between antennas has to be at least 5m and 2.6m respectively. In this thesis, it is assumed for simplicity that the antenna spacing is sufficient that the channels are completely independent.

We assume in the present work that the diversity combining operation is coherent. Consider a space diversity system with N receive antennas. The signal received by the j^{th} antenna may be written as

$$r_j(t) = g_j(t)s_j(t) + n_j(t), \qquad (5.1)$$

where $s_j(t)$ is a copy of the transmitted signal, $g_j(t)$ is the channel gain and $n_j(t)$ is the additive noise component. As each $s_j(t)$ contains the transmitted information, it can be argued that the linearly combined composite signal

$$r(t) = r_1(t) + r_2(t) + ... + r_N(t) = \sum_{j=1}^{N} g_j(t)s_j(t) + \sum_{j=1}^{N} n_j(t) \qquad (5.2)$$

will be a more accurate representation of the received signal, as the transmitted signals will add constructively, while the noise components, being random, will combine incoherently [37], leading to a higher local SNR. In general, if we know the properties of the channels over which the N signals are transmitted, we can use a weighted sum of the received signals, emphasizing certain channels to maximize the effective received SNR, i.e.

$$r(t) = a_1 r_1(t) + a_2 r_2(t) + ... + a_N r_N(t) = \sum_{j=1}^{N} a_j r_j(t), \qquad (5.3)$$

where the weights a_j, $j = 1, \ldots, N$ are known as the combining coefficients [37]. Note that the above is only true if the signals $r_j(t)$ have the same phase. Therefore, it is important to make sure that the received signals are co-phased when diversity combining takes place.

5.2 Diversity Combining Techniques

There are different ways to determine the coefficients a_j. These are referred to as diversity combining techniques and each involves some kind of tradeoff between performance and implementation complexity. Three common diversity combining techniques have been used in the literature: selection combining (SC), equal gain combining (EGC) and maximal ratio combining (MRC) [37]. This section will briefly outline each of them and compare their theoretical performance using the average output signal to noise power ratios (or simply power ratio) $\overline{p}$ of the system, calculated from the local power ratios p_j, $j = 1, \ldots, N$, for each channel.

5.2.1 Selection Combining

SC "combines" the signals from different receivers by only using the strongest received signal r_k. It is, strictly speaking, not a combining technique but more of a switching technique. The signals that are not selected are discarded and do not contribute to *r(t)* [37], and hence SC is perhaps the simplest diversity technique. Figure 5.1 shows an *N* channel SC system. Let *k* equal the index of the channel for which the local power ratio $p_k \geq p_j$ for all *j*. SC then gives the combining coefficients

$$a_j = \begin{cases} 1, & for\ j = k \\ 0, & for\ j \neq k \end{cases}. \tag{5.4}$$

In the SC system block diagram of Figure 5.1, there is an important block "Means of determining maximum p_j" which chooses the best antenna. There are several ways to do this. Smallest BER controlled diversity is the most effective, but the most computationally expensive way. In this method, a test signal is used to get the received signals from all the antennas, and the antenna whose signal has the fewest errors is used. This is done periodically and the antenna with the best signal is chosen dynamically. This method performs best when the channel does not change greatly between two test signals. Another criterion is received signal strength indication (RSSI) controlled selection diversity. The antenna with the highest RSSI is chosen by monitoring the field strength at the receive antennas [18, 42]. Note that SC does not require any knowledge of the received phases, as no linear combining occurs. Therefore, it can be used with either noncoherent or differentially coherent modulation schemes [54].

To calculate the average power ratio $\overline{p}$, we note that for a Rayleigh fading channel the local power ratio p_j has the distribution [37]

$$G(p_j) = 1 - e^{-p_j}, \tag{5.5}$$

which is derived from the Rayleigh fading distribution of the received signal envelope, assuming AWGN. Now, for SC, the realized output power

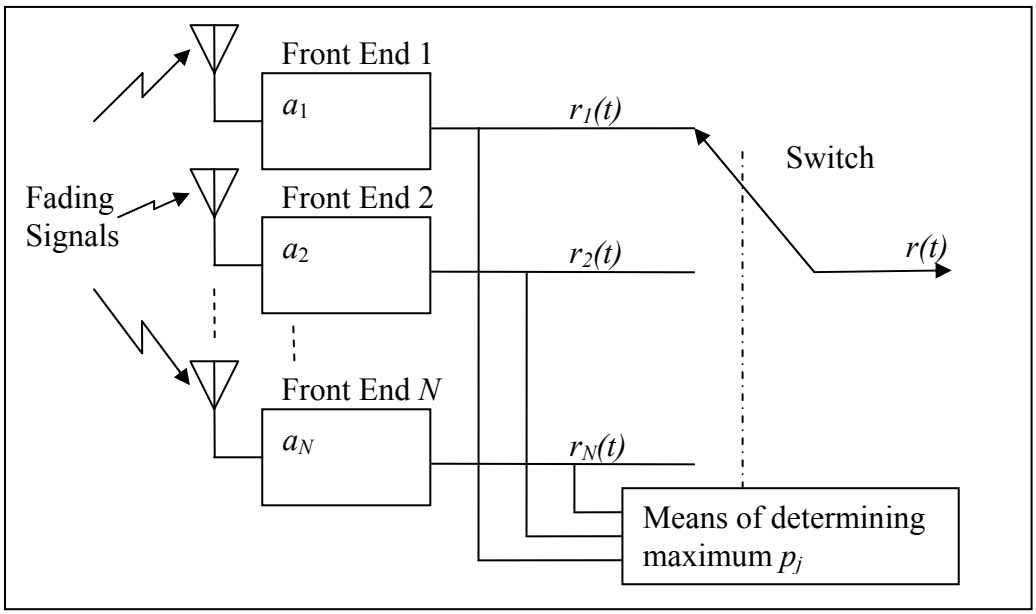

Figure 5.1 Selection diversity combining with *N*=3 [37].

ratio p is simply the maximum local power ratio for all channels under consideration, i.e. the largest value of p_j. To get a realized power ratio of p, we note that by definition of SC, $p_j \le p$ for all values of j (with at least one value of j such that $p_j = p$. Therefore, the probability of having a power ratio of p is equal to the product of $P(p_j \le p)$ for $j = 0, 1 \ldots N$, given that each channel is independent. This results in a distribution of the realized output power ratio p as [37]

$$S(p) = [G(p)]^N = \left(1 - e^{-p}\right)^N. \tag{5.6}$$

Then the average power ratio $\overline{p}$ is by definition given by [37]

$$\overline{p}(N) = \int_{-\infty}^{\infty} p dS_N(p) = \int_{-\infty}^{\infty} pN\left(1 - e^{-p}\right)^{N-1} e^{-p} dp, \tag{5.7}$$

By using the change of variables $y = 1\text{-}e^{-p}$, the integral becomes [37]

$$\overline{p}(N) = \int_0^1 -ln(1-y)y^{N-1} dy, \tag{5.8}$$

which by utilizing the series expansion

$$\ln(1-y) = \sum_{k=1}^{\infty} \frac{y^k}{k} \tag{5.9}$$

gives the following:

$$\begin{aligned} \overline{p}(N) &= \int_0^1 -\ln(1-y) y^{N-1} dy \\ &= \int_0^1 -\sum_{k=1}^{\infty} \frac{y^k}{k} y^{N-1} dy \\ &= \int_0^1 -\sum_{k=1}^{\infty} \frac{y^{N+k-1}}{k} dy \end{aligned} \tag{5.10}$$

Evaluating the integral, one gets the simple expression:

$$\overline{p}(N) = \sum_{k=1}^{N} \frac{1}{k}. \tag{5.11}$$

Hence, $\overline{p}(2) = 1+1/2 = 3/2$, $\overline{p}(3) = 1+1/2+1/3 = 11/6$, etc. When the N^{th} channel is added, $\overline{p}$ is only increased by $1/N$. Therefore, when $N \le 4$, there is a significant change. However when $N \ge 4$, increasing the number of channels does not increase the average local power ratio significantly and the performance of SC does not improve greatly.

5.2.2 Equal Gain Combining

In EGC, all channels are assigned equal gain. In other words, EGC simply adds together the received signals $r_j(t)$, giving each antenna a unity weight for an N channel EGC system [37], i.e.

$$a_j = 1, \quad j = 1,2,....,N. \tag{5.12}$$

Figure 5.2 shows a two channel EGC system. While the determination of the combining coefficient is not needed as it is predefined as 1, phase estimation must be carried out to ensure that the linear combination is phase coherent. Hence, the EGC technique is more complex than the SC design. For EGC, the resultant signal is given by the sum of the individual signals from each channel, i.e.

$$r(t) = \sum_{j=1}^{N} r_j(t). \tag{5.13}$$

Therefore, by definition, the output power ratio is [37]

$$p(t) = \frac{r(t)^2}{\sum \overline{n_j(t)^2}} = \frac{1}{N}\left[\sum_{j=1}^{N} r_j(t)\right]^2, \tag{5.14}$$

where $n_j(t)$ is the noise power for the j^{th} channel and $n_j(t)^2 = 1$ for all j by definition. This can be expanded to give

$$p(t) = \frac{1}{N}\left[\sum_{j=1}^{N} r_j(t)\right]^2 = \frac{1}{N}\sum_{j=1}^{N}\left[r_j{}^2(t) + \sum_{i \neq j}^{N} r_i(t) r_j(t)\right]. \tag{5.15}$$

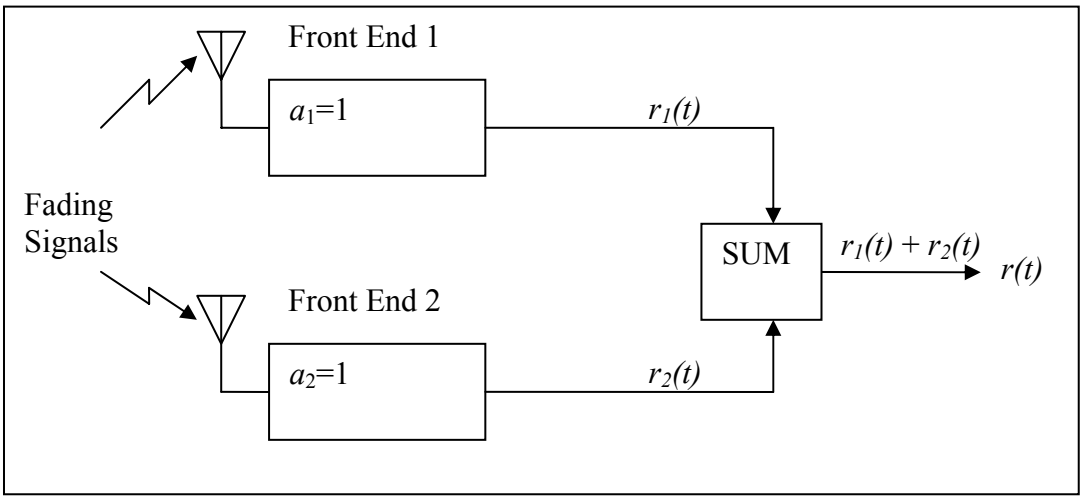

Figure 5.2 Equal gain diversity combining with *N*=2 [37].

Assuming the channels are independent, the average power ratio can be written as

$$\overline{p(t)} = \frac{1}{N}\sum_{j=1}^{N}\left[\overline{r_j^{\,2}(t)} + \sum_{i\neq j}^{N}\overline{r_i(t)}\,\overline{r_j(t)}\right]. \qquad (5.16)$$

Note that $\overline{r_j^{\,2}(t)} = 1$ and $\overline{r_i(t)} = \overline{r_j(t)} = R$ for all $i \neq j$, where R $(0 \le R^2 \le 1)$ is a dimensionless constant which varies with the channel model [37]. Furthermore, there are $N(N\text{-}1)$ terms in the summation $\sum_{j=1}^{N}\sum_{i\neq j}^{N}\overline{r_i(t)}\,\overline{r_j(t)}$. Putting these into (5.16), the average power ratio of EGC becomes [37]

$$\overline{p}(N) = 1 + (N-1)R^2. \qquad (5.17)$$

For a Rayleigh distribution, $R^2 = \pi/4 \approx 0.785$ [37]. Eqn. (5.17) suggests that $\overline{p}(N)$ is linearly proportional to the number of channels, which shows that increasing the number of antennas has more effect on the performance of EGC than SC.

5.2.3 Maximal Ratio Combining

MRC is optimal in that it can be arrived at based on likelihood function arguments and indeed is closely related to maximum likelihood detection [81]. We assume that the local noise power is the same in all the channels of the MRC system. Two conditions need to be satisfied to achieve the maximum output power ratio. Firstly, the weight assigned to each channel is proportional to the local rms value of the signal x_j. Secondly, the weight of each channel is inversely proportional to the mean square noise $\overline{n_j^{\,2}}$ in that channel. Therefore, MRC dictates that [37]

$$\begin{aligned} a_j &= \frac{x_j}{\overline{n_j^2}} \\ x_j(t) &= \sqrt{s_j^2} \end{aligned} \quad . \qquad (5.18)$$

Figure 5.3 shows a two channel MRC system. Theoretically, perfect channel estimation is required for MRC [54], and therefore, MRC is the most complex of the three combining techniques. In practice, a receiver employing MRC coherently combines the signals from each antenna by using the complex conjugate of their respective fading gains and noise variances [82, 83]. To ensure the signals are coherently summed, the MRC receiver needs to take into account the fading amplitude (proportionally to the received signal strength), phase and delay of each signal.

By definition, MRC has the property that the instantaneous power ratio following combining has the form [37]

$$p(N) = \sum_{j=1}^{N} p_j, \tag{5.19}$$

Then, the average power ratio $\overline{p}$ of MRC is given by [37]

$$\overline{p}(N) = \sum_{j=1}^{N} \overline{p}_j. \tag{5.20}$$

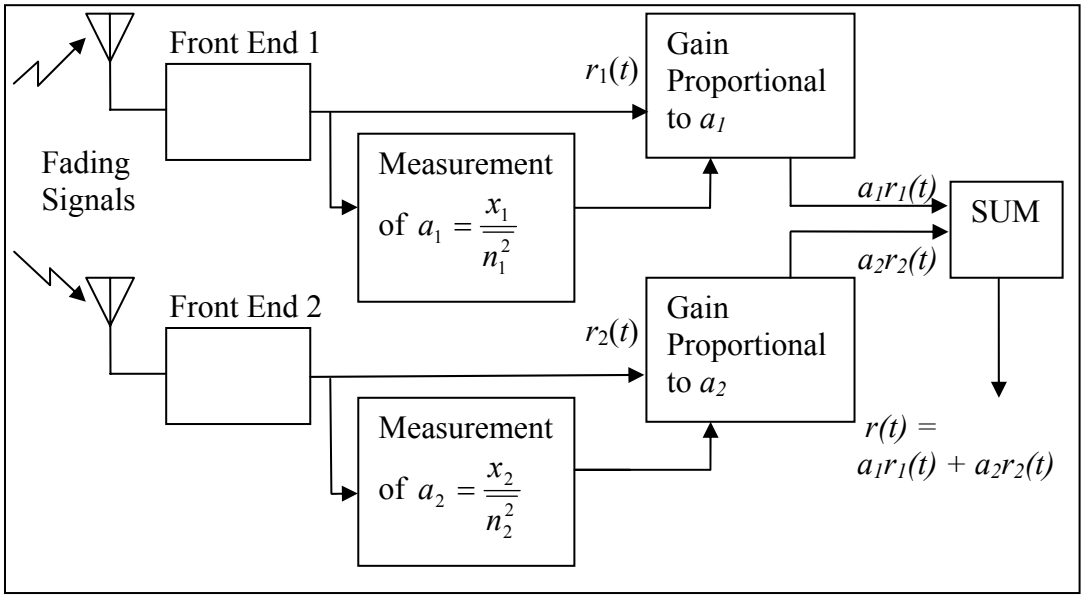

Figure 5.3 Maximal ratio diversity combining with *N*=2 [37].

Using the standard assumption of $r_j^2(t) = 1$ and $n_j(t)^2 = 1$ that has been used in the previous sections, we get $\overline{p}_j = 1$, which gives

$$\overline{p}(N) = N. \tag{5.21}$$

5.2.3 Comparing theoretical performances

From (5.11), (5.17) and (5.21), it can be seen that for SC, $\overline{p}$ increases only as $1/N$ with an increasing number of channels N, while both EGC and MRC performance increase linearly with increasing N. The theoretical relationship between N and $\overline{p}$ is shown in Figure 5.4, where the improvement observed with increasing N is plotted for each of the three combining techniques predicted using the theoretical model. A more detailed analysis of the figure is shown in Table 5.1, which compares the

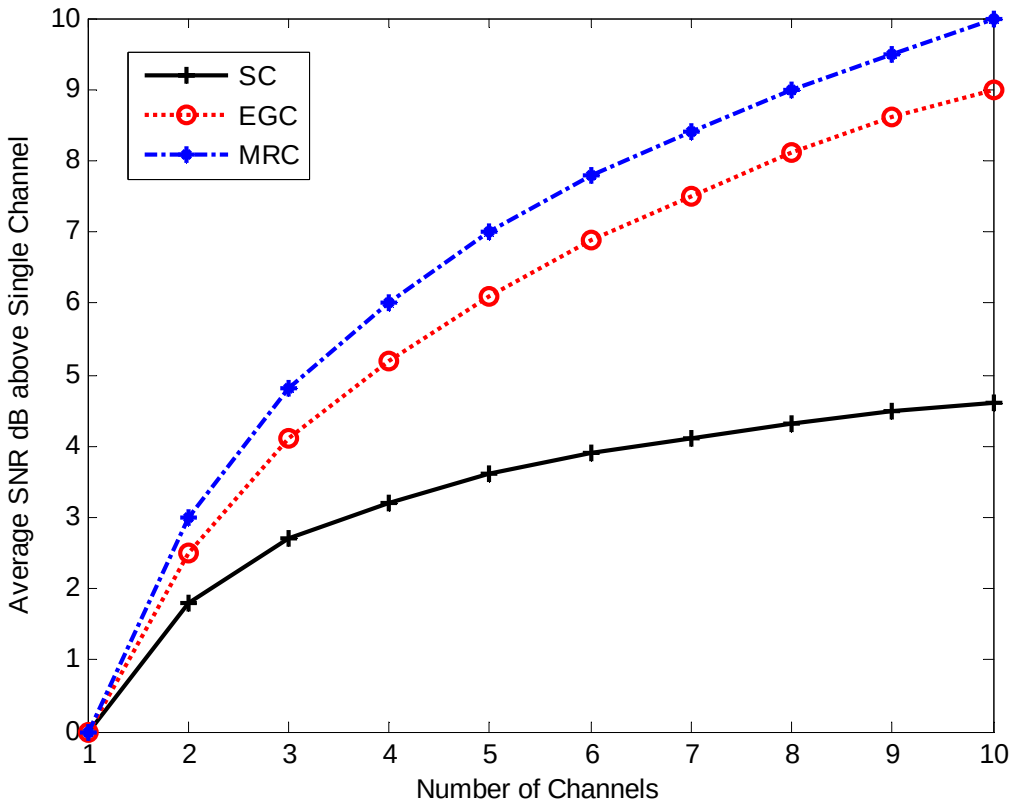

Figure 5.4 Diversity improvement (in dB) in average SNR, for Rayleigh fading locally coherent signals in locally incoherent noise with constant local rms values[37].

Number of Channels *N*	**Gain (dB) Achieved using MRC over:**		
	EGC	**SC**	**No diversity (Single channel)**
2	0.49	1.25	3.01
3	0.67	2.14	4.71
4	0.76	2.83	6.02
6	0.85	3.89	7.78
8	0.90	4.89	9.03
∞	1.05	∞	∞

Table 5.1 Comparative Average SNR of the different combining techniques for an AWGN channel [37].

theoretical performance of MRC and the other two techniques numerically with different numbers of channels. It can be seen that even by increasing the numbers of channels, EGC and MRC would never differ by more than 1.05dB, while their diversity improvements are much higher than when using SC. A 3 dB improvement in performance can be achieved with MRC just by using dual diversity (i.e. two antennas).

5.3 Diversity with PSP

To study the effect of diversity, the effect of multiple receivers is simulated by using multiple channels with different channel parameters and therefore independent fading. As the aim of the study is to look at the feasibility and performance of triple diversity, the system is simulated with two to four channels corresponding to dual, triple and quadruple diversity respectively, and the results are compared with those for a single channel. In order to do this, the diversity combining is incorporated with the PSP receiver design described in Chapter 4.

In order to implement diversity with PSP, one has to keep in mind that diversity considers the combining of the actual signals. Yet PSP is needed to obtain the channel information, which is needed for finding the appropriate gain for the diversity schemes. Therefore, the appropriate way is to use PSP to estimate the

channel gain for each diversity channel. The estimated gain is then used to determine the diversity gains which are applied to each channel to correct the branch metrics that are input into the MLSE receiver. Figure 5.5 shows a block diagram of the algorithm used in this thesis, combining PSP and diversity combining. Figure 5.5a shows the

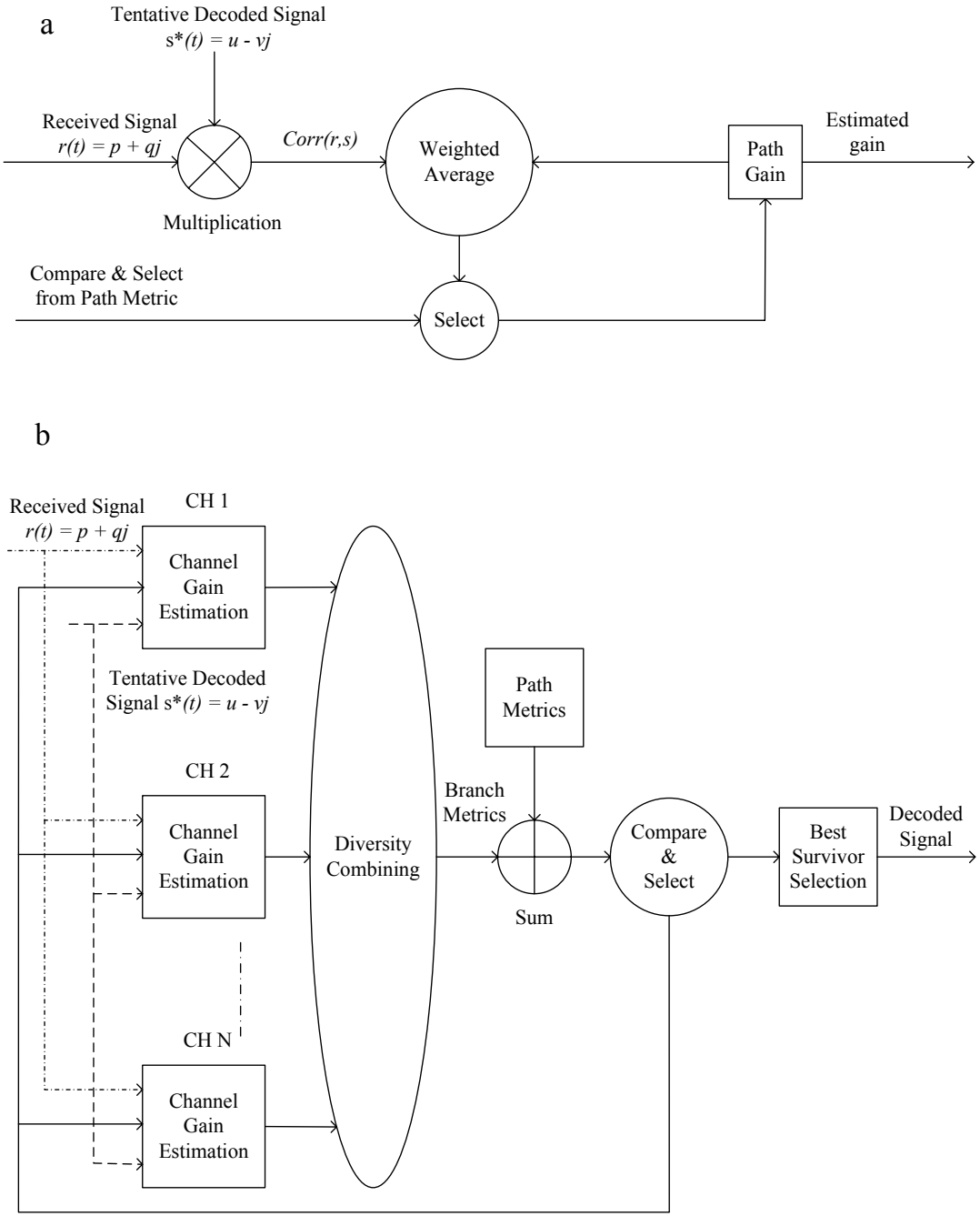

Figure 5.5 Block diagram of a PSP-based MLSE receiver with diversity combining: a) The algorithm used for PSP gain estimation for each channel; b) Diversity combining of estimated gain and the received signals to calculate the branch metrics and best survivor. Note that each of the "Channel Gain Estimation" blocks contain the algorithm specified in a).

block diagram corresponding to the gain estimation stage of the algorithm, which uses PSP to estimate the gain of a particular channel. As described in Section 4.4, the gain is estimated by PSP through calculating the correlation function between the received signal $r(t) = p + jq$ and each tentative decoded signal $s(t) = u + jv$. This gives the noisy estimate of the channel gain, $corr(r,s)$, which is then used to estimate the gain $g(t) = m + jn$ used at the next symbol time by weighted averaging with the previous gains following the current best survivor, which is in turn extracted from a path gain matrix which stores all the estimated gains for each survivor in the past.

Since each diversity channel has a different gain, this PSP gain estimation is performed on each of the diversity channels, as shown in Figure 5.5b. Each of the "Channel gain estimation" blocks corresponds to the block described in Figure 5.5a. The output from each of these blocks, the estimated complex gain from each channel, is then combined or selected depending on the diversity combining technique to calculate a single branch metric for each possible survivor. In particular, for SC, the received signal strength from each channel is compared, and the channel with the largest strength is selected. The branch metrics are calculated using only the received signal and the estimated gain from that channel. For EGC, the magnitude of the combiner gain is 1 for each channel, so that the received signals are simply added together. However, as the signals must be in phase before being added, the phase component for the fading must be compensated. Therefore, the gain applied to the branch metrics becomes $\cos\varphi_N + j\sin\varphi_N$, where φ_N is the phase of the PSP-estimated complex channel gain for the N^{th} channel. For MRC, the combiner gain is proportional to the SNR of the received signal in each channel. As the SNR is proportional to the amplitude or magnitude of the channel gain, the combiner gain magnitude is the amplitude of the estimated channel gain calculated from PSP. Again, since the signals need to be in phase, the phase component of the fading needs to be considered. This means that effectively, the diversity gain required for MRC is simply the conjugate of the complex gain estimated for each channel from PSP. In the final step, the calculated branch metrics for each survivor are added to the path metric of the corresponding survivor as described in Chapter 3, from which the best survivor is selected. This best survivor is then used to decode the most probable transmitted symbol, and is also fed back to the gain estimation and path metric calculation stage as shown in the block diagram.

As described in Chapter 4, a PSP-based MLSE receiver provides channel estimation for each surviving path in the VA to account for channel effects in a low delay manner. Therefore, when diversity is incorporated with PSP-based receivers, separate channel estimates are obtained for each channel in the PSP process. This implies that the channel information must be kept after the PSP algorithm has operated, meaning that diversity combining takes place after the PSP MLSE receiver has produced its channel estimates. This will expand the required computational resources as a set of surviving paths must be stored for each channel, and the number of sets increases in proportion to the number of channels used. However, the channel estimation already provides the fading amplitude and the channel phase, which is needed for MRC and hence no extra effort is needed to acquire the phase and amplitude for MRC diversity combining. It is therefore expected that the MRC scheme, now with the same complexity as the EGC scheme but with improved performance, will be the first choice for the design of a diversity scheme with PSP MLSE receivers for the P25 system.

5.4 Simulation Results

The performance of the PSP MLSE receiver is simulated using no diversity (single channel), dual diversity, triple diversity and quadruple diversity with SC, EGC and MRC diversity combining schemes across a wide range of Doppler frequencies in a Rayleigh fading channel. In particular, to simulate independent channels, the information symbol is first encoded with the H-CPM transmitting algorithm as described in Chapter 2. Three independent fading channels (or two/four for dual/quadruple diversity) are then applied to the transmitted waveforms, resulting in three (two/four) independently faded received signals. Each of these is then fed into the algorithm shown in Figure 5.5 for demodulation and decoding. Again, the error rate performance under different conditions is observed, from which the effects of diversity order, the diversity combining scheme and the various Doppler frequencies are investigated.

5.4.1 Effect of Diversity Combining Technique and Diversity Order

Figure 5.6 compares the PSP MLSE receiver BER performance with triple diversity using the SC, EGC and MRC diversity schemes at Doppler frequencies of 5Hz, 40Hz, 80Hz and 333Hz in a Rayleigh fading channel. It is clear from the graphs that MRC has the best performance and EGC outperforms SC. In particular, at high SNR, EGC and MRC exhibit larger diversity gain than SC. Figure 5.7 shows the effect of diversity order on the performance of a PSP MLSE receiver in a Rayleigh fading channel. It can be seen that as expected, the receiver performance improves as the number of receiving channels increases. In particular, it can be seen that there is a significant decrease in BER in going from a single channel to two channels. The performance improvement in going from dual diversity to triple diversity is also quite evident on the graph. It can be seen that triple diversity with SC performs better than dual diversity with MRC, even though MRC is a better combining technique.

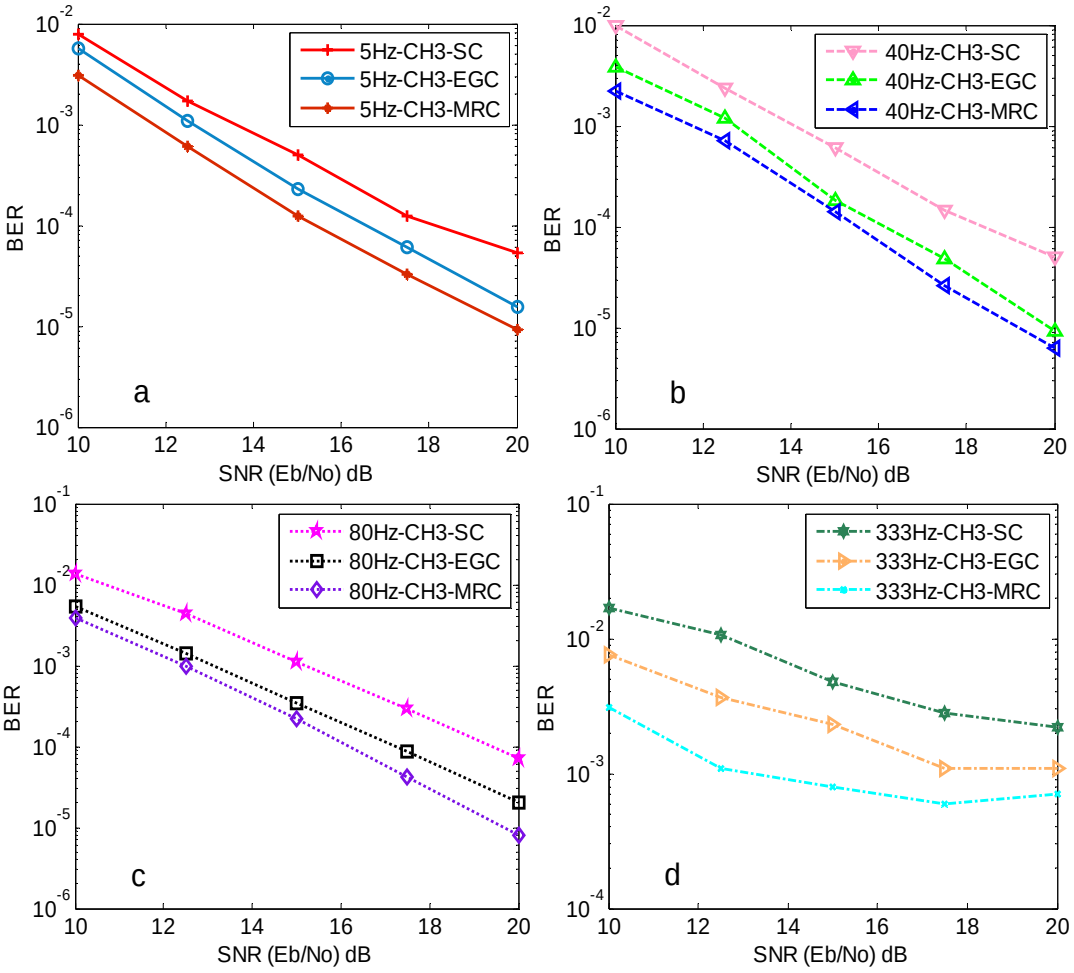

Figure 5.6 BER performance comparison of SC, EGC and MRC for PSP-based receivers at different Doppler frequencies listed in the figure. Symbol time $T = 1/6000$.

Table 5.2 shows the increased effective SNR level for each combining technique with dual diversity over no diversity at a BER = 10^{-2}, as extracted from Figure 5.7. A significant diversity gain is achieved as expected. Table 5.3 and Table 5.4 show the increased SNR level for each combining technique using different numbers of receiver channels at a BER = 10^{-3}, as extracted from Figure 5.7. As can be seen from Table 5.2 and Table 5.3, as diversity order increases, an increased diversity gain is obtained. However, the most significant diversity gain improvement is achieved by going from no diversity to dual diversity as opposed to going from dual to triple or triple to quadruple diversity. This matches theoretical expectations. Also

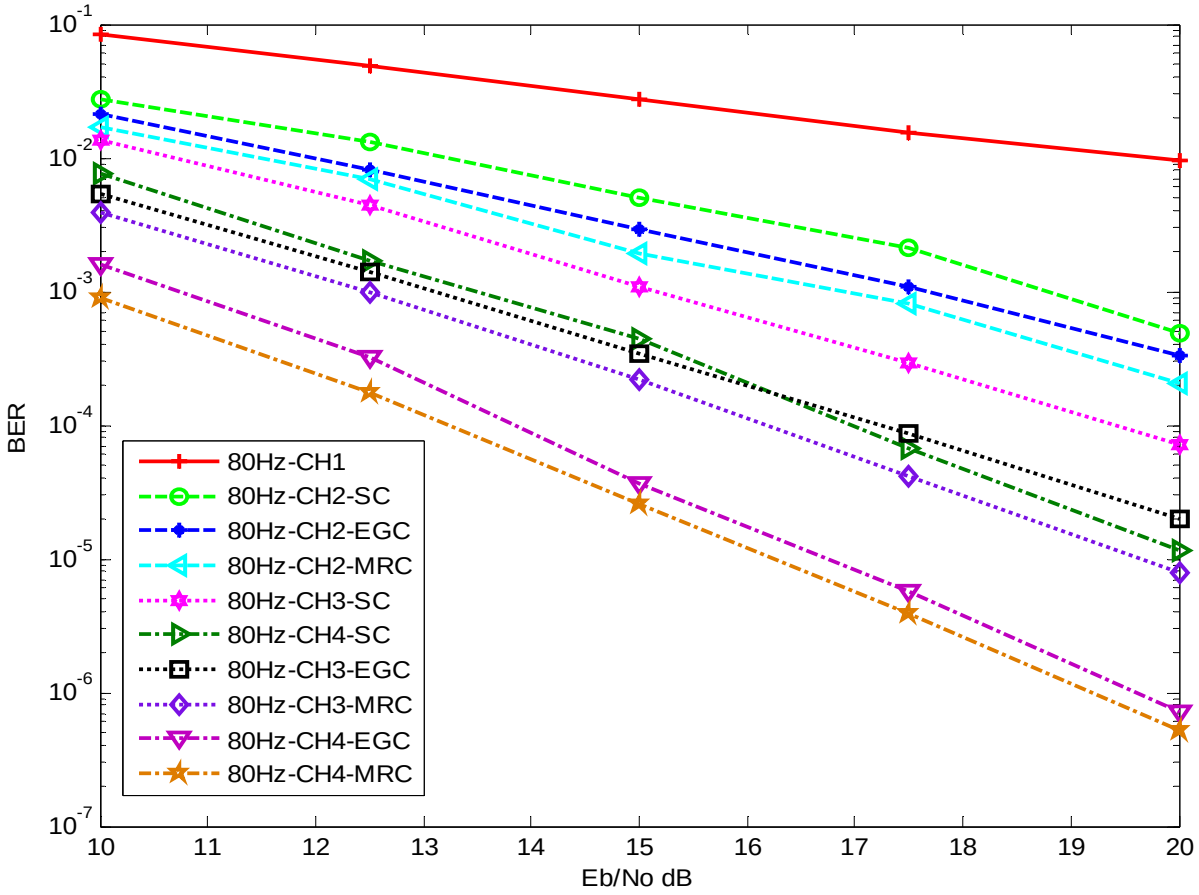

Figure 5.7 BER performance comparison of no diversity (CH1), dual (CH2), triple (CH3) and quadruple (CH4) diversity systems in Rayleigh fading channel at Doppler frequency of 80Hz. Symbol time $T = 1/6000$.

displayed in Table 5.3 and Table 5.4 is the improvement observed from going to 4 antennas or quadruple diversity. It can be seen that while going from a single channel to 4 channels results in a larger increase in dB level, the relative diversity gain achieved is much less than the improvement seen from single to dual or dual to triple diversity. Furthermore, the computational complexity, the hardware cost and physical system requirements are further increased if four antennas are used. There is also no significant increase in receiver coverage, while more effort is needed to keep a small correlation coefficient among the antennas for near-independent fading. These suggest that triple diversity is an excellent approach for implementing a diversity receiver.

Number of Channels *N*	**Diversity Gain (dB) at BER = 10^{-2}**		
	SC	**EGC**	**MRC**
2	6.4	7.7	8.2

Table 5.2 Diversity gain increment achieved with three diversity combining techniques at dual diversity over no diversity.

Number of Channels *N*	**Gain (dB) over Dual Diversity at BER = 10^{-3}**		
	SC	**EGC**	**MRC**
3	3.6	4.3	4.35
4	5.3	7.0	7.2

Table 5.3 Diversity gain increment achieved with three diversity combining techniques at triple diversity and quadruple diversity over dual diversity.

Number of Channels *N*	**Gain (dB) of Four Fold Diversity over Triple Diversity at BER = 10^{-3}**		
	SC	**EGC**	**MRC**
4	1.7	2.7	2.85

Table 5.4 Diversity gain increment achieved with three diversity combining techniques at quadruple diversity over triple diversity.

5.4.2 Effect of Doppler frequency

The effect of Doppler frequency on the performance of the three diversity combining techniques in a triple diversity system was also investigated. Rayleigh fading with Doppler frequencies of 5 Hz, 40 Hz, 80 Hz and 333 Hz was simulated, and the corresponding error performance of the PSP receiver with triple diversity was tested. Note that 5 Hz, 40 Hz and 80 Hz are typical Doppler frequencies used to specify and compare system performance of modern mobile radio wireless systems. 333 Hz corresponds to the Doppler condition expected when the receiver is used on a helicopter (which is possible in public service applications). Figure 5.8 shows the error performance of SC, EGC and MRC at different frequencies. It can be seen that the difference in the performance between MRC and SC increases with Doppler frequency. In particular, at 5 Hz, the difference between MRC and SC is approximately 2 dB at 10^{-3} BER, which becomes ~3 dB for 80 Hz and over 10 dB for 333 Hz. On the other hand, the difference between MRC and ECG seems to diminish as the Doppler frequency is increased from ~ 1 dB at 5 Hz and 40 Hz to less than 0.5 dB at 80 Hz for 10^{-3} BER, only to increase dramatically again at 333 Hz. Nevertheless, the most important point is that for all conditions, MRC gives the best error performance. It is also clear that at the lower Doppler frequencies, the increase in SNR has a significant effect on error performance, but this improvement due to increased SNR becomes much less significant compared to the effect of diversity at the higher Doppler frequencies. For example, for 5 Hz and 40 Hz, the BER decreases approximately 2.5 orders of magnitude by going from an SNR of 10 to 20 dB. This is reduced to approximately 2 orders of magnitude for Doppler frequencies of 80 Hz. At 333 Hz, the effect of SNR is dramatically diminished, with less than an order of magnitude decrease in BER despite a 10 dB increase in SNR, while the use of MRC diversity decreases the BER by up to 10 times across the whole SNR range. This highlights the importance and effectiveness of diversity combining in fast fading channels.

Observing the data across the graphs, it can be seen that in general, error performance degrades with increasing Doppler frequency. This is true for both SC and EGC, although for MRC the performance degradation is almost negligible, especially at low SNR. Nevertheless, BER variation from 5 Hz up to 333 Hz is less

than 1 dB above a BER of 10^{-3}, with the error performance between 5 Hz and 40 Hz being essentially the same. However, as SNR increases, the separation in performance

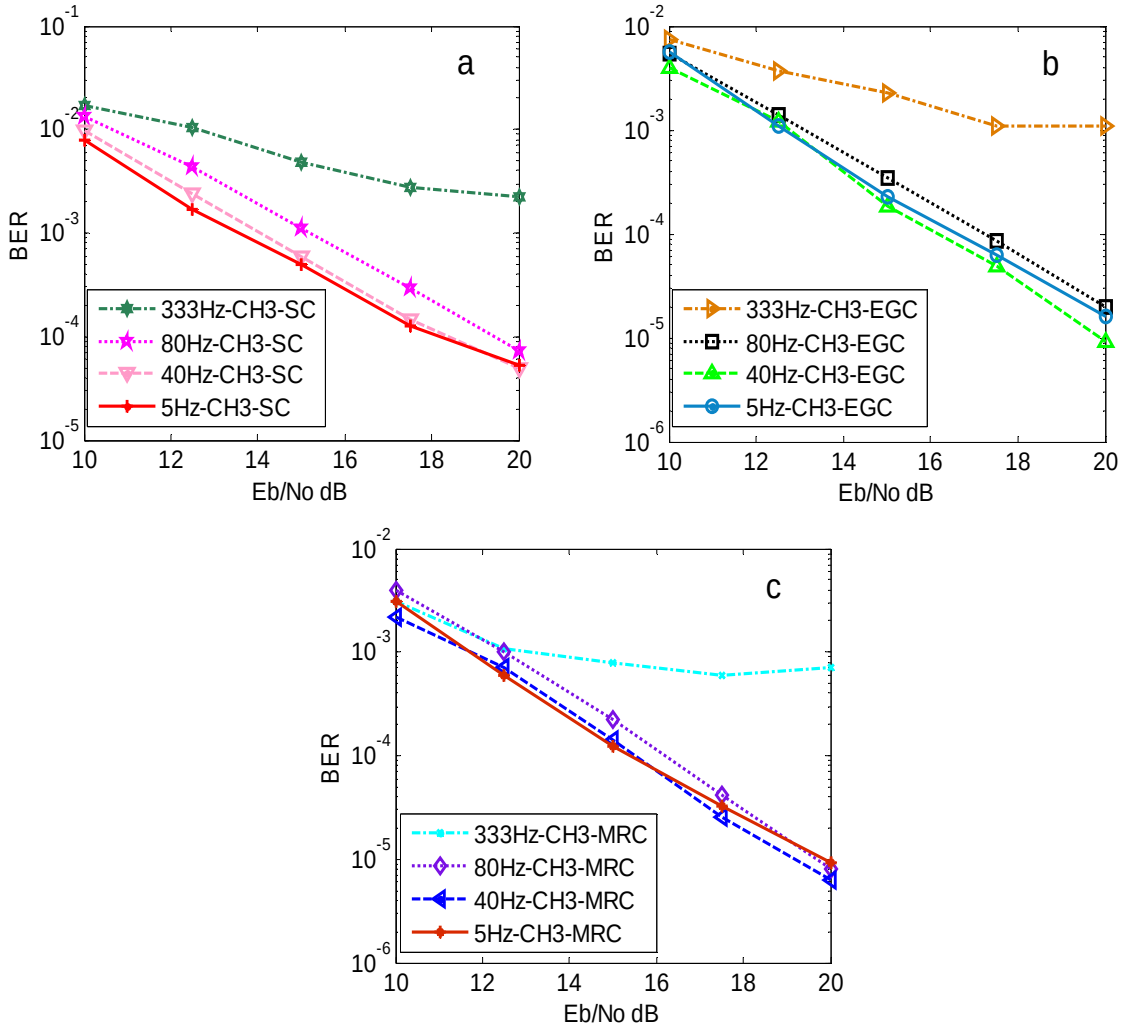

Figure 5.8 BER performance comparison of employing SC, EGC and MRC across a range of Doppler frequencies listed in the figure. Symbol time $T = 1/6000$.

for the different frequencies increases. While the error performances are close to each other at the lower Doppler frequencies, the performance at 333 Hz is now almost 10 dB worse. This saturation of the BER to the error floor of ~5×10^{-4} suggests that even with diversity, this Doppler frequency is too fast to be tracked. However, from Figure 5.8 we know that even with this relatively high BER, we expect that a receiver using any of the diversity combining techniques will still be orders of magnitude better in error performance than the single channel PSP receiver at this Doppler frequency. Overall, from Figure 5.8, it is clear that the MRC receiver is the best performer, even

for fast fading situations, with negligible degradation in performance for fast fading channels up to a Doppler frequency of 80 Hz.

5.5 Summary

In this chapter, it has been demonstrated that a triple diversity MRC scheme achieves significant diversity gain. Incorporated with PSP-based receivers, MRC does not need extra effort to acquire the fading amplitude and the channel phase for diversity combining. It was shown in the simulation that this scheme performed very well with the standard 80 Hz Doppler frequency regime, improving the error performance by more than 10 dB over a single channel PSP MLSE receiver. Of course, as mentioned in the beginning of the chapter, the simulation here assumes independent sub channels. Channel correlation is expected to degrade the error performance. Nevertheless, using triple diversity with PSP is obviously beneficial for the error performance and efficiency of the receiver. With the combination of triple diversity and the reduced state PSP MLSE receiver described in Chapter 3 and 4, much of the design specification for the H-CPM receiver for the P25 base station is achieved [6].

Chapter 6

Conclusion

Let us first remind ourselves of the two main goals of this thesis: firstly, to design a suboptimal, low complexity, high performance H-CPM base station receiver, which meets the APCO P25 Phase 2 standards; and secondly, to apply diversity combining using three antennas to achieve improvement in overall receiver performance. In this chapter, the results obtained are summarised and possible future research directions are described, based on the findings of the study.

6.1 MLSE receiver design

The receiver design was carried out in a simulated environment developed in MATLAB. Through the use of a simulated environment, and disregarding some practical parts of the design like symbol synchronization, an efficient receiver design was developed, with most of the effort going into developing the signal processing algorithm for the receiver. The end product is an MLSE based receiver design, which can be implemented for practical use. The design consisted of two stages. In the first stage, a trellis state reduction algorithm was derived to reduce the complexity of the optimal MLSE receiver, under AWGN conditions. In the second stage, fading was introduced and a channel estimation algorithm was incorporated into the MLSE receiver for fading channels.

Complexity reduction of the optimal MLSE receiver was achieved by using both the tilted phase concept of Rimoldi [15] and frequency pulse truncation [59]. By effectively eliminating the difference in the possible phase states at odd and even symbol times, the tilted phase approach allows the effective number of states searched per symbol time to be halved from 384 to 192, without reducing the actual number of trellis states used at any instant. As a result, the computational complexity of the receiver was reduced by half, with no degradation in error performance. This is

confirmed from the simulated BER performance, which shows no loss at all for the 192 state receiver when compared to the original MLSE receiver. Further reduction in receiver complexity was achieved by frequency pulse truncation, which assumes that the small amplitude of the tails of the frequency pulses is equal to zero. In particular, the truncation of the frequency pulse tail for $t > 3T$ translates to rolling the last symbol of the correlative state into the phase state, reducing the number of states from 192 to 48. The truncation of the tail at $t < T$ effectively ignores the first symbol in the correlative state, leading to a useful trellis structure of 12 states described by only one correlative symbol and the phase state. As this approach approximates the frequency pulse with a shorter duration pulse, some BER performance degradation is expected. Under AWGN conditions, a SNR degradation of 0.07 dB was found at 2% and 5% BER in comparing the 384 state and 12 state receivers. The loss is negligible at low SNR. In the light of the computation complexity decrease of over 95% in going from 384 to 12 states, it is clear that a MLSE-based 12 state receiver provides a good basis for a suboptimum low complexity receiver in a P25 base station.

The problem for reduced state receivers in fading channels is apparent from the start, as it was clear that fast fading introduces distortion to the received signal that MLSE receivers without channel estimators cannot take into account. This problem was solved by using PSP [30], where a weighted sum of previous received symbols in the surviving path is used to predict the fading channel gain. This is then incorporated into the received signal to undo the channel effects, thus allowing the MLSE receiver to perform the decoding of the signal. It was found that PSP can be used to estimate the channel state efficiently and without delay by estimating the channel gain for each surviving path, thereby incorporating the channel gain estimation within the VA. In particular, two schemes for channel estimation, block averaging and weighted sum, are used to estimate the current channel gain using past channel information.

It was found that the block technique performs well under AWGN and slow fading conditions, whereas under fast fading conditions, the weighted sum technique is a better choice. Under AWGN conditions, standard averaging PSP has essentially the same performance as a MLSE receiver with no PSP, a benchmark for static conditions. On the other hand, the weighted sum PSP result in a 2-dB degradation in performance under AWGN conditions. In Rayleigh fading, both techniques resulted in over 10 dB improvement in performance compared to the MLSE receiver with no PSP. However, the weighted sum PSP resulted in a further 10 dB improvement

compared to the standard averaging technique, even for extremely fast fading of Doppler frequency 333 Hz (fade rate 0.0555). Furthermore, the performance of the weighted sum PSP receiver at Doppler frequencies of 5 Hz, 40 Hz and 80 Hz are comparable if not better (at high SNR) than those reported by Tyco Ltd [1]. From these results, it was concluded that the suboptimal receiver for the P25 system would be one which uses the standard average PSP for static conditions and weighted sum PSP for fading conditions, given that the Doppler spread of the channel can be accurately estimated. Note that both the estimation of Doppler spread and the development of an alternative adaptive approach to the receiver design is outside the scope of this thesis.

In conclusion, a low complexity PSP-based MLSE receiver has been designed for H-CPM. Under AWGN conditions, there is a negligible SNR degradation of 0.07 dB at 2% and 5% BER compared to the near optimum (full number of trellis states) H-CPM receiver. The receiver proposed in this thesis sacrifices little in performance but achieves a significant reduction in implementation complexity. The application of PSP can be used to combat fading and a MLSE receiver using a weighted sum PSP technique for a Rayleigh fading channel and a standard averaging PSP for an AWGN channel performs well under a wide range of channel conditions.

6.2 Diversity

This part of the study involved the use of diversity combining to mitigate the fading effects of the wireless channel. In particular, triple diversity is studied in this thesis. By combining three copies of the transmitted signals each of which has experienced independent fading, the fading effect can be compensated, allowing the signal to be successfully decoded. In this thesis, the effects of triple diversity compared to that of the commonly used dual diversity were investigated. Three different combining techniques were considered, namely, selection combining (SC), equal gain combining (EGC), and maximal ratio combining (MRC). It was found SC has the simplest implementation complexity, while EGC and MRC have the same implementation complexity when used with PSP due to the estimated channel parameters' fading amplitude and phase being provided by the PSP algorithm.

Simulation results show that triple diversity introduces a substantial improvement in the performance compared to dual diversity. In particular, 3.6 dB, 5.3 dB and 5.7 dB improvement at BER = 10^{-3} was observed for SC, EGC and MRC respectively when using triple diversity in a Rayleigh fading channel. It was also observed that a further ~3 dB improvement can be obtained by going to four-fold diversity in a Rayleigh fading channel. However, as extra antennas bring an increase in complexity, hardware cost and the physical space needed (which is a major problem at a base station site), it was concluded that triple diversity is the best option for applying diversity in MLSE receivers.

The performances of SC, ECG and MRC triple diversity combining are compared at different Doppler spreads in Rayleigh fading channels. It was found that across all Doppler frequencies, MRC performs better than ECG, which in turn performs better than SC. The difference in performance among the three diversity techniques varies with Doppler frequency. In particular, it was observed that a 2 dB improvement at 10^{-3} BER over SC was obtained by using MRC. This increases to ~3 dB at 80 Hz and to over 10 dB at 333 Hz. On the other hand, the difference between ECG and MRC diminishes with increasing Doppler frequency, with the difference between the two decreasing from ~1 dB at 5 Hz to ~ 0.5 dB at 80 Hz. Overall, the Doppler frequency has limited effects on the BER performance of each receiver, with the performance between 5 Hz and 80 Hz in general being essentially the same for each diversity scheme.

In conclusion, the study of diversity combining shows that MRC under a triple diversity scheme is compatible with the reduced state MLSE and PSP algorithm, and provides a high performance, low delay MLSE detector for the P25 system under fast fading conditions.

6.3 Suggestions for Future Research

As seen throughout the thesis, there are a number of observations which suggest that further improvements could be achieved that could not be implemented due to time and resource constraints. Here we give a list of possible areas for further research which should be considered to further enhance the performance of the basic receiver design described in this thesis.

1. The PSP-based MLSE receiver is designed specifically for a Rayleigh flat fading channel. The performance of the receiver under different fading channels, as well as dispersive or ISI channels should be investigated.

2. Development of a LMS adaptive algorithm to evaluate the coefficients for channel estimation in the PSP algorithm.

3. Derive performance bounds for the H-CPM receiver with diversity combining.

4. Combine space-time coding and receiver space diversity for the H-CPM receiver to further improve the performance.

5. Apply convolutional encoding to H-CPM to further improve the performance [84].

6. Even though PSP limits the error propagation in the channel estimation and provides a low delay solution even under fast fading conditions, it suffers from high computational complexity. Further reduction in the PSP-based MLSE receiver complexity is desirable for a practical system [51].

7. Develop a hardware implementation of the proposed suboptimal receiver design.

6.3 Final remarks

In this thesis, we have described a possible design of a suboptimal receiver for the APCO P25 Phase 2 base station system using diversity combining. We have illustrated a viable design which has low complexity and can withstand fading and which is well suitable for the APCO P25 Phase 2 system. Although some of the details with regard to practical aspects have not been clearly resolved, we have shown in this thesis the essentials and a proof-of-concept design that are vital for the actual implementation of the receiver. Therefore, while this thesis cannot be used on its own as a design document, it should form the basis for the design of an APCO P25 Phase 2 base station receiver.

7 References

[1] M. Hartless, "Compare 12 kbps Downlink H-CPM vs p/4-DQPSK," Tyco Electronics, [Online]. Available: ftp://ftp.tiaonline.org/TR-8/APIC/TDMA/Files%202006/.

[2] F. R. Yu, H. Tang, and V. C. M. Leung, "QoS Provisioning in Public Safety Radio and Commercial Cellular Integrated Networks for First Responders and Critical Infrastructures," in *Proc. IPCCC*, 2007, pp. 570-575.

[3] TIA, "APCO project 25 system and standards definition," *TIA/EIA Telecommunications Systems Bulletin,* TSB102-A 1995.

[4] Krishna Balachandran, Kenneth C. Budka, Thomas P. Chu, Tewfik L. Doumi, Joseph H. Kang, Bell Labs, and L. Technologies, "Mobile responder communication networks for public safety," *IEE Communications Magazine,* January 2006.

[5] "APCO Project 25 - Standards for Public Safety Digital Radio. [Online]. Available: http://www.apcointl.org/frequency/project/information.html."

[6] TR-8, "07-100 -R5 TDMA - HarmonizedPHYdraft1v6 [Online]. Available: ftp.tiaonline.org/TR-8/APIC/TDMA/Files%202007/."

[7] J. B. Anderson, T.Aulin, and C.-E. W.Sunberg, *Digital Phase Modulation*. NY: Plenum, 1986.

[8] R. J. Young and J. H. Lodge, "Detection of CPM signals in fast Rayleigh flat-fading using adaptive channel estimation," *IEEE Trans. Veh. Tech.,* vol. 44, 1995.

[9] J. B. Anderson and A. Svensson, *Coded Modulation Systems*. NY: Kluwer Academic/Plenum, 2002.

[10] J. Anderson and D. Taylor, "A bandwidth-efficient class of signal-space codes," *IEEE Trans. Inform. Theory,* vol. 24, pp. 703-712, 1978.

[11] T.Aulin, "CPM - A power and bandwidth efficient digital constant envelop modulation scheme," Ph.D. Thesis, Lund University, Lund, Sweden, Nov. 1979.

[12] J. Anderson, C. E. Sundberg, T. Aulin, and N. Rydbeck, "Power-Bandwidth Performance of Smoothed Phase Modulation Codes," *IEEE Trans. Commn.,* vol. 29, pp. 187-195, 1981.

[13] T. Aulin and C. Sundberg, "Continuous Phase Modulation--Part I: Full Response Signaling," *IEEE Trans. Commn.,* vol. 29, pp. 196-209, 1981.

[14] T. Aulin, N. Rydbeck, and C. E. Sundberg, "Continuous Phase Modulation--Part II: Partial Response Signaling," *IEEE Trans. Commn.,* vol. 29, pp. 210-225, 1981.

[15] B. E. Rimoldi, "A decomposition approach to CPM," *IEEE Trans. Inform. Theory,* vol. 34, pp. 260-270, 1988.

[16] J. G. Proakis, *Digital Communications*, fourth ed. New York: McGraw-Hill, 2001.

[17] A. J. R. Francisco A. Monteiro, "Phase Error Resilience to I/Q Mismatch of a Simplified CPM Receiver," *IEEE Microwave Wireless Compon. Lett,* vol. 15, Sep. 2005.

[18] A. F. Molisch, J. Fuhl, and P. Proksch, "Bit error probability of MSK modulation with switched diversity in a mobile-radio channel with two independently-fading paths," in *Proc. PIMRC*. vol. 3, 1995, p. 1223.

[19] Marcelo S. Alencar and V. C. d. Rocha, *Communication systems*: Springer, 2005.

[20] B.-S. Feng, "A strategy to reduce the detection complexity of nonlinear continuous-phase modulation signals," M.E. Thesis, Chung Yuan Christian University, 2006.

[21] M. Kalkan, "CPM performance with diversity in mobile radio," in *Proc. Electrotechnical Conference*, 1994, pp. 32-34 vol.1.

[22] F. Adachi, "Postdetection selection diversity effects on digital FM land mobile radio," *IEEE Trans. Veh. Tech.,* vol. 31, pp. 166-172, 1982.

[23] J. P. Fonseka, "Soft-decision phase detection with Viterbi decoding for CPM signals," *IEEE Trans. Commn.,* vol. 47, pp. 1802-1810, 1999.

[24] S. J. Simmons, "Simplified coherent detection of CPM," *IEEE Trans. Commn.,* vol. 43, pp. 726-728, 1995.

[25] G. Colavolpe and R. Raheli, "Reduced-complexity detection and phase synchronization of CPM signals," *IEEE Trans. Commn.,* vol. 45, pp. 1070-1079, 1997.

[26] A. Barbieri and G. Colavolpe, "Simplified Soft-Output Detection of CPM Signals Over Coherent and Phase Noise Channels," *IEEE Trans. Wireless Commun.,* vol. 6, pp. 2486-2496, 2007.

[27] John B. Anderson, Tor Aulin, and C.-E. Sundberg, *Digital Phase Modulation*. New York: Plenum Press, 1986.

[28] E. Perrins and M. Rice, "Reduced-complexity detectors for Multi-h CPM in aeronautical telemetry," *IEEE Trans. Aerospace and Electronic Systems,* vol. 43, pp. 286-300, 2007.

[29] B. Amiri, "Per-Survivor Processing (PSP)," [Online]. Available: http://amiri.bahador.googlepages.com/Report_251.pdf.

[30] R. Raheli, A. Polydoros, and T. Ching-Kae, "Per-Survivor Processing: a general approach to MLSE in uncertain environments," *IEEE Trans. Commn.,* vol. 43, pp. 354-364, 1995.

[31] G. M. Vitetta and D. P. Taylor, "Viterbi decoding of differentially encoded PSK signals transmitted over Rayleigh frequency-flat fading channels," *IEEE Trans. Commn.,* vol. 43, pp. 1256-1259, 1995.

[32] M. J. Miller, "Detection of CPFSK signals using per survivor processing," in *Proc. MILCOM*, 1998, pp. 524-528 vol.2.

[33] M. N. Patwary and P. B. Rapajic, "Decision Feedback Per-survivor Processing: New Reduced Complexity Adaptive MLSE Receiver," in *Proc. APC*, 2005, pp. 802-806.

[34] Z. Bin and M. C. Valenti, "Per-survivor based detection of DPSK modulated high rate turbo codes over Rayleigh fading channels," in *Proc. SSC*, 2001, pp. 1026-1030 vol.2.

[35] J. H. Yi and J. H. Lee, "PSAIC decoder for space-time trellis-coded DS-CDMA system," *Electronics Letters,* vol. 41, pp. 344-346, 2005.

[36] P. Kovintavewat, J. R. Barry, M. F. Erden, and E. M. Kurtas, "Reduced-complexity per-survivor iterative timing recovery for coded partial response channels," in *Proc. ICASSP '05*, pp. iii/841-iii/844 Vol. 3.

[37] D. G. Brennan, "Linear diversity combining techniques," *Proc. IEEE,* vol. 91, pp. 331-356, 2003.

[38] J. K. Cavers, *Mobile Channel Characteristics, Second Edition*. Columbia, Canada: Shady Island Press, 2003.

[39] Philip Balaban and J. Salz, "Dual diversity combining and equalization in digital cellular mobile radio," *IEEE Trans. Veh. Tech.,* vol. 40, May 1991.

[40] P. Reid, "Diversity for an Emerging Digital Radio Standard," A Third Professional Year Project Report, University of Canterbury, 26 September 2002.

[41] M. R. Chaaban, Y. H. Chung, and A. M. D. Turkmani, "Diversity reception at the base station of a GSM/DCS1800 system," in *Proc. IEEE VTC'94*, pp. 709-713 vol.1.

[42] A. F. Molisch, H. Novak, J. F. Fuhl, and E. Bonek, "Reduction of the error floor of MSK by selection diversity," *IEEE Trans. Vehi. Tech.,* vol. 47, pp. 1281-1291, 1998.

[43] I. Ghareeb and S. Abu-Surra, "Differential detection of GMSK signals with postdetection MRC over correlated and unbalanced Nakagami-m fading channels," *IEE Commun. Proc.,* vol. 152, pp. 221-228, 2005.

[44] A. J. Rodrigues and A. A. Albuquerque, "Diversity techniques with multi-h CPM for satellite mobile systems," in *Proc. VTC*. vol. 1, 1996, pp. 551-555 vol.1.

[45] I. Korn and J. P. Fonseka, "GMSK with limiter-discriminator detector in Nakagami fading channel with and without selection combining," *IEEE Trans. Commn.,* vol. 51, pp. 1271-1273, 2003.

[46] W. Refai and S. C. Gupta, "Space diversity of CPM over fading channels with interfering signals," in *Proc ICC*, 1988, pp. 1641-1645 vol.3.

[47] F. Adachi and J. D. Parsons, "Error rate performance of digital FM mobile radio with postdetection diversity," *IEEE Trans. Commn.,* vol. 37, pp. 200-210, 1989.

[48] J. Cheng and T. Berger, "Performance analysis for MRC and postdetection EGC over generalized gamma fading channels," in *Proc. WCNC*. vol. 1, 2003, pp. 120-125 vol.1.

[49] J. Cheng and T. Berger, "Capacity and performance analysis for hybrid selection/maximal-ratio combining in Nakagami fading with unequal fading parameters and branch powers," in *Proc. ICC*. vol. 5, 2003, pp. 3031-3035 vol.5.

[50] I. Korn, "M-ary CPFSK-DPD with L-diversity maximum ratio combining in Rician fast-fading channels," *IEEE Trans. Veh. Tech.,* vol. 45, pp. 613-621, 1996.

[51] B. Xu Jin and M. Du Li, "Blind MLSE with spatial diversity combining and its simplified algorithm," in *Proc. ICCT*, 1998, p. 5 pp. vol.2.

[52] C. E. Sundberg, "Continuous phase modulation," *IEEE Communications Magazine,* vol. 24, pp. 25-38, 1986.

[53] J. B. Anderson and C. E. W. Sundberg, "Advances in constant envelope coded modulation," *IEEE Communications Magazine,* vol. 29, pp. 36-45, 1991.

[54] M.K.Simon and M. S. Alouini, *Digital Communication over Fading Channels: A Unified Approach to Performance Analysis*. NY: Wiley-Interscience, 2000.

[55] S. Haykin, *Communication systems*, 4th ed.: John Wilev & Sons, Inc., 2001.

[56] W. C. Jakes, *Microwave mobile communications*. Piscataway, NJ: IEEE Press, 1994.

[57] R. H. Clarke, "A statistical theory of mobile-radio reception," *Bell Syst. Tech. J.,* pp. 957-1000, Jul.-Aug. 1968.

[58] M. J. Gertsman and J. H. Lodge, "Symbol-by-symbol MAP demodulation of CPM and PSK signals on Rayleigh flat-fading channels," *IEEE Trans. Commn.,* vol. 45, pp. 788-799, 1997.

[59] A. Svensson, C.-E. Sundberg, and T. Aulin, "A Class of Reduced-Complexity Viterbi Detectors for Partial Response Continuous Phase Modulation," *IEEE Trans. Commun.,* vol. Com-32, October 1984 1984.

[60] G. D. Forney, "The Viterbi Algorithm," *Proc. of IEEE,* vol. 61, pp. 268-278, 1973.

[61] C. Horn, "C4FM Receiver Design," Tait Electronics Ltd Internal Report, 2004.

[62] A. J. Viterbi, "Error bounds for convolutional codes and an asymptotically optimal decoding algorithm," *IEEE Trans. Inform. Theory, IT-13, 260-269,* April 1967.

[63] G. Fettweis and H. Meyr, "Parallel Viterbi algorithm implementation: breaking the ACS-bottleneck," *IEEE Trans. Commn.,* vol. 37, pp. 785-790, 1989.

[64] E. A. Ince, Y. J. Guo, and S. K. Barton, "T-Algorithm Detection of Partial Response Continuous Phase Modulated Signals over Multipath Channels."

[65] T. Larsson, "Optimal design of CPM decoders based on state-space partitioning," in *Proc. ICC, Geneva*, 1993, pp. 123-127 vol.1.

[66] M. V. Eyuboglu, M. V. Eyuboglu, and S. U. H. Qureshi, "Reduced-state sequence estimation with set partitioning and decision feedback," *IEEE Trans. Commn.,* vol. 36, pp. 13-20, 1988.

[67] E. S. Perrins, "Reduced Complexity Detection Methods for Continuous Phase Modulation," Ph.D. Thesis, Brigham Young University, December 2005.

[68] E. Perrins and M. Rice, "A new performance bound for PAM-based CPM detectors," *IEEE Trans. Commn.,* vol. 53, pp. 1688-1696, 2005.

[69] P. Moqvist and T. M. Aulin, "Orthogonalization by principal components applied to CPM," *IEEE Trans. Commn.,* vol. 51, pp. 1838-1845, 2003.

[70] U. Mengali and M. Morelli, "Decomposition of M-ary CPM signals into PAM waveforms," *IEEE Trans. Inform. Theory,* vol. 41, pp. 1265-1275, 1995.

[71] W. Tang, "A Receiver for Continuous Phase Modulation in Walsh Signal Space," Ph.D. Thesis, University of Manitoba, Winniepeg, Manitoba, Canada, September 1998.

[72] "PSP and AID Processing for the Next Generation of Digital Communications White Paper.," Trellisware Technologies, Inc. [Online]. Available: http://www.trellisware.com/assets/pdfs/AID_PSP_Whitepaper.pdf.

[73] M. J. Omidi, S. Pasupathy, and P. G. Gulak, "Joint Data and Kalman Estimation for Rayleigh Fading Channels," *Wireless Pers. Commun.,* vol. 10, pg 319-339, 1999.

[74] J. K. Caver, "MLSE applied to CPM," Report Prepared for Tait Electronics Ltd, 2003.

[75] L. Krasny, H. Arslan, D. Koilpillai, and S. Chennakeshu, "Doppler spread estimation in mobile radio systems," in *Proc. PIMRC*, London, England, 2000, pp. 197-199.

[76] M. Hook, C. Johansson, and H. Olofsson, "Frequency diversity gain in indoor GSM systems," in *Proc. VTC*, 1996, pp. 316-320 vol.1.

[77] R. van Nobelen and D. P. Taylor, "Analysis of the pairwise error probability of non-interleaved codes on the Rayleigh-fading channel," in *Proc. GLOBECOM*, 1994, pp. 181-185.

[78] S. Verdu, *Multiuser Detection*, 1st ed. NY: Cambridge University Press, 1998.

[79] W. C. Y. Lee, "Mobile radio signal correlation versus antenna height and spacing," *IEEE Trans. Vehi. Tech.,* vol. 26, pp. 290-292, 1977.

[80] R. G. Vaughan and J. B. Andersen, "Antenna diversity in mobile communications," *IEEE Trans. Vehi. Tech.,* vol. 36, pp. 149-172, 1987.

[81] G. L. Stüber, *Principles of Mobile Communication*. Norwell, MA: Kluwer Academic Publishers, 1996.

[82] K. Young-Chai, K. Young-Chai, L. Tao, and J. Gibong, "Effect of noise variance in the channel estimation on dual-MRC over Rayleigh fading channels," in *Proc. VTC*, 2003, pp. 2538-2542 vol.4.

[83] L. B. M. Ning Kong, "Average SNR of a Generalized Diversity Selection Combining Scheme," *IEEE Commun. Letters,* vol. 3, March 1999.

[84] A. Svensson, "Reduced state sequence detection of partial response continuous phase modulation," in *Inst. Elec. Eng. -I*, 1991, pp. 256-268.